THE PROCEEDINGS OF THE PHYSICAL SOCIETY

VOL. 61, PART 3 1 September 1948 No. 345

A Theory of Transient Creep in Metals

BY C. L. SMITH
Cavendish Laboratory, Cambridge

MS. received 25 *March* 1948

ABSTRACT. A new approach to the theory of transient creep in metals is described and the relation $\epsilon = \text{const.}\ T(1-e^{-Ct})/t$ deduced, connecting the creep strain ϵ, the absolute temperature T and the time t. C is a constant.

This relation is compared with experimentally obtained curves.

§ 1. INTRODUCTION

FROM observations on the creep of non-alloyed metals at constant stress, Andrade (1911, 1914) found that the creep curves could be very satisfactorily represented by the formula

$$l = l_0(1+\beta t^{1/3})e^{\alpha t}, \qquad \ldots\ldots(1)$$

where l is the length of the specimen after time t, and l_0 the length at the moment $t=0$ when the sudden extension, occurring immediately after the application of the stress, is assumed to have ended. α and β are constants which depend on stress and temperature. If $\beta = 0$, $l = l_0 e^{\alpha t}$ and $(1/l)(dl/dt) = \alpha$.

With increasing time, the creep rate tends asymptotically towards the value given by this equation; at low temperatures α is practically zero. Andrade called this "viscous" flow; it is not Newtonian in that the strain rate $(1/l)(dl/dt)$ is not proportional to the stress. According to Becker (1925), such flow may occur by a process of thermally activated rearrangement of small numbers of atoms. To this category belongs recovery creep, which takes place at a constant rate such that there is equilibrium between strain hardening and thermal softening.

If the temperature is low relative to the melting point of the metal, $\alpha = 0$ and $dl/dt = \frac{1}{3} l_0 \beta t^{-2/3}$. The creep rate then tends asymptotically to approach zero with increasing time. This component of creep was called "β" flow by Andrade; Orowan (1947) has suggested the expression "transient creep" or "transient component of creep". It is this, the "β" flow, or transient creep, with which we shall be concerned in what follows.

Since Andrade's original work, transient creep has received little attention until recently, when several papers (Cottrell and Aytekin 1947, Los, unpublished, Mott and Nabarro 1948, Orowan 1947) have revived interest in the problem. In one of these, Orowan (1947) has suggested an expression for the creep rate by considering it as a thermally activated process, dependent on the form of the stress–strain curve; this is

$$d\epsilon/dt = (A/\epsilon^2)\exp(-B\epsilon^2 h^2/kT),$$

where $d\epsilon/dt$ is the creep rate, A and B are constants, h is the slope of the

yield stress–strain curve at the point under consideration, and ϵ is the extension measured from the point when the instantaneous extension, immediately following the application of the stress, is assumed to have ended.

In this expression the exponential term, $\exp(-B\epsilon^2h^2/kT)$, expresses the probability of a successful thermal activation occurring; the term A/ϵ^2 is an empirical factor giving the length of the glide avalanche ensuing from one successful activation.

In what follows, a treatment of transient creep is suggested which, although very much simplified, does not contain such an empirical factor.

§2. THEORY

The immediate effect of the application of the load in a creep test is an extension which is practically instantaneous if the inertia of the testing machine is small. This is followed by rapid plastic flow, which decreases in velocity more or less rapidly, and finally goes over into slow plastic flow or creep. We assume that, at the instant when sudden extension is complete, there exists in the specimen a very large number of spots of stress concentration where the local stress is higher than the mean applied stress, but lower than the local yield stress. This will occur where dislocations become trapped at energy barriers, as, for example, at the sites of impurity atoms or crystallite boundaries. Each of these spots can be characterized by an activation energy E, such that a local stress fluctuation, caused by thermal agitation, will raise the stress in a volume V up to the yield stress and initiate glide at that point.

The significance of the volume V is that the stress fluctuation must occur in a volume large enough for the local glide process not to be annihilated by the elastic forces in the surroundings when the stress fluctuation has ceased. The energy required to produce this stress fluctuation is E, the activation energy. Since the stress concentration will vary from point to point, the specimen in a given state will be characterized by a relationship between the energy E and the number of spots $f(E)\,dE$ with activation energies between E and $(E+dE)$.

As plastic flow continues, the distribution function $f(E)$ changes. We must first investigate the form of the function describing this variation with time. Let the function at time t be $f(E,t)=f$; we denote $f(E,0)$ briefly by f_0. Consider only the spots with activation energies between E and $(E+dE)$ at time t: their number will be $f(E,t)\,dE=f\,dE$. During the ensuing short interval of time dt, some will be lost by thermal activation from which glide ensues; let this number be dN, where

$$dN=-C(f\,dE)e^{-E/kT}\,dt. \qquad \ldots\ldots(2)$$

In addition, the glide which occurs during time dt will produce new spots between E and $(E+dE)$. The number of spots produced may depend on many factors, in particular on the past treatment of the specimen; since we do not know how it is influenced by these factors, we shall assume, for simplicity, that no new spots are created during creep.

With this assumption, equation (2) becomes

$$dN=d(f\,dE)=-C(f\,dE)e^{-E/kT}\,dt. \qquad \ldots\ldots(2\,a)$$

Equation (2 *a*) has a solution of the form

$$f=f_0e^{-\lambda t}, \quad \text{where} \quad \lambda=Ce^{-E/kT}, \qquad \ldots\ldots(3)$$

or

$$f(E,t)=f(E,0)e^{-\lambda t}. \qquad \ldots\ldots(4)$$

If the average amount of glide resulting from the activation of a spot is a, then the glide in time dt from the spots with activation energies between E and $(E+dE)$ will be

$$aC(f_0e^{-\lambda t})e^{-E/kT}\,dE\,dt. \qquad \ldots\ldots(5)$$

This follows by substituting the value of f from equation (4) into equation (2).

By integrating this expression over all possible energies E, we obtain for the creep rate $d\epsilon/dt$ the expression

$$\frac{d\epsilon}{dt} = aC\int_{E=0}^{E=\infty}(f_0e^{-\lambda t})e^{-E/kT}\,dE. \qquad \ldots\ldots(6)$$

The integral in (6) cannot be evaluated unless the function f_0 is known, and neither theoretical nor experimental work can, at the moment, give any indication of its form. If, however, a suitably simple form for the function $f(E, 0)$ is chosen, the integral (6) can be expressed by known functions. We shall assume, therefore, a distribution $f(E, 0) = \text{const.} = p$, such that there is an equal number of spots in equal energy intervals dE. The glide rate at time t, from equation (6), is then given by

$$\frac{d\epsilon}{dt} = aCp\int_0^{\infty} e^{-\lambda t}e^{-E/kT}\,dE. \qquad \ldots\ldots(7)$$

Substituting $dE = kT(d\lambda/C)e^{E/kT}$ (see equation (3)) in (7), we have

$$\frac{d\epsilon}{dt} = apkT\int_{E=0}^{E=\infty} e^{-\lambda t}\,d\lambda = apkT\left[\frac{e^{-\lambda t}}{-t}\right]_{\lambda=C}^{\lambda=0} = apkT\left\{\frac{1-e^{-Ct}}{t}\right\}. \qquad \ldots\ldots(8)$$

It will be noticed that the limits of integration are taken from $E=0$ to $E=\infty$. Clearly, spots cannot have an activation energy greater than some maximum value $E_{\max}$; but since higher energy spots would make only a negligible contribution to the creep rate, the upper limit can be taken as $E_{\max}=\infty$ in order to simplify the final result.

§ 3. DISCUSSION

From equation (8) we see that the creep rate is proportional to (i) the absolute temperature T, and (ii) the function $F(t)$ defined by $F(t)=(1-e^{-Ct})/t$.

In what follows we shall discuss only the function $F(t)$ describing the form of the transient creep curve at a constant temperature.

For values of t such that $Ct \ll 1$, $F(t)$ is a constant, since

$$F(t) = \frac{1-e^{-Ct}}{t} = \frac{1-(1-Ct+C^2t^2/2!\ldots)}{t} = C + (\text{small terms}),$$

and the creep strain ϵ is, therefore, a linear function of the time $\epsilon = akpT(Ct)$.

When, however, $Ct \gg 1$, $F(t)$ approximates to $1/t$ and the creep strain

$$\epsilon = \text{const.}\ (apkT)\ln(\text{const.}\ t).$$

In figure 1 curves are plotted of $y=1/Ct$ and also $y=(1-e^{-Ct})/Ct$.

In the former case $y\to\infty$ as $t\to 0$, and in the latter $y\to 1$ as $t\to 0$. These curves show that the approximation $1/Ct$ fails when Ct is small, and it can be seen that for values of $Ct \lesssim 3$ the deviation is appreciable, but for values of $Ct \gtrsim 3$ the approximation is very good. To determine for what values of t the deviation is appreciable, it is necessary to know the value of C.

C has the character of a frequency, and by making certain assumptions Mott and Nabarro (1948) conclude that its order of magnitude should be 100–1000 times smaller than that of the frequency of the atomic oscillations in a lattice. They

deduce this by considering a precipitation-hardened metal containing line dislocations arrested at the sites of precipitate atoms which are assumed to be, on the average, about 200 A. apart. The conclusion is that C is the frequency of the normal mode of oscillation of such dislocations 200 A. long, from which is obtained a value for C of $10^8 - 10^9$ sec^{-1}. This value will decrease with increasing distance between the points at which the dislocation is temporarily arrested, but even under the most favourable circumstances (i.e. with very high purity metals) it is difficult to see how an increase in the distance apart by a factor of more than 10^3 or 10^4 could be achieved. In this case C would become $10^4 - 10^5$ sec^{-1}. From this we see that the approximation $F(t) = 1/t$ should be accurate for all values of t greater than about 10^{-4} sec.

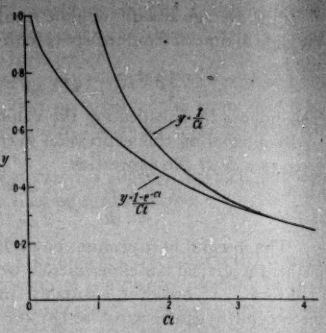

Figure 1.

By considering the movement of line dislocations over energy barriers, Mott and Nabarro also obtain a relation between creep strain and time

$$\epsilon = \text{const.}\ T^{2/3}(\ln Ct)^{2/3}.$$

This expression, of course, leads to $\epsilon \to -\infty$ for $t \to 0$; however, $t \simeq 1/C$ is the smallest value of t to which a physical sense can be attached.

A logarithmic relation between creep strain and time, $\epsilon = D \ln Et$, has already been suggested by several authors (Chevenard 1934, Phillips 1905, Tapsell and Prosser 1934), who have shown that it gives a good agreement with experimental results within the range of variables considered. In prolonged tests, however, it is found that the creep strain given by the above relation is less than that observed experimentally; Andrade's expression, on the other hand, under similar circumstances, would, in general, give too high values for the creep strain.

Examples of specimen creep curves are shown in figures 2–4.

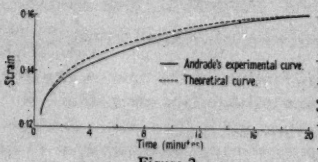

Figure 2.

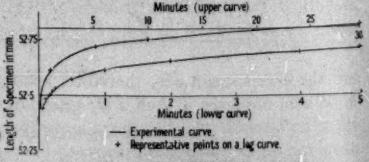

Figure 3.
The lower curve is the early part of the upper curve with an extended time scale.

The curve in figure 2 is taken from Andrade's paper (1914) and represents a creep test in which a lead specimen at $-78°$ C. was subjected to a stress of 401 kg/cm^2. At this temperature creep may be considered to be wholly transient.

Figure 3 shows a creep curve for copper * taken at room temperature at a constant stress of 1764 kg/cm^2. The stress was kept constant by the use of a

* This was kindly supplied by J. Los (unpublished).

spring-loading testing machine in which the decrease in the cross-sectional area of the specimen was compensated by a reduction in applied load produced by the relaxation of the spring. In addition, in this experiment the inertia of the moving parts of the apparatus was kept as small as possible; it should therefore provide a reliable test for the theory, and it is seen that the logarithmic function does, in fact, provide a good fit. An attempt was also made to fit Andrade's expression $l=l_0(1+\beta t^{1/3})e^{\alpha t}$ to this curve. It was found that this could only be achieved by giving α a small negative value, to which, of course, no physical interpretation can be attached. A very good fit was, however, obtained with $\alpha=0$ and the exponent of the time 0·10 instead of 0·33 as above, i.e. $l=l_0(1+\beta t^{0\cdot1})$.

Finally, figure 4 shows the initial part of the flow curve for a zinc single crystal at room temperature. In this case there was without doubt a super-imposed component of viscous creep which was taken into account by an additional term proportional to t, i.e. $\epsilon=D\ln(Et)+Ft$.

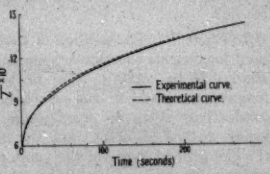

Figure 4. Zinc single crystal.

With three unknown constants, the experimental and theoretical curves can be made to coincide at three points; these were chosen to be at $t=3$ sec., $t=16$ sec., and $t=260$ sec. The agreement is again seen to be quite good. In fact, when it is remembered that the form of the distribution function $f(E,0)$ was chosen arbitrarily, and purely from the point of view of simplicity in mathematical manipulation, the agreement between the theoretical and experimental results is unexpectedly good.

Before such a simple theory can be advanced further, it is necessary to know the form of the function $f(E,0)$ more accurately, and also the manner in which this function changes as flow progresses. This would involve an investigation of the mechanism by which new spots are formed during creep. When this is accomplished, a theory on the lines outlined above will certainly give a more complete picture of transient creep.

ACKNOWLEDGMENT

The author would like to thank Dr. E. Orowan for many helpful discussions, and the British Iron and Steel Research Association, under whose auspices the work was done, for financial assistance.

REFERENCES

Andrade, E. N. da C., 1911, *Proc. Roy. Soc.* A, **84**, 1; 1914, *Ibid.*, **90**, 329.
Becker, R., 1925, *Phys. Z.*, **26**, 919.
Chevenard, P., 1934, *Revue de Metallurgie*, November, p. 473.
Cottrell, A. H., and Aytekin, V., 1947, *Nature, Lond.*, **160**, 328.
Mott, N. F., and Nabarro, F. R. N., 1948, *Report of Conference on Strength of Solids* (London: Physical Society), p. 1.
Orowan, E., 1947, *West of Scotland Iron and Steel Institute.*
Phillips, P., 1905, *Phil. Mag.*, **9**, 513.
Tapsell, H. J., and Prosser, E. E., 1934, *Engineering*, **137**, 212.

The Thermal Conductivity of some Insulating Materials at Low Temperatures

By C. S. CHOW *
Imperial College, London
* Now returned to China

Communicated by Sir Alfred Egerton ; MS. received 21 *May* 1947, *and in amended form* 8 *January* 1948

ABSTRACT. The method of Lamb and Wilson modified for use at low temperatures is used for thermal conductivity measurements of insulating materials in the range of temperature +18 to −180° c. For finely granulated and loosely packed fibrous materials, the temperature gradient was experimentally determined and the intermediate values of the conductivity along the temperature gradient were obtained. For coarsely granulated or loosely packed materials, only the mean conductivity is observed.

The general shape of the conductivity–temperature curve in relation to the density of packing for various materials is discussed. For compressible fibrous insulators, the variation of conductivity with packing densities at low temperatures has been found similar to that at normal or moderate high temperatures. Granulated cork, vermiculite, cotton waste, sawdust and slag wool were amongst the materials investigated.

§1. INTRODUCTION

A CONSIDERABLE amount of work has been done on the thermal conductivity of common insulating materials both at normal and at high temperatures, but data concerning the conductivities at low temperatures are very limited.

The present investigation was carried out in the Department of Chemical Technology, Imperial College, during the early period of the war, in connection with work on the liquefaction of methane. Results relating to some useful insulating materials for a temperature range of about 10° to −180° c. were obtained and are here reported.

The plate method has been used by Ezer Griffiths (1928/9, 1932, 1936, 1940/41) and by Rowley, Jordan and Lander (1945) for determination of the heat conductivities of materials to −75° c. and −40° c. respectively and to −183° c. by Wilkes (1946). The spherical shell method has been used by Gröber (1909, 1910) and by Raisch and Weyh (1932) for measurements to −183° c.

The method used in the present investigation is based on that used at normal temperature by Lamb and Wilson (1899), but includes the introduction of a guard-ring arrangement. This method was chosen because it is easier to set up two concentric cylinders than to provide spherical shells. The insulating materials can be packed conveniently between the cylinders, and thermocouple elements can be fixed in precise positions to determine the temperature distribution along the heat flow path.

§2. APPARATUS AND METHOD OF EXPERIMENTS

In figure 1 is shown the design and arrangement of the apparatus. It consists of two concentric cylinders, the space between them being packed with the material under test. The inner cylinder was 2 in. in diameter, 19 in. long with 1/16 in.

wall thickness; it was maintained at a low temperature with a suitable cooling agent such as liquid oxygen and acted as the "axial cooler". The outer cylinder, which served both as "heater" and water flow calorimeter, was double-walled, 12·5 in. long by 10 in. internal diameter. The wall space was baffled so as to distribute the water flow evenly round the circumference.

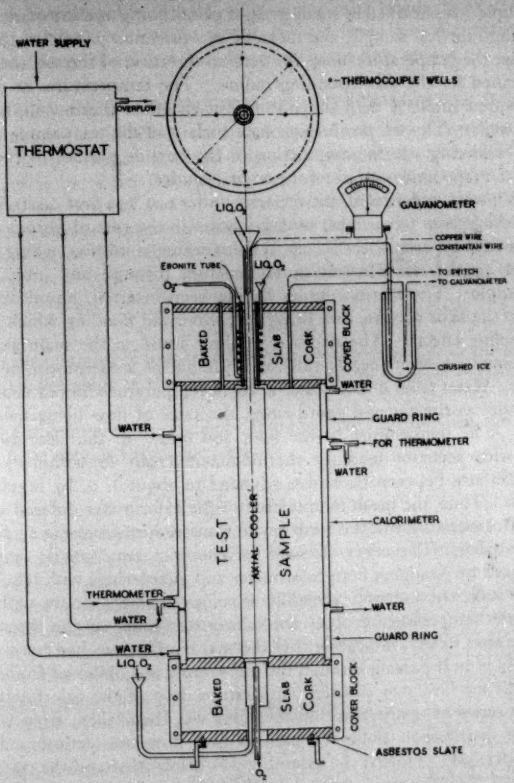

Figure 1. Apparatus.

Above and below the calorimeter were copper water jackets of the same diameter which served as "guard-rings", and the assembly was fitted at both ends with insulating cover-blocks which were equipped with auxiliary "axial coolers". Both guard-rings and cover-blocks were designed to eliminate "edge effects" from the heat flow, so that all the heat transferred from the calorimeter to the cooler could be assumed to flow at every point radially through the test material, i.e. in a direction perpendicular to the cylinder axis. The top cover-block was equipped at different radii with 3/16 in. holes parallel to the axis, which served as thermocouple wells.

Temperature measurements were made by means of copper–constantan thermocouples. The copper wire was 0·012 in. in diameter, and the constantan 0·007 in. The couples were calibrated at the normal boiling points of various pure cooling agents (liquid oxygen, methane, ethylene, dry ice etc.), and the readings thus obtained were then compared with the available data in the literature. Each thermocouple was sheathed in small straight glass-tubing and introduced through a "well" into the test sample, and movable in a direction parallel to the cylinder axis, so that the temperature along the vertical direction of the test sample could be determined for the corresponding radius. The temperatures at other radii were measured similarly with the aid of glass-sheathed thermocouples through the other wells. The temperature on each surface of the test sample was determined by soldering one thermojunction to the outside surface of the cylinder and another to the inner surface of the outer cylinder.

To conduct an experiment, the material under test was first carefully packed, attention being given to evenness of distribution in the case of fibrous materials. Then the whole apparatus was set up in the working condition, taking necessary precautions against the penetration of moisture through any interstices into the test sample. The thermocouples having been inserted, liquid oxygen was poured into the axial coolers, care being taken to avoid flooding which produced external cooling effects. The depth of cooling liquid in the main axial cooler was maintained constant (nearly full) with the aid of a thermocouple and galvanometer. Water from a thermostat at room temperature flowed continuously through both calorimeter and guard-rings, the rates of flow being made steady and equal. The temperature of the inlet and outlet to the calorimeter were measured with accurate mercury thermometers (read to within $\pm 0{\cdot}01°$ c.), and the difference between them was adjusted to about 1° c. by regulating the rate of flow. Thus, the mean temperature of the calorimeter differed very little from room temperature and the tendency to transfer heat from the surroundings could be avoided. The effect of small variations in atmospheric temperature was minimized by wrapping both calorimeter and guard-rings with felt.

After a sufficient interval (generally from six to eight hours with a good insulator), the temperature drop of the calorimeter water or the thermocouple readings became steady, indicating that thermal equilibrium had been attained. The quantity of heat passing through the test sample was obtained from observations of both the flow rate and the temperature drop of the calorimeter water. A complete series of temperature observations was then taken, from which the temperature distribution along the path of heat flow was determined for the material under test. Finally, the assembly was dismantled and the test material weighed.

It may be noted that the method used for determining the temperature gradient as described above is only applicable to the conditions in which there is no difficulty in inserting the glass-sheathed thermocouples into the test sample. For the materials like cotton waste (in tangled thread form), this method cannot be applied. In such a case, only the temperature on each surface of the test sample can be taken; i.e. only a single value for the thermal conductivity (mean conductivity) is determined at a given temperature difference. For some materials which, in practice, are difficult to pack evenly, the method has also failed to give reliable results. However, in this apparatus, though only liquid oxygen was used, other cooling agents such as dry ice in toluene, if necessary,

can also be used for determining the conductivity values of the test material at other mean temperatures. It would thus be possible, by employing the same apparatus, to estimate the temperature coefficient of the thermal conductivity of those materials for which the temperature gradient is difficult to determine. With regard to those materials for which the temperature gradient can be determined with a reasonable degree of accuracy, the conductivity–temperature relationship for each material is readily derived from the experimental data at the given temperature difference as described in the next section.

§3. METHOD OF CALCULATION AND EXPERIMENTAL RESULTS

In the apparatus described the heat leakage from the ends is assumed to be negligible through the use of guard-rings, and the direction of heat flow is taken at all points to be radial through the section of the test sample under study. Then the cross-sectional area of the path is $2\pi rL$ at radius r (where L is the length of the calorimeter and r the distance from the cylinder axis) and the temperature at every point on such a cylindrical shell is constant. If the temperature gradient can be determined, the conductivity k is obtained from the formula,

$$k = \frac{q}{2\pi rL} \cdot \frac{1}{(dt/dr)}, \qquad \ldots\ldots(1)$$

where q is the quantity of heat transferred in unit time, and dt/dr the temperature gradient (i.e. the slope of the temperature distribution curve, t vs r) at the point of radius r.

When the temperature gradient cannot be determined, then the mean conductivity k_m is obtained from the formula,

$$k_m = \frac{q}{2\pi L/\ln(r_2/r_1)} \cdot \frac{1}{t_1 - t_2}, \qquad \ldots\ldots(2)$$

where t_1 and t_2 represent temperatures on the outside and inside surfaces of the test sample, and $2\pi L/\ln(r_2/r_1)$ is called the shape factor (Langmuir, Adams and Meikle 1913).

That these assumptions are justified may be illustrated by reference to the experimental results for finely granulated cork, packed to obtain a uniform bulk density. In figure 2 (*a*) are shown the observed longitudinal temperature readings on the cylindrical shell at several different radii. The first experiment was repeated after repacking, when the bulk density differed by 0·1 lb/cu. ft. It can be seen that while there is no evidence of appreciable "edge effects" there are some slight irregularities in the temperature readings, the maximum deviation from the mean being

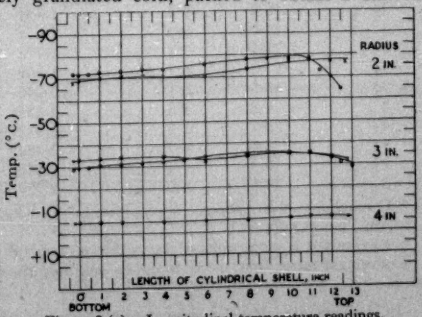

Figure 2 (*a*). Longitudinal temperature readings. Granulated slab cork.
Grain size: 49·5% 10–20 mesh and 59·5% through 20 mesh.
—○— for density of 6·3 lb/cu. ft.
—×— for density of 6·4 lb/cu. ft.

generally less than 10%. However, taking into account the small variations in grain size and the probable experimental error (for example, the inexact location of the thermojunctions), such a result is satisfactory. Taking the average height of ordinate for each curve to represent the temperature on the corresponding shell the results in table 1 are obtained. These are plotted in figure 3. The difference in the rate of heat transfer in the two experiments is only about 0·4 B.T.U./hour (less than 2%).

Table 1

Density lb/cu.ft.	Radius (inch)							Mean temp. of water (° c.)	Δt (° c.)	Rate of flow cm³/min.
	1	2	3	4	4½	4¾	5			
	Temperature (° c.)									
6·3	−181	−75	−32·5	−5·0	—	—	14·5	17·0	0·73	131·0
6·4	−181	−74	−33·5	−5·5	7·0	11·0	14·5	16·5	0·80	121·4

By graphical differentiation of the t–r curve (figure 3) the temperature gradient against radius is obtained, and from these values the thermal conductivity at various temperatures is calculated by means of equation (1). The detailed results so obtained are set out in table 2, from which the conductivity–temperature curve is plotted (see figure 4 (a)).

Table 2. Granulated slab cork (baked).

Density: 6·3–6·4 lb/cu. ft. q=22·75 B.T.U./hr. Grain size { 49·5% 10–20 mesh. 50·5% through 20 mesh.

Radius r (inch)	t (° c.)	$\frac{dt}{dr}$ (° F./ft.)	$2\pi rL$ (sq. ft.)	Conductivity, k (from eq. (1)) B.T.U.*	C.G.S.†
1	−181	48·5 × 86·4	0·545	0·0099	0·000041
1¼	−141	33·0 ,,	0·681	0·0117	0·000048
1½	−113	23·8 ,,	0·818	0·0135	0·000056
1¾	− 91·5	18·5 ,,	0·954	0·0149	0·000062
2	− 75	14·5 ,,	1·090	0·0166	0·000069
2¼	− 62	12·3 ,,	1·227	0·0174	0·000072
2½	− 50·6	10·7 ,,	1·363	0·0180	0·000074
2¾	− 40·8	9·3 ,,	1·499	0·0189	0·000078
3	− 32·0	8·2 ,,	1·636	0·0196	0·000081
3¼	− 24·3	7·3 ,,	1·772	0·0203	0·000084
3½	− 17·2	6·7 ,,	1·909	0·0206	0·000085
3¾	− 10·8	6·1 ,,	2·045	0·0211	0·000087
4	− 4·8	5·6 ,,	2·181	0·0215	0·000089
4¼	0·7	5·2 ,,	2·317	0·0218	0·000090
4½	5·8	4·7 ,,	2·454	0·0227	0·000094
4¾	10·3	4·4 ,,	2·590	0·0230	0·000095
5	14·5	4·0 ,,	2·727	0·0241	0·000099

* Throughout this paper, k expressed in B.T.U. is in consistent units, i.e. B.T.U./(hr.) (sq. ft.) (° F./ft.).

† k expressed in C.G.S. units is gram-cal/(sec.) (cm²) (° c./cm.)

Conversion factor from B.T.U. to C.G.S.—multiply the former by 0·00413 to obtain the latter.

In the case of coarsely granulated materials the curves corresponding to figure 2 (a) show wider deviations, the temperature being generally lower at the bottom and higher at the top of each cylindrical shell. Furthermore, for each corresponding shell the general shape of such curves depends largely on the

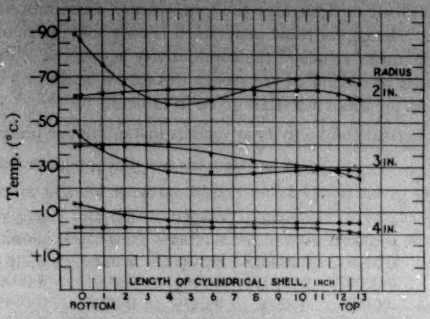

Figure 2 (*b*). Longitudinal temperature readings.
Slag wool.
—O— for density of 9·2 lb/cu. ft.
—X— for density of 12·3 lb/cu. ft.

relative proportions of the fractions of different grain size, and for the same packing the smaller the radius the greater are the deviations at the two ends of the shell.

For coarsely granulated materials as well as fibrous materials loosely packed, the curves such as shown in figure 2 (*b*) for slag wool at the density of 9·2 lb/cu. ft. are typical examples of the wide variations in temperature; the variations are generally much greater when the density of packing becomes still lower. In

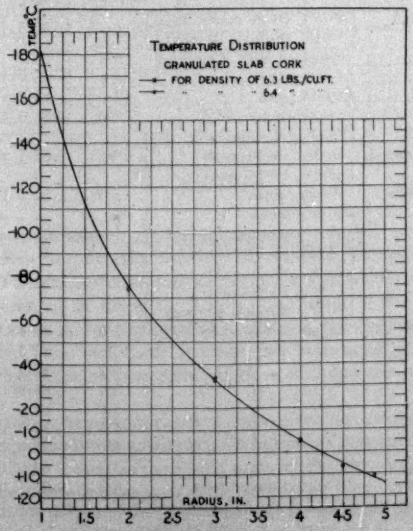

Figure 3.

such cases it is difficult to determine the temperature distributions with a satisfactory accuracy. Hence, for these materials it is only safe to calculate by means of equation (2) the mean values of the conductivity across the wide temperature range. The results so calculated are shown in table 4, including also the mean conductivity values for those materials given in table 3.

Table 3. Thermal conductivity at various instantaneous temperatures.

Temp. (° c.)	Units (see table 2)	No. of test materials (see descriptions in table 4) 1A	2A	3A	4	5	6
0	B.T.U.	0·0218	0·0380	0·0211	0·0358	0·0230	0·0224
	C.G.S.	0·000090	0·000157	0·000087	0·000148	0·000095	0·000093
− 40	B.T.U.	0·0190	0·0330	0·0183	0·0276	0·0187	0·0190
	C.G.S.	0·000079	0·000136	0·000076	0·000114	0·000077	0·000079
− 80	B.T.U.	0·0160	0·0275	0·0155	0·0225	0·0145	0·0155
	C.G.S.	0·000066	0·000114	0·000064	0·000093	0·000060	0·000064
−120	B.T.U.	0·0132	0·0227	0·0126	0·0192	0·0112	0·0120
	C.G.S.	0·000055	0·000094	0·000052	0·000079	0·00046	0·000050
−160	B.T.U.	0·0105	0·0191	0·0098	0·0170	0·0088	0·0089
	C.G.S.	0·000043	0·000079	0·000040	0·000070	0·000036	0·000037
−200*	B.T.U.	0·0085	0·0163	0·0070	0·0157	0·0062	0·0064
	C.G.S.	0·000035	0·000067	0·000029	0·000065	0·000026	0·000026

* Values extrapolated.

Table 4. Mean thermal conductivity

(Cold face temperature −181° c.)

No.	Material	Description	Bulk density lb/cu. ft.	Mean temp. (° c.)	Mean thermal conductivity B.T.U.(1)	C.G.S.(2)
1A	Granulated cork (baked)	49·5% 10–20 mesh 50·5% through 20 mesh	6·3	−82·5	0·0159	0·000066
1A	do.	Repeated after re-packing	6·4	−82·7	0·0162	0·000067
1B	do.	4–10 mesh	5·4	−83·4	0·0168	0·000070
2A	Vermiculite*	10–14 mesh	13·5	−86·2	0·0271	0·000112
2B	do.	4–10 mesh	9·0	−86·0	0·0199	0·000082
2C	Vermiculite (mixed)	7·9% 3–4 mesh 26·5% 4–10 mesh 65·6% 10–14 mesh	9·8	−85·7	0·0244	0·000101
3A	Sea-weed product	Powder form	8·0	−82·3	0·0155	0·000064
3B	do.	50·0% block 49·5% powder	7·3	−83·2	0·0201	0·000083
4	Sawdust (air-dried)	4·0% on 10 mesh 24·4% 10–20 mesh 61·6% 20–40 mesh 10·0% through 40 mesh	15·5	−82·3	0·0243	0·000100
5	Wadding	Crude cotton-wool	2·6	−83·4	0·0149	0·000062
6A	Slag wool		12·3	−82·3	0·0150	0·000062
6B	do.		9·2	−85·9	0·0115	0·000048
6C	do.		8·1	−84·9	0·0107	0·000044
6D	do.		7·0	−84·6	0·0113	0·000047
6E	do.		5·9	−83·9	0·0125	0·000052
6F	do.		5·0	−83·0	0·0134	0·000055
6G	do.		3·7	−83·0	0·0183	0·000076
7	Cotton waste	Tangled thread form	8·2	−86·7	0·0232	0·000092

* Vermiculite (in the expanded form) was received from the importers ground and graded 3–14 mesh. It was tested as received and then sieved so as to give two fractions, 4–10 and 10–14 mesh. These fractions were examined separately.

† Sawdust was a mixture of soft pine with a small amount of oak.

(1) B.T.U. per hour per sq. ft. for 1 ft. thickness and 1° F. temperature difference.

(2) Gm-cal. per sec. per cm^3 for 1 cm. thickness and 1° c. temperature difference.

For fibrous materials loosely packed the shape of the curves is particularly dependent on the uniformity of packing. This is illustrated by the curves in figure 2(*b*) for slag wool at two packing densities. The curves for the lower density (9·2 lb/cu. ft.) indicate the effect of compression of the bottom layer material under its own weight as well as that of uneven distribution of the packing material, while for much higher density of packing (12·3 lb/cu.ft.) very slight irregularities in the temperature readings are shown, with the one exception of the curve for 3 in. radius which is probably due to the effect of uneven distribution.

In general, for fibrous materials tightly packed such as slag wool at the density of 12·3 lb/cu. ft. and for materials finely granulated or in the form of powder, the variations in temperature for each cylindrical shell are very small, and therefore the temperature distribution along the path of flow can be determined with a

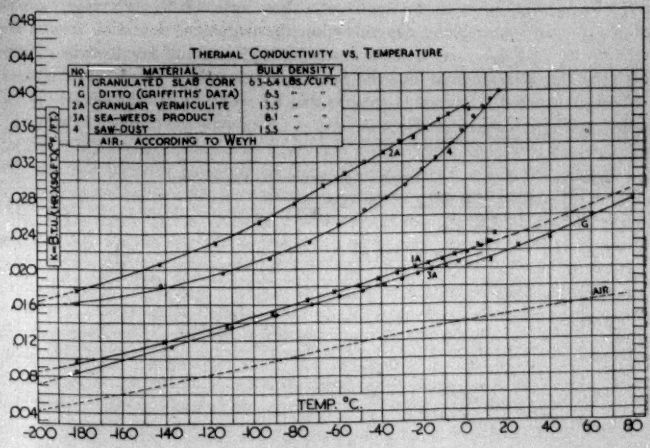

Figure 4 (*a*).

reasonable degree of accuracy. The conductivity–temperature relationships are derived by the method described above, the results so obtained being shown in figure 4(*b*). The results at several temperatures as taken from these smoothed curves are presented in table 3. Above 0° c. values of the conductivity are less certain than at lower temperatures, since in this region the variation of temperature gradient with path is small and consequently the influence of errors in temperature measurement on the calculated results is considerably increased.

The conductivity–temperature curve is also given for sawdust. This material consists of a large fraction of small particles but only a very small fraction of large particles or "chips", and, as the whole mass of the test sample can be evenly distributed, the packing density is fairly uniform. The curves corresponding to figure 2 show no particular irregularities; the temperature gradient is therefore determined without any great uncertainty.

§4. DISCUSSION OF RESULTS

As shown in figure 4 (*a*), the conductivity–temperature relationship is approximately linear over a wide range of temperature when insulating materials tested are closely packed to a uniform density (Nos. 1A, 3A, 6A etc.). However, when materials tested are not closely packed to give a uniform density, the variation of conductivity with temperature seems to deviate from the linear relationship, the degree of deviation being dependent on the tightness and uniformity of packing (cf. No. 6 and No. 5) (Rowley *et al.* 1945). The conductivity–temperature curve is most concave upwards for material most loosely packed.

The results indicated by figures 4 (*a*) and (*b*) can be compared with those shown in table 4 at the same temperatures; when k varies linearly with t (see curves 1A, 3A, 6A), the experimental value of k_m is correctly represented at t_m, no matter what the temperature drop across the test sample may be. However, if k is not a linear function of t, the two results show appreciable difference from each other, this difference being dependent on the degree of deviation from a linear relationship of the k–t curve. For instance, in the case of sawdust the difference between the experimental and the instantaneous values of the conductivity at $-82{\cdot}3°$ C. is about 2·5 times as great as that for wadding at $-83{\cdot}4°$ C.

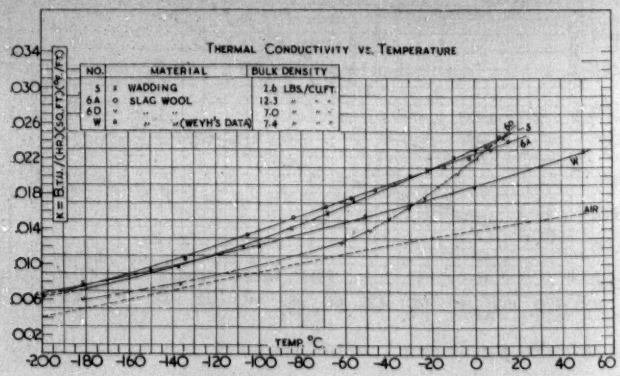

Figure 4 (*b*).

In a comparison of the conductivity data for a given material obtained by different methods, it is of importance to ascertain that the material tested by different investigators not only has the same properties (such as source of raw material, method of manufacture, density etc.) but also is tested in the same temperature range.

For slag wool the results reported by Raisch and Weyh (1932) give quite fair agreement with the present data in the low temperature range, but the mean values across wide temperature ranges cannot in fact represent the true behaviour of the conductivity for loosely packed materials.

For finely granulated slab cork, the conductivity was found to be approximately linear with temperature, and the extrapolation of its k–t curve (No. 1A) in the direction of higher temperature yields figures which compare well with

Griffiths' results (1940/41) for the same material at 6·5 lb/cu. ft. as shown in figure 4(*a*) (No. G).

For compressible materials the thermal conductivity is a function of the density of packing at a given temperature, and for each material there is an "optimum" density which corresponds to a minimum conductivity (20) (Griffiths 1940/41). In table 4 it is seen that the mean conductivity for slag wool at about −84° c. has a minimum value at about 8 lb/cu. ft. packing density, which is in agreement with Griffiths' results obtained in a 20 in. apparatus (1928/29, 1932, 1936, 1940/41).

It is also clear that, for a given granular material the conductivity depends on grain size, but the variation of conductivity with grain size may be different in nature for a different kind of granular material within the same range of grain size. Thus, in table 4, the apparent mean conductivity for granulated cork becomes higher when the test sample consists of comparatively large grains (4–10 mesh), while for granular vermiculite the conductivity becomes still lower as the proportion of the large grains (4–10 mesh) present is higher. This is probably connected with the porosity and other physical properties of the materials tested.

As already pointed out by various investigators, the amount of heat transferred through an insulating material is dependent on the conductivity of the material itself, and the transfer through air cells or interspaces within the pack is not only by conduction but also by radiation and convection. The relative amount of heat transferred by each of these processes is associated with the density of packing and the grain size of the material. It is generally agreed that, at higher densities of packing the conduction of heat by the material itself plays an increasingly important rôle, but at low densities or in a coarsely granulated material there are different views on the mechanism of the heat transfer through air spaces. According to Griffiths, convection takes place in the air spaces as observed in experiments on granular materials with a hot plate in a vertical position. Other authors suggest radiation as an important factor (Rowley *et al.* 1945), which causes the increase in slope of the curve.

In the present experiments, decrease of bulk density with the height occurred in loosely packed and coarsely granulated materials; consequently the thermal resistivity near the bottom with comparatively large densities was found to be appreciably greater than that towards the top, as can be illustrated by the curves for the longitudinal temperature readings (figure 2(*b*)). This behaviour is rather different from that observed by Griffiths. Furthermore, the k–t curve obtained was also seen to be most concave upward for the most loosely packed material.

When the effect of radiation and convection is reduced to a minimum, the apparent conductivity of an insulating material is obviously dependent on the conductivity of the material itself and of air in the interspaces. For materials of even porous structure the effect due to any radiation or convection may be negligibly small, so that the difference between the apparent conductivities of such materials could be taken to indicate the difference between the true conductivities of the solid part of the test samples. If such materials are also similar in physical structure, then the general shape of their k–t curves would be similar to each other, as can be seen from the apparent similarity of the two curves (figure 4(*a*)) for finely granulated cork (No. 1A) and powdered seaweeds product

(No. 3A). In line with the same view, the k–t curve for wadding (figure 4 (*b*)), though slightly different from that for slag wool at 12·3 lb/cu. ft., might become similar to the latter if the wadding were packed to the same degree of tightness and evenness.

Since most thermal insulators consist of porous or granular materials, the conductivity of air is regarded as the possible minimum value. The k–t curve for air according to Raisch and Weyh (1932) is shown in figure 4 for comparison. The materials tested with the apparent conductivity values nearest to the conductivity of air are granular baked slab cork, powdered seaweeds product, slag wool and wadding.

It must be pointed out that the materials tested with comparatively low conductivity values are not all useful for low temperature work. In selecting an insulation for practical applications, there are other important factors which must be taken into consideration, such as moisture resistance, mechanical and thermal strength, density, and cost (cf. Quarmby 1942).

ACKNOWLEDGMENTS

The author wishes to record his indebtedness to Prof. Sir A. C. Egerton, Sec.R.S., Head of the Department of Chemical Engineering and Applied Chemistry, Imperial College, for continued interest and encouragement; to Prof. D. M. Newitt, F.R.S., for helpful advice on the design of the apparatus, and to Dr. J. H. Burgoyne for assistance in the work. Finally, the author is particularly indebted to the Universities' China Committee in London for a grant which made possible the carrying out of the work.

REFERENCES

Egerton, A., and Pearce, M., 1945, *J. Inst. Fuel*, **18**, 168 (see refs. cited).
Griffiths, E., 1928/9, *Proc. Phys. Soc.*, **41**, 151,; 1932, *Structural Energy*, **10**, 202 ; 1936, *Chem. Engng. Congr.*, **1**, 366 ; 1940/41, *Proc. Brit. Assocn. Refrig.*, **37**, 15.
Griffiths, E., and Awbery, J. H., 1935, *Proc. Brit. Assocn. Refrig.*, **31**, 93.
Griffiths, E., Powell, R. W., and Hickman, M. J., 1942, *J. Inst. Fuel*, March.
Gröber, H., 1909, *Z. ges. Kalte., Ind.*, **16**, 84 ; 1910, *Z. Ver. dtsch. Ing.*, **54**, 1319.
Lamb, C. G., and Wilson, W. G., 1899, *Proc. Roy. Soc.*, **65**, 285.
Langmuir, I., Adams, E. Q., and Meikle, G. S., 1913, *Trans. Amer. Electrochem. Soc.*, **24**, 55.
Quarmby, B., 1942, *British Plastics*, **13**, 376 ; **14**, 32.
Raisch, E., and Weyh, W., 1932, *Z. ges. Kalte., Ind.*, **39**, 123.
Rowley, F. B., Jordan, R. C., and Lander, C., 1945, *Refrig. Engng.*, **50**, 541.
Wilkes, J., 1946, *Refrig. Engng.*, **52**, 37.

The Emission of Negative Ions from Oxide Coated Cathodes

By R. H. SLOANE and C. S. WATT*
Queen's University, Belfast
* Now at Cavendish Laboratory, Cambridge

MS. received 1 *December* 1947

ABSTRACT. The negative ions emitted from an oxide coated cathode and nearby electrodes have been analysed, using both a demountable metal mass spectrometer and glass sealed-off tubes to which normal cathode-ray tube high-vacuum technique could be applied. The mass-to-charge ratios of a large number of negative ions from the different electrodes have been determined. Retarding potential measurements have enabled energy distribution curves to be plotted for the more intense ion beams, and permit of discrimination between negative ions produced thermionically and those produced by bombardment. Some observations have been made on the dependence of the ionic thermal emission on the cathode temperature, and the variation of this emission with time after changes in cathode temperature, accelerating field and cathode surface conditions. The results are discussed and compared with those of other workers in this field.

§ 1. INTRODUCTION

It has long been known that the so-called "black spot" which develops on the screen of some high-vacuum cathode-ray tubes is produced by negatively charged heavy particles (von Ardenne 1935, Levy and West 1936) which are projected from the cathode region and focused on to the screen by the electrostatic lens. Bachman and Carnahan (1938) and Broadway and Pearce (1939) have been able to produce radial lines of black spots or negative ion mass spectra on the screen by applying a strong transverse magnetic field in the neighbourhood of the electron gun. More recently a paper by Schaefer and Walcher (1943) has become available describing results which were obtained by using a cathode-ray tube gun followed by a mass spectrometer with 48° deflection and an electrometer detector. Schaefer and Walcher, however, confined their attention to a demountable apparatus using grease sealed ground joints. The work described in the present paper is a comprehensive analysis of the negative ions from oxide coated cathodes and neighbouring electrodes, made with both a demountable metal apparatus and glass sealed-off tubes to which normal cathode-ray tube high-vacuum technique could be applied. Each complete apparatus constituted a mass spectrometer of the Dempster type, and permitted definite identification of the mass-to-charge ratios of the several negative ions observed, as well as determination of the energy distribution of the more abundant ions. It was also possible to investigate the dependence of the ionic thermal emission on the cathode temperature, and the variation of this ionic emission with time after changes in cathode temperature, accelerating field and cathode surface conditions. The experimental work was done between 1938 and 1940 but, apart from a preliminary note (Sloane and Cathcart 1939), publication in detail has had to be postponed on account of the war.

The general scope of the investigation is: (*a*) It makes an addition to the comparatively scanty information available concerning the mass numbers of atoms and radicles which form stable negative ions. (*b*) It provides new data for the emission from oxide coated cathodes. (*c*) It gives new information in

connection with the still incompletely understood phenomenon of cathodic sputtering. (*d*) It has a bearing on the design of cathode-ray tubes (Sharpe 1946, Bachman 1945).

The apparatus employed is described in § 2 and the main results obtained are recorded in § 3. Our results are discussed and compared with those of the other workers in this field in § 4.

§ 2. APPARATUS

(i) *Sealed-off glass tubes*

Two sealed-off glass tubes were used. The essential features of the first are shown in figure 1. It included a negative ion source I, a magnetic deflection chamber D and a receiving chamber R. The source consisted of an indirectly heated oxide coated cathode 8 mm. long, with its heater connected to F_1 and F_2, and its emitting surface connected to C. The cathode was surrounded by a cylindrical anode 1·0 cm. in diameter, which was connected to G_1. A slit (1 cm. × 3 mm.) in the lower side of the anode was covered with tantalum gauze made from 36 gauge wires spaced 0·5 mm. apart, which will be referred to as the first gauze. A second similar tantalum gauze connected to G_2 was placed between the first gauze and the source slit (8 mm. × 0·75 mm.), the latter being connected to S_1. All the electrodes, except the cathode and the two gauzes, were made of nickel-chrome which had previously been degassed in a vacuum furnace. G_2 was usually connected to S_1. The inner surface of D was coated with colloidal graphite ("Aquadag") which gave both good electrostatic screening and a rough surface which reduced reflection of the ions at the wall to a minimum.

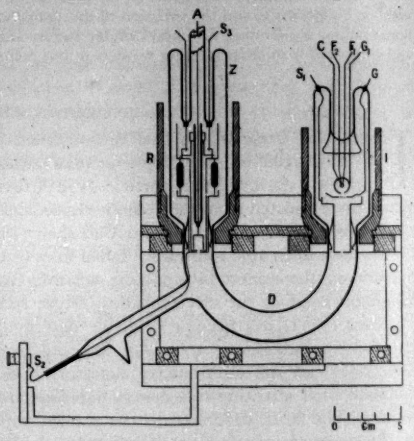

Figure 1. First glass sealed-off tube and mounting. In the tube, glass is shown by heavy lines, metal by lighter lines. The iron magnetic screen is shaded with full lines, the brass supports with alternate broken lines.

The Faraday cylinder, connected to A, was provided with guard rings and an electrostatic screen carrying the collecting slit, which was connected to S_3. This screen was connected electrically to another screen (not shown in the diagram) round the outside of the glass envelope Z. This in turn formed part of the electrostatic screen for the lead from the Faraday cylinder to the grid of an electrometer valve (Osram Type T) used to record the negative ion current. In this way the Faraday cylinder and its leads were screened completely except for the small opening of the collecting slit S_3 (6 mm. × 0·75 mm.). A second wider slit (9 mm. × 2·6 mm.) connected to S_2 was placed in front of the collecting slit. Contact was made with the Aquadag by means of spring strips as shown,

and, in order to eliminate any possible potential drop along the Aquadag between the source and the collecting slits, S_1 was connected metallically to S_2.

After assembly the tube was degassed for several hours in a furnace under vacuum. The electrodes in the source side were further degassed by eddy current heating, and the cathode activated in the usual way. The tube was then sealed-off and mounted in the same electromagnet as was used with the metal mass spectrometer (§2(ii)). The pole pieces were spaced by brass pillars which supported iron magnetic screens surrounding the source and detector chambers as shown in figure 1.

The negative ion accelerating voltage (V_n) was maintained steady at up to 2800 volts by a chain of neon tube stabilizers (Cossor Type S130). A potentiometer connected across a pre-selected section of this chain allowed fine adjustment of V_n.

The second tube, of which less use was made since it had a less good vacuum, had a somewhat similar electrode system, but with G_2 omitted. Advantage was taken of the small quantity of residual gas for some experiments described in §3(vii). Even in this tube the gas pressure was certainly not more than 10^{-4} mm. Hg and probably not more than 10^{-5} mm.

(ii) *The metal demountable system*

This mass spectrometer was the one previously described by Sloane and Press (1938b). It had heavy pole pieces spaced 9 mm. apart by a vacuum tight nickel-plated brass rectangular frame, and was constructed to permit of simultaneous deflection of two beams through 180°. In the present work only the larger of the two arcs was used and some slight structural modifications were made. The electrode systems were somewhat similar to those in the glass tubes. On the source side there was an oxide coated cathode C with a nickel backing plate at the same potential, a single gauze G and a slit S_1 (7 mm. × 0·75 mm.), while on the detecting side the Faraday cylinder was mounted behind two slits S_2 (8 mm. × 3 mm.), and S_3 (9 mm. × 0·75 mm.), S_3 being in the electrostatic screen surrounding the Faraday cylinder, as in the sealed-off tube. Both the source and detecting chambers were magnetically screened. All joints were made vacuum tight with a grease of low vapour pressure (Apiezon L).

§3. EXPERIMENTAL RESULTS

Mass spectra were recorded in all cases by keeping the magnetic deflecting field constant and applying a variable voltage V_n between C and S_1, so as to accelerate negative ions towards S_1. By varying V_n, one negative ion beam after another was brought through the slits into the Faraday cylinder. A voltage V_1, accelerating negative ions in the same direction, was applied between the cathode C and the gauze G in the metal apparatus and second glass sealed-off tube, and between C and G_1 in the first glass sealed-off tube.

The resolving power of each apparatus was arranged so as to separate all peaks of interest without unnecessarily reducing the currents to be measured, which it was convenient to keep greater than 10^{-15} amp.

(i) *Ion spectra : metal demountable system*

Two mass spectra, typical of a large number obtained using the demountable metal system, are shown in figure 2. These were taken after a new cathode

had been activated and operated under normal conditions for five hours. The spectrum (a) was obtained with a total cathode emission of 2·4 ma., while spectrum (b) was obtained with the cathode temperature a little higher and the emission varying slowly from 3·1 ma. to 4 ma. during observations in which the light ions were recorded first. V_1 was 100 v. for spectrum (a) and 200 v. for spectrum (b). The voltage scale along the top of the diagram gives V_n.

Since V_1 was applied between C and G, while the main variable accelerating voltage V_n was applied between C and S_1, it follows that V_n and $V_n - V_1$, together with any initial energy possessed, determined the energy with which negative ions liberated from the cathode and gauze respectively passed downward into the deflecting chamber D. An ion from the gauze would, therefore, enter the

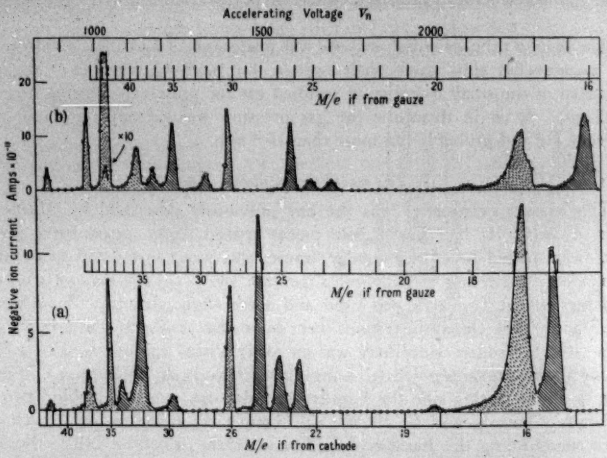

Figure 2. Negative ion mass spectra taken with the metal demountable apparatus. Peaks shaded with broken lines are due to ions from the cathode, those shaded with full lines to ions from the gauze.

(a) $V_1 = 100$ volts. (b) $V_1 = 200$ volts.

Faraday cylinder at a value of V_n greater by an amount V_1 than the value in the case of a similar ion from the cathode. If V_1 were increased and a new spectrum taken, peaks due to ions from the gauze would move to higher values of V_n, while those from the cathode would remain fixed. An example of the resulting displacement is seen in figure 2. This method was used to determine the place of origin of the different ions throughout all of our work. The peaks shaded with full lines in figure 2 and elsewhere are due to ions from the gauze, and those shaded with broken lines to ions from the cathode. Where variation of V_1 revealed overlapping of two peaks from gauze and cathode respectively, the approximate relative intensities are indicated by double shading. Where ion beams were particularly intense both the base and, on a reduced scale, the peak are shown. The mass-to-charge ratio (M/e) scales in figure 2 have been calculated by taking the position of the ion with $M/e = 26$ in atomic mass units, from the cathode, as standard (see § 3 (ii)), and staggering the scales for ions from the

gauze by an amount V_1. The current scale for spectrum (b) is smaller than for spectrum (a). The peaks at mass numbers 42, 35 and 37 from the cathode have increased appreciably in intensity with increase in V_1, while that at mass number 26 has increased slightly. Peaks at mass numbers 32 from the cathode and 35 from the gauze are superimposed in (a) but separated in (b).

No ions of mass number greater than 42 were found in these cases although search was made for them, and the available accelerating voltage was not high enough to allow a search for ions lighter than 16. Using a lower value of magnetic field a beam of small intensity at mass number 12 was observed.

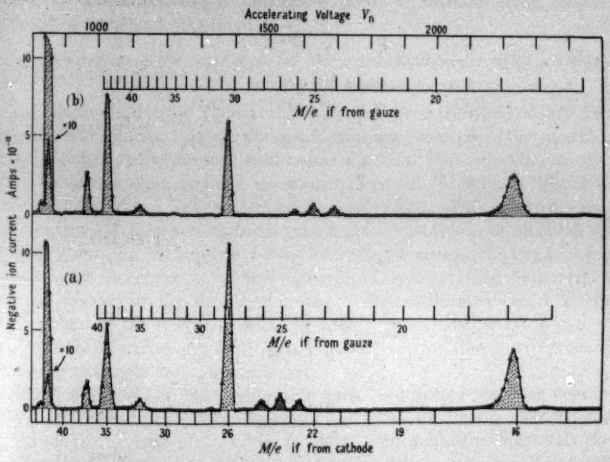

Figure 3. Negative ion mass spectra taken three days after those shown in figure 2, a partial vacuum having been maintained in the meantime. The shading of the peaks is the same as in figure 2.

(a) V_1=100 volts. (b) V_1=200 volts.

Figure 3 shows two spectra taken three days after those shown in figure 2. In the interval a partial vacuum had been maintained (pressure about 10^{-3} mm. Hg) with the cathode cold and all accelerating voltages reduced to zero. An attempt was made to reform the cathode, which was then aged for three and a half hours before readings were commenced for spectrum (a) with V_1 100 v. The second spectrum (b) was taken with V_1 200 v. The cathode emission varied from about 3 ma. at high values of V_n to about 1·5 ma. at low values of V_n in each case. The relative heights of the peaks are quite different from those in figure 2, and the only peaks recorded from the gauze with any appreciable intensity are those for mass numbers 24, 25 and 26. Both spectra have small peaks at mass numbers 27 and approximately 43 from the cathode. It will be noticed that 26 from the cathode is less intense in the second spectrum, but it does not necessarily follow that this is due entirely to increase of V_1, since it was noticed that with V_1 100 v. the peak height slowly decreased with time. It must be emphasized that it is not justifiable to make direct comparisons between the intensities of ion peaks

Table 1. Negative ions identified by different observers using oxide coated cathodes

1	2	3	4	5	6	7	8
1	—	—	H^-	H^-	H^-	H^-	H^-
12	C^-	C^-	C^-	C^-		C^-	C^-
13	—	—	CH^-	—	CH^-	—	—
14	—	—	—	—	CH_2^-	—	—
16	O^-	O^-	O^-	O^-	—	O^- or CH_4^-	O^-
17	—	—	—	—	OH^-	—	—
18	—	—	—	—	H_2O^-	H_2O^-	—
19	—	F^-	F^-	F^-	—	F^-	—
23	—	—	—	—	Na^-	—	—
24	—	C_2^-	—	C_2^-	C_2^-	—	—
25	—	C_2H^-	—	C_2H^-	C_2H^-	—	—
26	CN^-	CN^-	CN^-	CN^-	$C_2H_2^-$	CN^- or $C_2H_2^-$	CN^- or $C_2H_2^-$
27	Al^-	Al^-	—	—	—	—	—
30	—	—	—	—	—	NO^- or $HCHO^-$	—
32	O_2^-	O_2^-	O_2^-	O_2^-	O_2^-	O_2^-	O_2^-
33	—	—	—	—	?	—	—
34	—	—	—	—	?	—	—
35	$^{35}Cl^-$	$^{35}Cl^-$	$^{35}Cl^-$	$^{35}Cl^-$	$^{35}Cl^-$	$^{35}Cl^-$	$^{35}Cl^-$
37	$^{37}Cl^-$	$^{37}Cl^-$	$^{37}Cl^-$	$^{37}Cl^-$	$^{37}Cl^-$	$^{37}Cl^-$	$^{37}Cl^-$
39	—	—	—	? $^{39}K^-$	—	—	—
40	—	—	? Ca^-	—	Ca^-	Ca^-	—
42	CNO^-	—	—	—	?	—	CNO^- or $C_3H_6^-$
43	?	—	—	—	?	diffuse 42·7*	—
48	—	—	broad diffuse peak*	—	?	—	"suspicion" of 48*
56	—	—	—	—	CaO^-	CaO^-	—
58	—	—	—	—	Ni^-	—	—
60	—	—	—	—	Ni^-	—	—
62	—	—	—	—	?	—	—
68	—	—	—	—	?	—	—
74	—	—	—	—	—	$Ca(OH)_2^-$	—
79	—	—	$^{79}Br^-$	—	—	80 ?	unresolved Br^-
81	—	—	$^{80}Br^-$	—	—		
101	—	—	—	—	—	$CaCO_3^-$ or SrO^-	—
120	—	—	—	—	—	SrO_2^-	
127	—	—	—	—	—	—	I^-
168	—	—	—	—	—	BaO_2^-	—
261	—	—	—	—	—	$Ba(NO_3)_2^-$	—

Cols. 2–5 : observations by Sloane and Watt.
2–3, using demountable system.
4–5, using glass sealed-off tubes.
2, 4, at cathode, 3, 5, at gauze.

Col. 1 : mass-to-charge ratio of ion.
Col. 6 : observations by Schaefer and Walcher.
Col. 7 : observations by Bachman and Carnahan.
Col. 8 : observations by Broadway and Pearce.

* See § 4.

for widely different mass numbers, since the spectra were plotted by varying the accelerating voltage. This means that different ion beams traversed the semi-circular arc to the Faraday cylinder with different energies and consequently possibly suffered different losses. In addition to this the ion optical effects in the source chamber were different. It was not convenient to arrange for good focusing without sacrificing the simplicity of design which appeared essential if the area of bombarded surfaces was to be kept small.

All negative ions detected by the use of the metal mass spectrometer have their identifications, in some cases tentative (see §4), listed in columns 2 and 3 of table 1. Column 1 of the same table gives the mass-to-charge ratios (mass numbers) of these and other ions.

(ii) *Calibration of the mass scale for the metal spectrometer using a Kunsman positive ion source*

The value of M/e for a particular beam can be calculated roughly from the magnetic field, the accelerating voltage V_n and the geometry of the spectrometer; but to obtain a more definite calibration a special Faraday cylinder was used with a Kunsman alkali positive ion source (Tyndall 1938) fitted behind a small opening in its base. When the source was heated, alkali positive ions could be drawn through the opening and accelerated into the deflection chamber through the slits S_3 and S_2. They could then be made to traverse the negative ion path in the reverse direction to S_1, and be detected by measuring the current to the electrode system in the source chamber. This calibration could be effected, without altering the magnetic field, by merely interchanging the source supply leads and the electrometer lead. Any possible errors due to irreproducibility of the magnetic field were thus avoided.

Figure 4 shows the Na^+ calibration peak (a) together with the negative ion peaks (b) for mass numbers 26 from the cathode and 24, 25 and 26 from the gauze, for the particular case of V_1 equal to 100 v., and establishes definitely the M/e scale for the negative ions. This was confirmed by comparing the positions of the two potassium positive ion peaks (mass numbers 39 and 41) with those due to the two chlorine negative ions (mass numbers 35 and 37).

(iii) *Ion spectra : glass sealed-off tube*

A representative spectrum taken with the first glass sealed-off tube is shown in figure 5. In this case the cathode emission was 27 ma. and V_1 100 v. The gauze G_2 was connected to the slit S_1. Using the same method for finding the place of origin of the ions as in the case of the demountable system, the ions listed in columns 4 and 5 of table 1 were identified. In the present case, the mass scale was fixed taking the chlorine isotope of mass 35 as standard, and ions of mass less than 12 were not studied. With V_1 120 v., other conditions being the same, the small peak apparently in region 32 from the cathode became resolved into two; one remained fixed and was therefore due to an ion of mass number 32 from the cathode, whilst the other which moved was due to an ion of mass number 39 from the gauze. It is for this reason that these peaks have been shaded as in figure 5. The diffuse unresolved peak in the region where V_n is approximately 370 v. may be due to ions from the cathode with mass numbers in the range 40 to 60. It does not move as V_1 is changed, but has not been shaded as it may include some ions from the gauze. The same applies to part of the unshaded

background for smaller masses. The diffuse peak will be discussed later (§4). No ions with mass number greater than 81 were observed although they were sought for using higher values of V_n and correspondingly higher values of magnetic field, with appropriately increased magnetic screening of the source chamber S.

Using a suitably small magnetic field, peaks due to hydrogen ions from the cathode and gauze appeared at the values of V_n shown in figure 6. For this spectrum V_1 was 120 v. and the cathode emission was 33·5 ma. These ions have

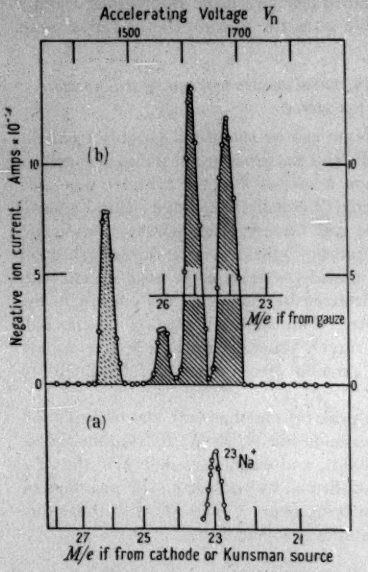

Figure 4. Calibration peaks for metal mass spectrometer. (*a*) Peak due to sodium positive ions from a Kunsman source placed behind the Faraday cylinder. (*b*) Peaks due to negative ions from the cathode and gauze, taken without altering the magnetic field in any way after taking (*a*). The shading of the peaks is the same as in figure 2. $V_1 = 100$ volts.

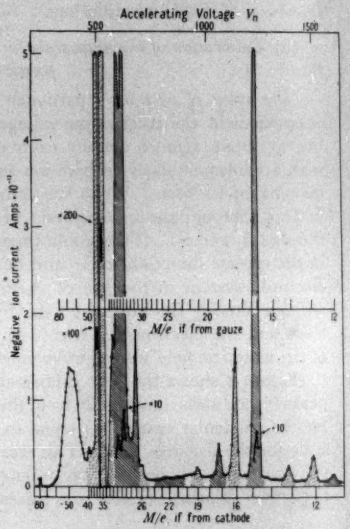

Figure 5. Negative ions mass spectrum taken with the first glass sealed-off tube shown in figure 1. The shading of the peaks is the same as in figure 2. $V_1 = 100$ volts.

been included in columns 4 and 5 of table 1. No ions with mass numbers between 12 and 1 were observed in this instance although it is known that $^6Li^-$ and $^7Li^-$ exist (Sloane and Love 1947).

After prolonged use of this tube a spectrum taken with voltages and magnetic field similar to those used for figure 5 revealed only the chlorine peaks from the cathode in any appreciable intensity, and even they had decreased until 37 showed a peak height of only $2{\cdot}2 \times 10^{-13}$ amp., compared with $1{\cdot}85 \times 10^{-11}$ in figure 5. The only other ions then detected were 16 from the cathode, 32, 35 and 37 from

the gauze, all less than 10^{-14} amp. peak height, and 16 from the gauze with a peak height of about 3×10^{-14} amp. Although the ion peak heights had decreased, the electron emission had increased for the same value of V_1. The decrease in the heights of the peaks from the gauze may have been due either to the tube vacuum having become harder so that the number of residual positive ions available for bombarding the gauze was less, or to the gauze having become thoroughly degassed, since at one stage it was run red hot, or to a combination of these two effects.

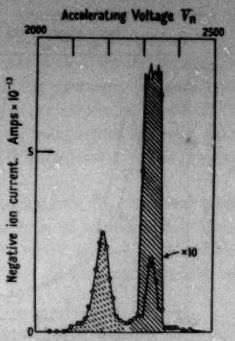

Figure 6. Peaks due to hydrogen atomic negative ions from the cathode (left) and gauze (right) in the first glass sealed-off tube. $V_1 = 120$ volts.

(iv) *Energy distribution*

Arnot and Milligan (1936) found that a negative ion produced from a surface by bombardment with the corresponding positive ion could have an energy in excess of that imparted to it by the accelerating electric fields in the apparatus. Later Sloane and Press (1938), using their double mass spectrometer, showed that a given positive ion could liberate different negative ions and that, in the cases investigated, these also could have excess energies.

In the present work a retarding potential method (Arnot and Milligan 1936, Sloane and Press 1938) was used for studying the energy distribution in the various negative ion beams. Particles of a given kind differing in momentum, due to their leaving their place of origin with a range of initial velocities, could be brought on to the slit S_2 in front of the Faraday cylinder by varying the accelerating voltage V_n. The total number of ions of a given kind approaching the slits, which left the source (cathode or gauze) with more than any particular initial energy V_r, could then be found by holding the Faraday cylinder, and its screening slit S_3, V_r volts negative to the source, whilst V_n was varied so that the whole inherently diffuse beam moved across the slits. Arnot and Milligan, using variation of magnetic field instead of V_n, found that the peak heights of the curves so obtained were proportional to the areas beneath the peaks, and it will again be assumed (Sloane and Press 1938) that this is also true when V_n is varied. The energy distribution curve of the ions is then obtained by first plotting a curve showing peak height against V_r, and then differentiating this with respect to V_r. Representative curves obtained in this way and showing the existence of initial energy, are shown in figures 7, 8, 9 and 10. Figures 7 and 8 were obtained using the demountable system and figures 9 and 10 using the first glass sealed-off tube. These results demonstrate clearly that a relatively large number of ions with mass numbers 16 from the cathode, 26 from the gauze and 1 from the cathode have considerable initial energy, while only a relatively small number of ions of mass number 1 from the gauze have any appreciable initial energy. The distribution curves for the ion of mass number 1 explain the different shapes of the two peaks in figure 6, the tail on the left hand side of the peak from the cathode being due to ions with initial energy. In the same way figure 7 explains the high energy tail to the left of 16 from the cathode in all spectra. Figure 11 shows a retarding potential curve, taken with the demountable

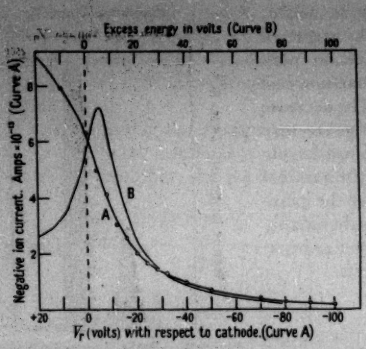

Figure 7. Retarding potential curve (A) and derived energy distribution curve (B) for oxygen (M/e=16) negative ions from the cathode in the metal demountable mass spectrometer. V_1=200 volts, cathode emission =6·2 ma., and V_n=2232 volts (connection to cathode) when V_r was zero.

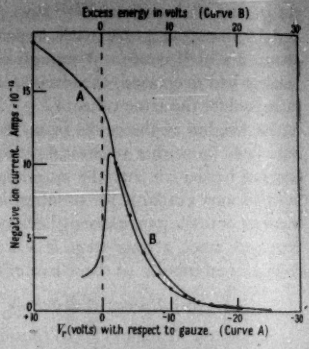

Figure 8. Retarding potential curve (A) and derived energy distribution curve (B) for negative ions with M/e=26 from the gauze in the metal demountable mass spectrometer. V_1=200 volts, cathode emission 10·3 ma., and V_n=1447 volts (connection to gauze) when V_r was zero.

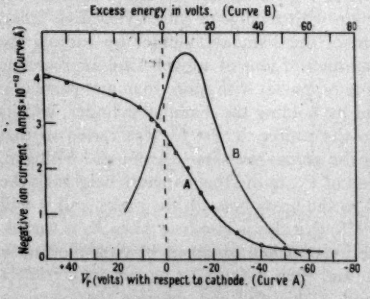

Figure 9. Retarding potential curve (A) and derived energy distribution curve (B) for hydrogen (M/e=1) negative ions from the cathode in the first glass sealed-off tube. V_1=100 volts, second gauze connected to slit, cathode emission 27·8 ma., heater current 1·3 A. (normal), and V_n=2340 volts (connection to cathode) when V_r was 60 volts accelerating.

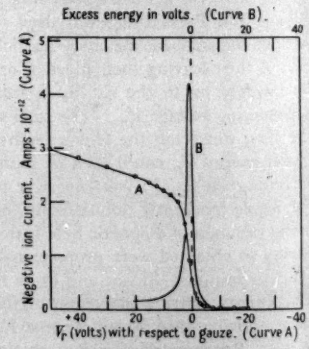

Figure 10. Retarding potential curve (A) and derived energy distribution curve (B) for hydrogen (M/e=1) negative ions from the gauze in the first glass sealed-off tube. Conditions are the same as for figure 9 except that V_n=2365 volts, the connection being made to the gauze.

system, for ions with no measurable initial energy, namely those of mass number 42 from the cathode. The curves for 35 and 37 from the cathode are similar except that they do not show the kink at the upper bend. The origin of the kink is unknown but it is not significant for the present discussion. All three curves fall abruptly when the Faraday cylinder is approximately 2·5 v. positive with

respect to the source, but if there were no contact potential differences and no fall of potential through the oxide coating they would presumably fall at zero volts. This stagger from zero gives a correction factor which should be applied when estimating the initial energies in the case of, for instance, figure 7, but it can frequently be ignored when the initial energies are of the order of 100 v. It should also be taken into account when setting the mass scales for ions from the gauze in all the mass spectra, but this refinement is unnecessary in the present instance.

When taking all these retarding potential measurements V_n was connected between S_1 and the source (cathode or gauze) of the ions of immediate interest, while V_r was applied by connecting a single variable small voltage between the source and the Faraday cylinder. Results obtained for all ions investigated are summarized in table 2.

Table 2. Summary of results for initial energy distribution

Ions from oxide cathode			Ions from tantalum gauze		
M/e	Apparatus	Initial energy	*M/e*	Apparatus	Initial energy
1	Sealed-off	Up to $\lessdot$ 60 v.	1	Sealed-off	Small tail up to $\lessdot$ 10 v.
16	Metal	Up to $\lessdot$ 100 v.	24	Metal	Up to $\lessdot$ 25 v.
			25	Metal	Up to $\lessdot$ 8 v.
26	Metal	Very small ($<$ 4 v.)	26	Metal	Up to $\lessdot$ 25 v.
35	Metal	None			
	Sealed-off	None			
37	Metal	None			
	Sealed-off	None			
42	Metal	None			

Of the other ions from the cathode, those with mass numbers 12, 13, 19, 27, 40, 43, 79 and 81 gave peaks which were too small for satisfactory retarding potential experiments to be performed. The peak due to the ion of mass number 32 from the cathode was not investigated by the retarding potential method, but it can be seen from figure 2 (b) to possess a considerable excess energy tail. In the same way figure 2 shows the ion beams of mass numbers 16, 32, 35 and 37 from the gauze contain large numbers of ions with appreciable excess energies. This is confirmed by figure 5, which also indicates that there are some fast ions of mass numbers 12 and 19. The possession of excess energies by the chlorine isotopes from the gauze explains why the peaks due to these ions

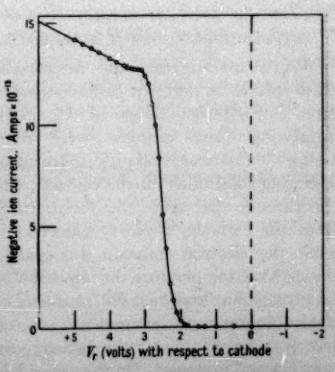

Figure 11. Retarding potential curve for negative ions with M/e=42 from the cathode in the metal demountable mass spectrometer. V_1= 200 volts, cathode emission=1·75 ma., and V_n=850 volts (connection to cathode). This exhibits no excess energies.

are not separated in figure 5, while those from the cathode, showing only an approximately Maxwellian distribution appropriate to the cathode temperature, are resolved.

(v) *Variation of chlorine peak heights with cathode temperature*

Figure 12 shows the rise and fall of the emission of $^{35}Cl^-$ and $^{37}Cl^-$ from the cathode for various cathode temperatures, determined by the heater currents shown. These curves were obtained using the first sealed-off tube after ageing, when the chlorine ions gave the only strong beams. V_1 was 150 v. The points shown are the maxima for each temperature (see next section). The curve relating electron emission and cathode temperature, which is also plotted in the figure, shows that when the heater current was raised above about 1·3 amp. the electron emission became space-charge-limited, although the ionic emission still increased rapidly. The subsidiary maximum and minimum appear to be real, since they repeat as shown. It may be significant that they occur at the points where the electron current becomes space-charge-limited, as they were absent from a similar set of curves taken with the second sealed-off tube under conditions when there was no space-charge limitation. The shoulders on the falling parts of the ionic curves in figure 12 were, however, present on the curves taken with the second tube.

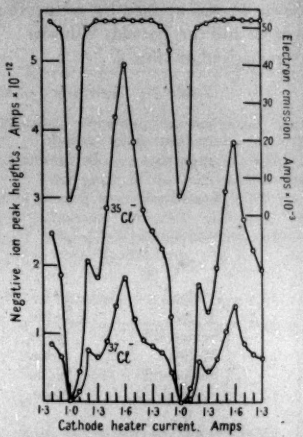
Negative ion peak heights. Amps • 10⁻¹²
Electron emission. Amps • 10⁻⁹
35Cl⁻
37Cl⁻
1·3 1·0 1·3 1·6 1·3 1·0 1·3 1·6 1·3
Cathode heater current. Amps

Figure 12. Variation of chlorine negative ion peak heights and electron emission (top curve) with cathode heater current, and hence cathode temperature. The heater current was lowered to 1·0 A. from its normal value of 1·3 A., raised to 1·6 A., reduced again to 1·0 A., raised again to 1·6 A., and finally reduced to 1·3 A. V_1=150 volts.

(vi) *Time changes in emission after alterations in electric field or cathode temperature*

While investigating the negative ion mass spectra at different cathode temperatures and different values of V_1, certain interesting time changes were noted. Using the first sealed-off tube under normal operating conditions for the cathode, when the cathode had aged, the variations of intensity of the only peaks observed from the cathode, those of chlorine, were investigated. It was found that, while the electron emission was space-charge-limited, on suddenly increasing the cathode temperature the emission of $^{35}Cl^-$ and $^{37}Cl^-$ increased immediately to a maximum and then fell *gradually* to a steady value, but on increasing V_1 the ion emission rose *gradually* to a maximum before falling slowly to an approximately constant value; the falling part of the curve often showed secondary maxima and minima. On the other hand, when V_1 was decreased from 100 to 50 v. the ion current fell immediately and quickly reached a steady value.

Similar time effects were observed with the slightly soft second sealed-off tube. Figure 13 shows the variation of the chlorine peak heights with time on changing V_1 in this tube. At X in this figure, V_1 was raised from 120 to 150 v.,

the electron emission increasing abruptly from 27·5 ma. to 39 ma. At Y, V_1 was raised to 180 v., the electron emission rising to 50 ma. At Z, V_1 was reduced again to 150 v., when the electron emission fell to 39 ma.

Somewhat similar results for the variation of negative ion emission with accelerating voltage have been recorded previously with a $PbCl_2$ source (Zentgraf 1929). It seems probable that the time changes in the emission of $^{35}Cl^-$ and $^{37}Cl^-$ from an oxide coated cathode are connected with electrolytic phenomena in the coating.

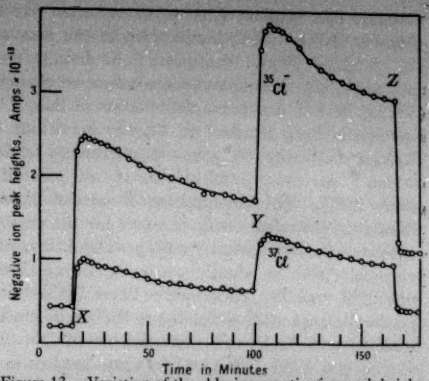

Figure 13. Variation of the chlorine negative ion peak heights with time after changes in V_1 in the slightly soft second sealed-off tube.

(vii) *Time changes in emission after change in cathode surface conditions due to positive ion bombardment*

The variation with surface conditions of the chlorine peak heights from the cathode and of the electron emission, for fixed values of V_1 and cathode temperature, could be studied by making use of the small amount of residual gas present in the second sealed-off tube. When preliminary measurements were being made with this tube it was observed that when the magnetic field was of such a value that large values of V_n were necessary to detect the chlorine ions, the electronic emission gradually decreased with time, while the peak heights of the chlorine ions gradually increased. This is believed to have been due to positive ions formed by electron collision in the residual gas bombarding the cathode and altering its surface. With small values of magnetic field and correspondingly small values of V_n this bombardment effect was negligible. These low values could therefore be used to observe the changes in emission due to recovery of the cathode after it had been bombarded for a long period using high values of V_n.

Repeated observations showed that on reducing V_n from a large to a small value suddenly, leaving V_1 and the cathode temperature unaltered, the chlorine peak heights decreased gradually with time while the electronic emission gradually increased.

§4. DISCUSSION

The ions detected by Bachman and Carnahan (1938), Broadway and Pearce (1939), Schaefer and Walcher (1943) and by us are listed for comparison in table 1. Column 1 of table 1 gives the mass-to-charge ratios (mass numbers) of all ions detected in any of the above investigations; columns 2 and 3 give the ions found by us to originate at the cathode and gauze respectively in the metal apparatus, while columns 4 and 5 list similar results for our sealed-off tubes; columns 6, 7 and 8 give the ions identified by Schaefer and Walcher, Bachman and Carnahan, and Broadway and Pearce respectively. It has been

assumed that negative ions with more than one electronic charge are unstable (Massey 1938). The identification of the ions with mass numbers 1, 12, 16, 19, 32, 35, 37, 79 and 81 appears to be definite, either from their isolation in the spectra (1, 12), their known electronegative character (16, 19), the isotope ratios (35, 37, 79, 81), or from a combination of these. The peak of mass number 32 has usually been ascribed to O_2^-, an ion which has been considered in detail (Bates and Massey 1943), but, as mentioned by Broadway and Pearce, it might be due in part to S^-, and sulphur is still believed to form a stable negative ion (Bates 1947). The identification of most of the others must be more tentative, although a good case could be made for the persistent ion at 26 being CN^-, on account of the electronegative properties of this radicle. $^{27}Al^-$ has been reported previously from an aluminium oxide source (Blewett and Jones 1936), and it is thought that this ion is stable (Bates 1947), but it is not certain that in these spectra the peak at 27 is not due to the ion of some hydrocarbon or other radicle. Schaefer and Walcher's identification of Na^- requires further investigation (Sloane and Love 1947). The same applies to the ion of mass number 39 which has been found using the first sealed-off tube, and has been reported previously by Ditchburn and Arnot (1929) and attributed tentatively to $^{39}K^-$. The identification of the organic negative ions is necessarily very tentative. The two principal ion groups studied with low resolving power by Sloane and Press (1938), where exact identification was of secondary importance, and interest was centred on the process of formation, are seen by comparison with the spectra described in this paper to have been almost certainly composed of ions with mass numbers 24, 25 and 26 in the one case, and 35 and 37 in the other.

Bachman and Carnahan mention that, in the case of a tube sealed-off after breakdown of the cathode, only ions of mass numbers 16, 26, 35 and 37 were observed, while 16 and 26 gradually disappeared. This is in accord with our experience while using the first sealed-off tube when, after considerable use, only 35 and 37 from the cathode could be detected with any appreciable intensity under normal conditions, and it is to be contrasted with the statement by Schaefer and Walcher that after a few hours 35 and 37 disappeared and were undetectable in their tube, although other ions persisted.

Bachman and Carnahan recorded a spot at mass number 42·7 which Bachman considered (private communication) might be complex. Our figure 3, obtained using the metal mass spectrometer, shows, in fact, this region resolved into 42 and 43, although in our apparatus 42 was much more intense than 43. Again, Bachman and Carnahan mention that this spot sometimes became smeared out into a large area. Figure 5 shows that we observed a diffuse peak in the region of 50 before the first sealed-off tube became aged, and a similar peak appeared with the second sealed-off tube. It is possible that this diffuse peak is to be correlated with the smeared-out spot referred to by Bachman and Carnahan, and a spot suspected by Broadway and Pearce at 48. Its origin is not clear.

Some of the spots observed by Bachman and Carnahan and by Broadway and Pearce were sharply focused while others were not. Broadway and Pearce concluded that the sharply focused spots were due to negative ions emitted directly from the cathode, whereas Bachman and Carnahan considered that they were due to ions arising on the cathode surface close to the axis of the electron gun as a result of positive ion bombardment. Our results show that some ions from the cathode, particularly those with mass numbers 35, 37 and 42, show no

excess energy and have apparently an approximately Maxwellian distribution of energy appropriate to the cathode temperature, while 26 shows a diminutive excess energy tail extending only to 4 v. These ions would therefore be expected to give sharply focused spots in cathode-ray tubes with electrostatic focusing; in fact, Bachman and Carnahan remark that 26, 35 and 37 were sharply focused, although Broadway and Pearce found 26 and 42 slightly diffuse. Further, these energy distributions support the view that 35 and 37 are emitted thermionically as a result of electrolytic action in the cathode. Additional support is afforded by our observations on the variations of the heights of the peaks due to the chlorine ions when either V_1 or the cathode temperature is altered (§3(vi)). The ion with mass number 42 may also be emitted by this process and 26 may be mainly so emitted.

There is, however, another possible mode of formation for these two ions. It is known (Broadway and Pearce 1939) that oxide cathodes readily adsorb particles of an electronegative character and, although the surface layer so formed appears to be very stable, some re-evaporation presumably takes place; it is possible that some of the released particles are negatively charged. The CNO^- ions, presumed to be responsible for the peak at mass number 42, are perhaps released by this mechanism. They appeared in our work only in the metal mass spectrometer, which was sealed with grease (unless indeed the broad diffuse peak at 50 in figure 5 is at least partly due to them) and this agrees with the observation by Broadway and Pearce that these ions appeared most strongly in the presence of grease vapours. The CN^- ions with mass number 26 may also be emitted mainly by this re-evaporation process, but the diminutive excess energy tail on their energy distribution curve is probably due to ions liberated by positive ion bombardment, unless it just possibly results from the dissociation of a larger molecule. There does not, however, appear to be any intimate connection between the intensities of 42 and 26 either in the present work or in that of Broadway and Pearce. This slight excess energy would account for Broadway and Pearce's observation of a slightly diffuse spot due to ions with mass number 26, if the bombardment process was enhanced in their tube in the case of this ion.

Both Bachman and Carnahan, and Broadway and Pearce find the O^- spots diffuse. Bachman and Carnahan explain this as being due to a large area of the cathode being bombarded, while Broadway and Pearce think it may be due to the ions concerned being formed by dissociation of O_2 after capture of an electron, or by conversion of oxygen positive ions (Arnot and Milligan 1936). Our retarding potential results for O^- show that this ion from the cathode has a large excess energy tail on the energy distribution curve, with some ions possessing up to 100 v. excess energy. It therefore seems probable that the diffuseness of the spots is due to this large energy spread, since sharply focused spots can result only from beams homogeneous in energy. The H^- ions from the cathode have a somewhat similar energy distribution, and this almost certainly accounts for the diffuseness of the H^- spot also referred to by Broadway and Pearce. We did not examine the peak at mass number 32 by the retarding potential method, but spectrum (b) of figure 2 shows this peak to have the curved low voltage side characteristic of peaks including ions with excess energy. Bachman and Carnahan state that this spot is diffuse. They also say the spot due to 12 is diffuse, but in our case the peak due to 12 was too faint for energy distribution

runs although its shape in the mass spectrum is consistent with its resulting from a beam including some ions with excess energy. Ions liberated from surfaces by positive ion bombardment seem always to be characterized by the possession of large excess energies (Arnot and Milligan 1936, Sloane and Press 1938), and, if this is so, it seems reasonable to conclude that at least a large part of each of 32, 16, 12 and 1 from the cathode is due to this process.

The observation by Becker (1929) and Detels (1927) that most of the oxygen emitted when space current is drawn is uncharged, although some ions are emitted, is consistent with the above conclusion if we envisage the oxygen flux as maintaining a surface layer which is then "sputtered" off (Sloane and Press 1938) as negative ions by the positive ion bombardment.

The oxygen peaks, among others, disappeared as our first sealed-off tube became aged, but when V_1 was increased and a large electron current was drawn from the aged cathode, 16 reappeared strongly. This result is in agreement with Becker's (1929) observation that oxygen can only be released from a well aged cathode by drawing a strong electron current. Schaefer and Walcher (1943) recorded O_2^- but not O^-. Barton (1925) also reported this phenomenon in the case of well formed and aged cathodes. However, his resolution was not high and our experience with the first sealed-off tube when aged gives experimental support to the suggestion by Broadway and Pearce that the ion observed by Barton may in fact have been chlorine. Blewett and Jones (1936) also detected O_2^- from a barium oxide emitter, but under conditions when chlorine contamination was certainly present.

Bachman and Carnahan (1938) mentioned that some spots were surrounded by small circles, in particular those due to mass numbers 26, 35 and 37, and that the circles might be "evidence furthering the theory of a gas source other than the cathode". Later Sloane and Cathcart (1939) pointed out that these circles might be due to bombardment of a gun aperture by positive ions and just possibly by negative ions from the cathode. The latter process was suspected by Sloane and Cathcart because in their early work the absence of ions with excess energy in the 26, 35 and 37 beams from the cathode was taken to show that the cathode was not bombarded by positive ions. In the apparent absence of positive ion bombardment Sloane and Cathcart were driven to the conclusion that the ions detected from the gauze were liberated under negative ion bombardment. Shortly afterwards however, they detected the excess energy tail on 16 from the cathode so that it appeared probable that positive ion bombardment played an important, if not the only, rôle. In a subsequent paper, Bachman (1940) pointed out that the bombarded aperture was the so-called grid and that it was at a potential negative to the cathode, so that negative ions would pass it by in favour of the first anode. He then proceeded to give a detailed explanation of the formation of the observed ring structure. In particular, he attributed the diffuseness of the rings to bombardment of the upper and inner sides of the aperture, in addition to the sharp aperture edge, by unfocused positive ions formed in the gas in the region between the grid and the first anode. Since the intensity distributions on proceeding radially through the ring patterns on the screen varied widely from ring to ring in a given spectrum it appears to us that the diffuseness is more likely to be due to the excess energies observed by us for all ions from the gauze which could be examined, as we have found that the energy distribution curves vary markedly from ion to ion. Bachman

also found that some rings showed a focused spot in the radially outermost section, while others did not. These spots he explained as being due to negative ions liberated from the aperture as a result of bombardment by a focused positive ion beam originating in the gas in the region between the first and second anodes. The appearance of these spots on some rings and not on others he explained by assuming that certain positive ions, present in the unfocused grid–first anode swarm responsible for the ring, were absent from the focused first anode–second anode beam. This explanation if correct makes his observations very interesting in that, while it is certain that bombardment of a contaminated surface by a given positive ion can give a whole spectrum of negative ions (Sloane and Press 1938), Bachman's observations support the view that this spectrum depends to some extent on the type of positive ion bombarding the surface.

Schaefer and Walcher (1943) list ions of mass numbers 24 and 25 from their oxide coated cathode, but since their cathode and the neighbouring grid were at the same potential they could not distinguish between these two electrodes as possible sources of ions. Our results suggest that 24 and 25 detected by them really arose from positive ion bombardment of the grid. We have never observed 24 or 25 from an oxide coated cathode, in agreement with Bachman (private communication). Schaefer and Walcher state that all peaks were sharp and mention that an energy spread of ± 10 v. at M/e 25 would have produced noticeable broadening. This is not compatible with our results.

Figure 12 shows that as the cathode temperature is increased, while V_1 is held constant, the chlorine ion current continues to increase rapidly with cathode temperature even after the electronic emission has become space-charge-limited. Schaefer and Walcher (1943) found a similar effect while investigating the dependence on cathode temperature of the emission of the ion ascribed to O_2^-, in the case of a formed cathode. The curves in figure 7 (*b*) of their paper show exactly the same trend as do those of our figure 12 when the heater current, and hence the cathode temperature, is increasing. It will be noticed that in our case, although the electron emission reaches the same values on the repeated cycle of heating and cooling, the chlorine ionic emission appears to be falling progressively. These facts might be interpreted as indicating that the electron and ionic emissions are not intimately connected, but Liebmann (1946 a, b) has shown that the electron optical emission picture of the thermionic cathode on the cathode-ray screen is reproduced in negative quite faithfully, except for a few details, by the ion burn; a fact which he apparently rightly interprets as indicating that the *local* electron current density at the cathode surface and the rate of negative ion production are in most cases closely correlated.

The results described in § 3 (vii) show that bombardment of the cathode by positive ions reduces the electronic emission, which subsequently recovers when the bombardment ceases. This effect was also observed by Schaefer and Walcher, using hydrocarbon positive ions for bombardment. They also found that the CH^- ion beam, the only one investigated by them in this connection, was not increased by the bombardment, but our results show definitely that bombardment increases the intensity of the chlorine ion beams, and that these decrease again when the bombardment is discontinued.

Throughout most of this discussion it has been assumed that the surface production of negative ions is due to one of two causes; either they are evaporated thermionically or they are sputtered off by bombardment with positive ions.

In the former case the energy distribution of the emitted ions will be thermal with a temperature that of the surface. In the latter case the energies are distributed over a very much wider range, the exact dependence of which on the masses of the bombarding and emitted ions, and on the energy of the bombarding ions, will be discussed in detail elsewhere. With both types of emission the question as to how the surface film is formed has been left practically open in this work. This question involves two distinct problems : the one that of migration of material to a surface from the interior of a solid, and the other that of the conditions of deposition of a surface film from low pressure gas. Both lie outside the scope of this investigation, but whatever mechanisms are ultimately found to explain these will require to be in accord with the results which have been obtained by us. It has also to be remembered that the study of negative ions as a whole, unlike that of positive ions, has still progressed comparatively little (Massey 1938, Bates and Massey 1943, Bates 1947), and that it may be found that processes other than these two may play a not unimportant part, as is in fact implied in Broadway and Pearce's discussion.

ACKNOWLEDGMENTS

The authors wish to thank Dr. Eliza B. Cathcart for assistance while taking observations during the early part of this work. They also wish to thank Professor K. G. Emeléus for continued interest, and are greatly indebted to the late Sir Clifford Paterson, F.R.S., Director of the Research Laboratories of the General Electric Company Ltd., for kindly providing the oxide coated cathodes used in all the experiments.

REFERENCES

VON ARDENNE, M., 1935, *Arch. Electrotech.*, **29**, 731.
ARNOT, F. L., 1937 a, *Proc. Roy. Soc.* A, **158**, 137 ; 1937 b, *Ibid.*, **158**, 157.
ARNOT, F. L., and BECKETT, C., 1938 a, *Nature, Lond.*, **141**, 1011 ; 1938 b, *Proc. Roy. Soc.* A, **168**, 103.
ARNOT, F. L., and MILLIGAN, J. C., 1936, *Proc. Roy. Soc.* A, **156**, 538.
BACHMAN, C. H., 1940, *J. Appl. Phys.*, **11**, 83 ; 1945, *Gen. Elect. Rev.*, **48**, 13.
BACHMAN, C. H., and CARNAHAN, C. W., 1938, *Proc. Inst. Radio Engrs.*, **26**, 529.
BARTON, H. A., 1925, *Phys. Rev.*, **26**, 360.
BATES, D. R., 1947, *Proc. Roy. Irish Acad.*, **51**, 151.
BATES, D. R., and MASSEY, H. S. W., 1943, *Philos. Trans. Roy. Soc.*, **239**, 269.
BECKER, J. D., 1929, *Phys. Rev.*, **34**, 1323.
BLEWETT, J. P., and JONES, E. J., 1936, *Phys. Rev.*, **50**, 464.
BROADWAY, L. F., and PEARCE, A. F., 1939, *Proc. Phys. Soc.*, **51**, 335.
DETELS, F., 1927, *Jb. drahtl. Telegr.*, **30**, 10.
DITCHBURN, R. W., and ARNOT, F. L., 1929, *Proc. Roy. Soc.* A, **123**, 516.
LEVY, L., and WEST, D. W., 1936, *J. Instn. Elect. Engrs.*, **79**, 11.
LIEBMANN, G., 1946 a, *Nature, Lond.*, **157**, 228 ; 1946 b, *Electronic Engng.*, **18**, 289.
MASSEY, H. S. W., 1938, *Negative Ions* (Cambridge : University Press).
SCHAEFER, H., and WALCHER, W., 1943, *Z. Phys.*, **121**, 679.
SHARPE, J., 1946, *Electronic Engng.*, **18**, 385.
SLOANE, R. H., and CATHCART, E. B., 1939, *Nature, Lond.*, **143**, 474.
SLOANE, R. H., and LOVE, H. M., 1947, *Nature, Lond.*, **159**, 302.
SLOANE, R. H., and PRESS, R., 1938 a, *Nature, Lond.*, **141**, 872 ; 1938 b, *Proc. Roy. Soc.* A, **168**, 284.
TYNDALL, A. M., 1938, *Mobility of Positive Ions in Gases* (Cambridge Phys. Tracts).
ZENTGRAF, M., 1929, *Ann. Phys., Lpz.*, **2**, 313.

Some New Aspects of High-Speed Oscillography

By D. M. MACKAY

Wheatstone Physics Laboratory, University of London, King's College

ABSTRACT. From a consideration of the mechanism of the cathode-ray oscillograph at very high speeds it is shown, in Part I, that conventional deflection systems do not fully realize the possibilities of the cathode-ray tube.

By a modification of the shape of the deflector-plates it is theoretically possible, under suitable conditions, to expand the time-scale obtainable with a given time-base generator up to infinity. This gain is obtained at the expense of definition, but brightness is not affected. Relativistic considerations are shown to be irrelevant.

The geometry of the deflected electron beam is examined, and an expression derived relating the shape of the effective time-base voltage wave-form, the time-scale, and the shape of the Y-plates.

Part II examines some practical factors ignored in the analysis of Part I. These cause various forms of trace distortion, which are classified as (i) intermodulation effects, (ii) mismatching distortion, (iii) transit-time effects, (iv) defocusing and equivalent effects.

Possible ways of overcoming a number of these difficulties are described. Some have already been employed with success, but others have not yet been followed up.

PART I: THE IDEAL CASE

§1. INTRODUCTION

THE upper limit to the attainable speed of a cathode-ray oscillograph is normally set by a combination of practical factors such as trace brightness, and theoretical limitations fundamentally inherent and insurmountable. It is characteristic of modern physics that the distinction between these two categories is rapidly disappearing, as analysis reveals the interrelation of their ultimate causes.

In the field of high-speed oscillography, however, it is still possible to draw a fairly well defined dividing line, and to consider separately the ideal case and the practical factors modifying it. The object of Part I is to examine the mechanism of the ideal cathode-ray oscillograph at high speeds, and to suggest a possible method of increasing the time-scale factor, theoretically up to infinity, without a corresponding increase in time-base voltage-gradient. Contrary to popular belief, it is shown that relativistic considerations set no limitation on writing speed, and that at high speeds the latter need not have any connection with the time-scale factor.

In Part II it is intended to examine some of the practical limitations of the technique, and to suggest some methods of at least partially overcoming them.

§2. THE NATURE OF THE DEFLECTED BEAM

Figure 1 represents part of a typical electrostatic deflection system in an "ideal" C.R. tube. A stream of electrons, assumed to have negligible cross-sectional area, moves in the direction OA with velocity v_t, and passes through a deflecting field E between two plates X_1, X_2, of negligible axial dimensions.

Figure 1.

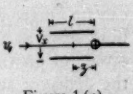

Figure 1 (*a*).

The electrons receive a transverse velocity v_t due to E, and travel at an angle θ to OA to strike a plane screen AB, normal to OA, at a point B whose distance from the axis is x'.

It is evident that if the distance OA be D,

$$x'/D = \tan\theta = v_t/v_f. \qquad \ldots\ldots(1)$$

Thus if v_f is constant,

(a) *The transverse velocity v_t of an electron producing a spot of light at a distance x' from the origin A is determined only by that distance*, i.e. in other words, the maximum electron velocity which has to be attained under given conditions of gun voltage etc. is a function only of trace *length*, and is independent of writing *speed*.

Differentiating equation (1), we have $dx'/dt = (D/v_f)(dv_t/dt)$, so that, under the same conditions,

(b) *The speed of the spot of light is determined by the rate of change of the transverse velocity imparted to successive electrons by the deflecting field.* This means that relativistic considerations do not affect the problem any more at high writing speeds than they do in the case of a steady deflection of the spot; the limit to writing speed, in the conventional oscillograph,* is set only by the available transverse acceleration.

What happens to the electron beam, then, when the writing speed approaches that of light? Evidently if the time taken for the spot to traverse the screen is short compared with the transit time from plates to screen, the stream of electrons producing the trace AB must form an expanding "kink" (as shown at A'B' in figure 2), travelling towards the screen with an axial velocity v_f. When the leading edge of this kink reaches the screen, a spot of light will be formed at the point of intersection, which will travel rapidly along the line AB with velocity $v_s = v_f \cot\phi + v_t$, or $v_s \simeq v_f \cot\phi$, where ϕ is the angle between screen and kink at the point of intersection (figure 2 (*a*)).

This physical picture suggests an interesting possibility: if the screen, instead of being normal to the tube axis, were inclined to it in such a way as to reduce ϕ, then v_s could be increased to any desired value up to infinity, without any increase in the transverse acceleration of the electron stream.

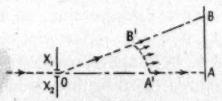

Figure 2.

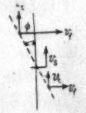

Figure 2 (*a*).

That such an arrangement could give an infinite writing speed is undeniable. But unfortunately—apart from the geometrical distortion of the picture which would occur at any speed—the tilting of the screen, and the increased writing speed caused by it, would have no visible effect on the picture, least of all on its "time-scale factor" (§ 3), for the spatial configuration of the electron stream is determined once the electrons have left the deflecting system, and the only effect of inclining the screen is to alter the speed of *delineation* of a picture whose time-scale is already fixed.

Evidently, in connection with high-speed oscillography, the electron stream can no longer be regarded as a beam or pointer pivoted at the deflector system, but rather as a formation of electrons setting out to delineate a picture on the screen or photographic plate. The course of each electron is predetermined by the deflector system, and the instant at which it strikes the screen is relatively

* Throughout this paper the term "oscillograph" will be used for convenience to cover both visual and photographic delineators of wave-form.

unimportant. The electrons can even arrive in reverse order, so that the spot of light travels in the negative direction of the time-scale (if ϕ is negative), without in any way affecting the appearance of the trace.

§ 3. THE TIME-SCALE FACTOR

The classification of the numerous terms used to describe the "speed" of an oscillograph—time-base speed, scan speed, sweep speed, writing speed, trace speed etc.—is by no means easy, since their connotation varies with different authors and different contexts. It seems clear, however, that there are already too many terms, and it is therefore with some trepidation that one ventures to suggest yet another, to represent a quantity which is not unambiguously defined by any of the above, but which is a parameter of fundamental interest to the user of an oscillograph.

An oscillograph with electrostatic deflection may be regarded as a device with two terminals between which a voltage $v_{\text{in}}=f(t)$ is applied (figure 3). It

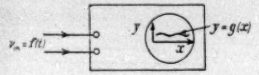

Figure 3.

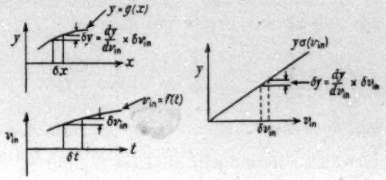

Figure 4.

produces on a screen a graph with the equation $y=g(x)$, where y is a function $\sigma(v_{\text{in}})$ of v_{in}, generally of the form

$$y=av_{\text{in}}+b. \qquad \ldots\ldots(2)$$

The fundamental criterion of speed, which we shall refer to as the *time-scale factor* S, may be defined formally as the ratio of the interval δx between two adjacent ordinates y and $(y+\delta y)$ on the screen, to the interval δt between the two corresponding values of the input voltage, v_{in} and $(v_{\text{in}}+\delta v_{\text{in}})$ (figure 4). In the limit, we may write

$$S=(dx/dy)(dy/dv_{\text{in}})(dv_{\text{in}}/dt). \qquad \ldots\ldots(3)$$

This quantity is the factor by which the X-scale must be multiplied to give the time-scale; it is that normally implied when one speaks of an oscillograph as having a writing speed of so many centimetres per microsecond.

It should be noted that S, as defined, has no relation to the speed of the spot delineating the wave-form. S is obtained theoretically by comparing corresponding intervals dx and dt on the two graphs, but dx/dt cannot be measured directly, since x as defined is not an explicit function of t, and is *not* the abscissa of the delineating spot. Accordingly equation (3) defines S in terms of three pairs of related quantities, the slopes of the x–y, y–v_{in} and v_{in}–t graphs, which can be measured. Writing $dy/dx=g'(x)$, $dy/dv_{\text{in}}=\sigma'(v_{\text{in}})$, $dv_{\text{in}}/dt=f'(t)$, we have

$$S=\sigma'(v_{\text{in}})f'(t)/g'(x). \qquad \ldots\ldots(4)$$

If equation (2) holds, $\sigma'=a$, and $S=af'(t)/g'(x)$.

In conventional low-speed oscillographs it is unnecessary to distinguish between this time-scale factor and the X-component of the writing speed, but in high-speed oscillographs the two quantities may differ considerably in magnitude, and even in sign (see also § 5).

§ 4. Y-DEFLECTION

We have seen that an increased writing-speed need not imply an expanded time-scale. It will now be shown that at high speeds a simple relation exists between the shape of the Y-deflection system and the time-scale factor, as a result of which, conversely, a great expansion of time-scale may be obtained without any corresponding increase in writing speed (Mackay 1946 a).

The simplified arrangement shown in figures 1 and 2 does not include any means of deflecting the electron stream in the Y-direction—i.e. out of the plane of the diagram. In this paper we shall consider only electrostatic deflection systems for this purpose, and figure 5 illustrates the conventional arrangement,

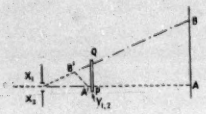

Figure 5.

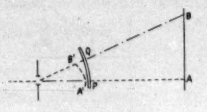

Figure 6.

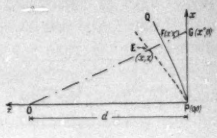

Figure 7.

in which a second pair of plates, Y_1 and Y_2, is used to produce a deflecting field at right angles to the tube axis and to the direction of the X-deflection. The axial dimension of the Y-plates is assumed negligibly small, so that the Y-deflection of a given electron may be regarded as taking place when that electron traverses the line PQ representing the locus of the deflecting field. For convenience the trace is assumed to start at the centre of the screen.

In the case of high-speed deflection considered (figure 5), the electron at A′ which is due to produce a spot of light at A receives its Y-deflection at the point P where A′A intersects the Y-plates; and the electron at B′, similarly, receives its deflection at Q. *The interval of time portrayed on the screen between* A *and* B *is therefore the interval between the instants of intersection of electrons* A′ *and* B′ *with the deflecting field.**

In other words, the important quantity is the transverse speed of the point of intersection of the electron stream with the line PQ.

If now we apply the "inclined approach" technique to the Y-plates, we have in this case the theoretical possibility of attaining an infinite time-scale factor. All that is necessary is to reduce the interval of time between the instants of intersection of A′ and B′ with the deflecting field. This can be done by bending the line PQ towards A′B′, as shown in figure 6, so that Q comes to meet B′, and the velocity of the point of intersection of A′B′ with PQ is increased in the same way as the writing speed in the previous case, *and without any corresponding decrease in trace brightness.*

We have thus increased S (equation (4)) by reducing $g'(x)$, since $g'(x)$ tends to zero as the shape of the kink approaches that for which all electrons receive the same Y-deflection. Alternatively, one may say that the time-scale of the *phenomenon*, as "seen" by the electron stream, has been *contracted.*

* Subject to the conditions of § 5.

§5. THE EXPANDED TIME-SCALE FACTOR

To derive the relation holding between the shape of the plates, the time-base voltage wave-form, and the resulting time-scale factor S, it is convenient to refer the X-deflection of the spot to a plane normal to the Y-axis and passing through P (figure 7), and to take P as origin of an (x, z) coordinate system with the positive direction of the z-axis to the left of P.

The incident electron stream moving from left to right with a constant z-axial component of velocity v_f is represented by EP, where E (x, z) is a typical electron, whose path intersects PQ at F (x', z') and the x-axis at G (x'', O). All electrons are assumed to receive x-deflection at the point O on the z-axis, the distance OP being d.

The time interval represented by the distance PG (x''), or its projection on the screen, will be the time taken by an electron to travel from E to F, *less* the time taken for the signal to travel along the Y-plates from P to Q (or the difference in times of arrival of the signal at P and Q). For any given value of v_f and arrangement of Y-plates, the latter time correction can be allowed for as a z-correction in the equation for PQ. We shall henceforth assume that the equation of PQ,

$$z' = \Psi(x') \qquad \ldots\ldots(5)$$

represents this "effective locus" of the Y-deflecting field.

With this assumption, we can state that the time interval T corresponding to PG is given by $T = (z - z')/v_f$, so that the time-scale factor

$$S = dx''/dT = v_f\, dx''/d(z - z'). \qquad \ldots\ldots(6)$$

The writing speed, on the other hand, is simply $v_f\, dx''/dz$.

The time-base (X-deflecting) field at O has been responsible for imparting different transverse velocities v_x to successive electrons passing through it, and each value of v_x thus fixed determines a corresponding value of x'', since $x''/d = v_x/v_f$. We can therefore express the action of this field in terms of x'' and time, or (since the time t between the passage of the electron at P and that at E through the X-field is $t = z/v_f$) in terms of x'' and z.

Thus instead of defining the X-deflection by the equation $v_x = V(t)$, we may write $x'' v_f/d = V(z/v_f)$ or, with z in terms of x'',

$$z = v_f V^{-1}(x'' v_f/d), \qquad \ldots\ldots(7)$$

where V^{-1} is the reciprocal operator to V.

We shall find it convenient to rewrite equation (7) as

$$z/v_f = U(x''). \qquad \ldots\ldots(8)$$

The equation of PQ, (5), may also be written in terms of x'', for

$$x' = x''(1 - z'/d), \qquad \ldots\ldots(9)$$

so that $z' = \Psi[x''(1 - z'/d)]$, which we may write as

$$z'/v_f = \Phi(x''). \qquad \ldots\ldots(10)$$

Hence the interval T corresponding to x'' is given by

$$T(x'') = U(x'') - \Phi(x''). \qquad \ldots\ldots(11)$$

This simple relation makes it possible, for a given plate shape, to derive the graph of x'' against T (the slope of which is S) merely by subtracting two ordinates.

provided that the X-deflecting wave-form is known. Alternatively the shape of plates required to give any characteristic can be derived directly from the given U and T curves (figure 8).

Equation (5) can conveniently be expressed in terms of the above functions, since

$$\frac{1}{S}=\frac{dT}{dx''}=\frac{1}{v_f}\frac{dz}{dx''}-\frac{1}{v_f}\frac{dz'}{dx''}$$

or

$$1/S=\dot{T}'=U'-\Phi' \text{ *}.$$

A particular case of some interest arises when a linear time-base generator is required to produce a linear time-scale, expanded by the technique described.

In this case $T(x'')$ and $U(x'')$ are both proportional to x'', so that from (11), $\Phi(x'')=U-T=kx''$. Now $z'=v_f\Phi=v_f kx''$ (from (10)), or from (9),

$$z'(d-z')=dv_f kx';$$

PQ therefore must form an arc of a parabola symmetrical about the line $z=d/2$.

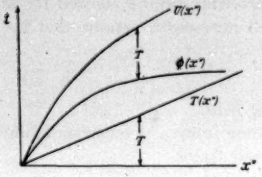

Figure 8.

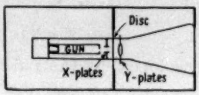

Figure 9.

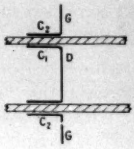

Figure 10.

The fact that Y-deflection does not take place at a constant distance from the screen implies that the Y-sensitivity will tend to vary as a function of X-deflection. This can be corrected for in the design of the plates, and should be borne in mind in relation to the second part of this paper.

§ 6. CONCLUSION

In this Part we have been concerned only with theoretical consideration of the ideal case in which many simplifying assumptions have been made. It is intended in Part II to discuss some of the practical limitations of this method of time-scale expansion. It is important, however, to note that even in the ideal case the technique is useful only when the time of rise of the deflecting voltage is already fairly short, since the complete kink A′B′ must occupy only a fraction of the distance between plates and screen.

Assuming a value for v_f of 3×10^9 cm/sec., this means that if the kink is to occupy not more than, say, 10 cm. in the axial direction, it must be formed in less than $10/(3\times10^9)$ sec., or about $1/300\,\mu$sec. Thus the technique requires initially a really high-speed time-base generator, such as a hydrogen thyratron circuit, in order to be effective.

The author has obtained a time-scale factor exceeding the speed of light with the aid of such a circuit, and a normal deflector system. In this case the kink must have been formed in less than $1/1000\,\mu$sec., so that a time of $1/300\,\mu$sec. is evidently quite attainable with present-day components. Once it is attained

* This equation deals with reciprocals of speed, for which no term appears as yet to have been coined, despite the large number of problems which would be simplified by its use. (Cf. use of " conductance " in resistance problems.)

the technique described enables the time-scale to be expanded, theoretically up to infinity if required, without further increase in time-base voltage-gradient.

PART II: PRACTICAL LIMITATIONS

§ 1. INTRODUCTION

In the analysis given in Part I, several simplifying assumptions were made. Some of these will not be discussed in detail here: it will be assumed, for example, that the trace produced will be of sufficient intensity to be detected, and that synchronism can be maintained between the time-base generator and the phenomenon under investigation. The first of these requirements is somewhat eased if the phenomenon is repetitive in character (e.g. the R.F. wave-form of a pulsed magnetron). The second is perhaps rendered more stringent in the latter case, although it will often be possible to extract a suitable time-base voltage from the driving circuit.

Our present interest, however, is to consider the ways in which the deflection mechanism of the cathode-ray tube itself differs in practice from the ideal case. We shall also examine some possibilities which suggest themselves as offering at least partial solutions to the practical problems raised.

Four principal factors restrict the usefulness of the conventional cathode-ray tube deflection mechanism at high speeds. These are:

(*a*) "Intermodulation" between signal- and time-base plates, introducing distortion of the time-scale. (*b*) Mismatching of the signal circuit by the Y-deflection system, introducing wave-form distortion. (*c*) Transit-time effects, causing distortion of the frequency-characteristic of the Y-deflection system, and hence of any non-sinusoidal wave-form being examined. The linearity of the time-scale may also be affected. (*d*) Positional uncertainty caused by the finite cross-section of the beam at the deflection system. This produces an effect equivalent to defocusing. These will now be considered in turn.

§ 2. INTERMODULATION

Intermodulation or "cross-talk" between X- and Y-plates is caused chiefly by direct capacitive pick-up of the unwanted signal by the plates concerned. In its most troublesome form the higher-frequency components of the Y-signal find their way to the X-plates and may even cause loops in the trace. In this case, other things being equal, the effect is most serious at low time-base speeds, so that, for a given value of inter-X-plate impedance, the problem is eased by increasing the time-base voltage gradient. Clearly, since the stray capacitance and the inter-X-plate impedance form a potential divider, it is an advantage to employ a time-base generator with as low an output impedance as possible.

At very high frequencies, however, the inductance of the leads to the X-plates sets a lower limit to the inter-plate impedance, and it becomes essential to employ thorough screening to minimize X-Y-plate stray capacitance. Although the use of such screens is fairly common, the earthing arrangements require special care at high frequencies, as a shield earthed via a high-inductance lead forms an excellent coupling device.

Two forms of shield construction have been used in the course of work on a high-speed oscilloscope for the investigation of current build-up in radar modulator valves (Mackay 1946 b). In both, a metal disc, slotted to permit

passage of the electron stream, was employed as a shield between X- and Y-plates. In one form of tube * the disc was made larger than the diameter of the tube neck, a copper–glass seal being employed, so that a continuous metallic shield could be arranged to enclose completely the portion of the tube containing the Y-plates and screen (figure 9).

The shielding obtained in this way was most satisfactory, but the production of a tube with a large glass–metal seal is not an easy problem. The second form of tube † employed was designed to obviate this. The slotted disc D (figure 10) had a diameter just less than that of the tube neck, and was fitted with a cylindrical collar C_1 of the same diameter. Outside the neck, an earthed "guard-ring" G coplanar with the disc formed a virtual extension of it, and was fitted with a second collar, corresponding in position to the first, and so acting as a capacitive by-pass of the earth lead from the disc. The latter was brought out to a thimble cap just behind the guard-ring.

In the same oscilloscope, the shielding provided by this tube also proved completely satisfactory up to the highest test frequency (600 Mc/s.) used.

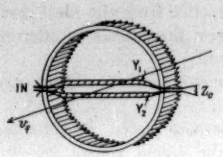

Figure 11.

Figure 12.

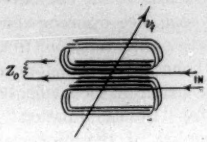

Figure 13.

Unfortunately work on the project was interrupted by the author's release from Admiralty service before tests at higher frequencies could be undertaken, but there seems no reason to doubt that this method of shielding could be satisfactory at frequencies several times higher than those used. The hard-valve time-base generator employed in these tests had an effective output capacitance of the order of 15 pF.

§3. MISMATCHING DISTORTION

In general the impedance presented by a deflector-plate system is capacitive, and since it is normally connected to the signal source via a cable with resistive or complex impedance, considerable distortion of the monitored wave-form can take place at high frequencies. Reflection of the signal can also introduce serious effects.

In an effort to overcome this difficulty, special Y-plate systems were incorporated in the tubes referred to in §2. They were designed as sections of parallel-tape transmission line of the same impedance as the coupling cable, and leads were brought out from each side of the tube neck, so that the signal could travel *through* the deflector system to a second cable or a suitable resistive termination at the other side (figure 11). (A similar scheme has been developed independently in U.S.A. (Rudenberg 1945), with parallel wires as deflectors.) Apart from the small reflections occurring at discontinuities in impedance at the glass seals, such techniques can virtually eliminate loading effects.

* Produced in the research laboratories of Messrs. A. C. Cossor.
† Produced in E.M.I. Research Laboratories.

§4. TRANSIT-TIME

The effect of transit-time on X-deflection is discussed briefly in an Appendix. Its most serious result is the modification of the form of the functions V and U (Part I), particularly just as the deflecting voltage begins to rise. At this instant a number of electrons, already part-way through the field before the change took place, will emerge with disproportionately low values of v_x. This has the same effect as a rounding of the leading edge of the time-base wave-form. Since distortion of this type can be allowed for in the design of the Y-plates, as described in Part I, it does not represent a fundamental limiting factor.

In the case of the Y-plates, however, transit-time is of vital importance. A limit is placed on their effective narrowness not only by considerations of sensitivity and impedance (which are directly related quantities), but also by the edge effects which occur between narrow tapes. These effects can be reduced by a decrease in the plate separation, but unless micro-oscillographic technique (von Ardenne 1938, Hollmann 1940, Lee 1946) be adopted, the thickness of the electron beam normally restricts the usefulness of such a decrease. The use of a magnetic lens system, arranged to bring the beam to a subsidiary "cross-over" at the Y-plates, might however be of some assistance in reducing the permissible plate separation.

A suggestion for extending considerably the upper-frequency response of a deflector system has been put forward recently (Mackay 1946 a), and is illustrated in figure 12. Essentially the method proposed is to divide each Y-plate into a series of segments, each fed from the preceding one by way of a loop of conductor such that the signal takes the same time as an electron to travel from segment to segment. Thus each electron encounters the signal several times in succession, always in the correct phase, and receives cumulative deflections. In fact the arrangement is equivalent to a "travelling-wave" system with a velocity equal to that of the electron stream. Since v_t is normally of the order of $\mathbf{c}/10$, it is necessary only to arrange that the signal path is about ten times the axial separation between successive segments. The "plates" might conveniently take the form of two distorted helices of D-shaped cross-section (figure 13), with earthed shields (not shown) so arranged as to maintain over the outer portions of the D's an impedance approximately equal to the characteristic impedance presented by the inner portions to the signal which is applied "in push-pull" to the input leads. The ends of the helices nearest to the screen are terminated in a suitable resistance, or may be connected to an output cable if required.

It is evident from Part I (§5) that an expansion of time-scale would be achieved if we could reduce the velocity of the signal along the path PQ (figure 7). It is possible in theory to do this by using a helically-wound conductor in place of each Y "plate" or wire, but this would tend to introduce slight irregularities in the sensitivity to Y-deflection, as a function of X-deflection.

§5. BEAM CROSS-SECTION

The cross-sectional dimensions of the stream of electrons (apart from their importance in defining the minimum plate separation) introduce a further limiting factor when the inclined-plate technique is used to increase the time-scale factor. This is best seen by reference to figure 14, in which AA'B' represents a magnified portion of the electron stream after X-deflection. The undeflected beam A'A

has a width a in the x, z plane, and since X-deflection is analogous to a shearing action, a typical cross-section LM of the kink A′B′, normal to the tube axis, will also have a width a.

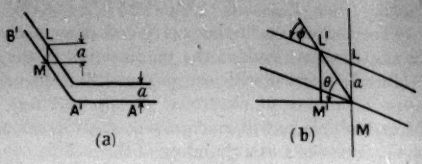

Figure 14.

Thus if conventional Y-plates of negligible axial length were employed, the width of the group of electrons LM receiving simultaneous deflections would be just a. If, however, the Y-plates are inclined at an angle θ to the tube axis, it is clear from figure 14 (b) that the effective width L′M of the electron stream is increased to $a\cos(\theta-\phi)/\sin\phi$, where ϕ is the angle between the plates and the kink. Consequently in this case the picture on the screen will show a defocusing effect as if the spot were elongated in the X-direction, although it may appear perfectly circular when at rest. Assuming that the cross-sectional area of the beam is fixed by other considerations, it might be best in such a case to make a as small as possible, at the expense of the width in the Y-direction, so that the spot is normally elliptical. (This width a is that of the beam before it has been brought to a focus. The spot size is normally much smaller.)

Since in fact the Y-field will have a finite width in the axial direction, this must further increase the width of beam simultaneously receiving a given deflection. Indeed it may well prove that this problem is the chief obstacle to the realization of the full possibilities of any inclined-plate method of time-scale expansion. Factors of the order of $\times 10$ might, however, be usefully attainable with present-day tubes having beam-widths of the order of 2–3 mm. Further improvement may be possible with suitable tube design.

§6. BRIGHTNESS

We have hitherto ignored the question of trace brightness as outside the scope of this paper. It has been mentioned however (Part I, §4) that the suggested method of scale expansion does not affect the brightness of the trace. The trace on the expanded time-scale is delineated by the same number of electrons as in the "conventional" case, so that the total illumination is independent of the degree of expansion obtained by inclining the Y-plates. The loss sustained is not in brightness, but in definition (§5).

Some indication of the possibilities with present-day materials was obtained in experiments conducted in 1946. At an accelerating voltage of 7 kv., and a repetition-rate of the order of 1000 c/s., the tubes referred to in §2 gave a trace visible under a viewing hood at writing speeds up to and exceeding the velocity of light. (A hydrogen thyratron time-base generator circuit was employed.) This speed is adequate for the adoption of the inclined-plate technique (Part I, §6).

§7. CONCLUSIONS

It has been shown that, in theory, any desired time-scale factor up to infinity can be attained in a C.R. oscillograph, by shaping the Y-plates to make use of the finite time taken by the beam to traverse the deflecting system. From examination

of the practical factors involved, the most useful lines to pursue towards this end would seem to be: (*a*) the reduction of beam cross-section at the Y-plates, to allow of a corresponding reduction in inter-plate separation, and to minimize "defocusing" effects; (*b*) design of the Y-plates as a parallel-wire transmission line of known characteristic impedance, preferably on a "travelling-wave" principle; (*c*) reduction of intermodulation effects to a minimum by means of efficient shielding. It is emphasized that although the theory outlined was developed in the course of oscillographic work at Admiralty Signal Establishment,* opportunities for practical investigations were limited to those few aspects which could be developed in the time available. Consequently the bulk of the present paper is presented only as a theoretical analysis of possibilities inherent in the oscillographic method, in the hope that further developments may be stimulated along the lines indicated.

ACKNOWLEDGMENTS

Part of the matter described forms the subject of Patent Applications made jointly with the Director of Scientific Research, Admiralty, and permission to publish the paper is gratefully acknowledged. The author also wishes to acknowledge the help and inspiration derived from discussions with many of his former colleagues in Admiralty Signal Establishment; he is particularly indebted to the able assistance of Mr. C. A. J. Clements in the experimental work.

APPENDIX

Effect of transit-time on X-deflection

The upper-limit effects of transit-time on X-deflection are most easily seen by considering the deflection produced by a "step" of voltage V_x, applied to X-plates of effective length l cm. (figure 1 (*a*)). At the instant of application, a section of the beam of length l is between the plates, and it is the electrons in this section which will form the kink responsible for the trace on the screen.

Taking as temporary origin the point O where the electrons leave the field, electrons at distance ζ to the left of O will experience the field due to V_x for a time ζ/v_f.

Hence their transverse velocity v_x on leaving O is given by $v_x = kV_x\zeta/v_f$, and the kink (figure 7) therefore is parabolic with the equation

$$x = v_x(d-z)/v_f = kV_x z(d-z)/v_f^2,$$

since $z = \zeta$ when the origin is transferred to P.

Thus even an infinitely high time-base–voltage gradient is able to produce only a comparatively slowly-rising kink, whose slope depends mainly on the amplitude of the voltage step.

REFERENCES

VON ARDENNE, M., 1938, *Z. Phys.*, **109**, 553.
HOLLMANN, H. E., 1940, *Proc. Inst. Radio Engrs.*, **28**, 218.
LEE, G. M., 1946, *Proc. Inst. Radio Engrs.*, **34**, 121.
MACKAY, D. M., 1946 a, *Brit. Prov. Pat. Spec.* 18071/46 ; 1946 b, unpublished A.S.E. Report.
RUDENBERG, H. G., 1945, *J. Appl. Phys.*, **16**, 279.

* Now Admiralty Signal and Radar Establishment.

Theoretical Design of Linear Accelerator for Electrons

By W. WALKINSHAW
Atomic Energy Research Establishment, Malvern

Communicated by J. D. Cockcroft; MS. received 17 *March* 1948

ABSTRACT. A circular corrugated waveguide is considered as an electron accelerator. The dependence of phase velocity on frequency and guide dimensions is obtained analytically and is in close agreement with experiment. Tables have been computed for designing accelerator tubes for any frequency and R.F. power.

§ 1. INTRODUCTION

A SHORT account of an experimental section of a travelling wave type of linear accelerator for electrons has been given in a recent paper (Fry, Harvie, Mullett and Walkinshaw 1947). It is our present purpose to describe in greater detail the theoretical analysis on which its design was based. Briefly, the accelerator tube consists of a circular waveguide propagating a wave with an axial component of electric field. Electrons, introduced in a monokinetic stream at the fed end of the guide, form bunches which "surf-ride" in an accelerating field and are maintained in phase with the wave by increasing the phase velocity at the same rate as the mean electron velocity. Ordinary laboratory waveguides cannot be used for this purpose, since their phase velocity is always greater than the velocity of light, but by making deep corrugations in the outer wall magnetic energy can be stored, and it is thus possible to decrease the phase velocity of the wave in a manner analogous to inductive loading of a transmission line in a delay network.

A first design requirement is a sufficiently accurate theory relating the phase velocity of the wave to the radio-frequency and the geometrical parameters of the corrugated guide. This is carried out and a most satisfactory agreement is found between theory and practice : for example, low power measurements made by Mullett and Loach (1948) at 3000 Mc/s. on a two-metre length of corrugated guide have shown a phase error of 18° at the end of the section; that is, an error of one part in four hundred in phase velocity. An account of this theory is given in § 2; numerical data are given in § 3 for the design of accelerator tubes.

Electrons are injected with an initial velocity considerably less than the velocity of light. The phase velocity of the wave is then increased slowly with distance at a rate depending on the available peak accelerating field. The mean acceleration rate must always be less than this peak accelerating field or the electrons fail to form stable bunches. To keep the accelerator length as short as possible some compromise must be made between the fraction of electrons trapped in the wave and the rapidity of the acceleration process. An analytical treatment of this part of the design will be found in § 3.

§ 2. UNIFORM CORRUGATED WAVEGUIDE

2.1. *Frequency equation*

Our purpose is to excite a travelling wave which has a phase velocity less than the velocity of light and an axial component of electric field. Let us examine therefore the simplest type of wave which has these properties, that is, a circularly

symmetrical solution of the electromagnetic field equations with axial and radial components of electric field and a circular magnetic component. Thus we get (Stratton 1941)

$$\left.\begin{aligned} E\rho &= E_0(i\beta/\chi)\,J_1(\chi\rho)\,\exp[-i\beta z+i\omega t],\\ E_z &= E_0 J_0(\chi\rho)\,\exp[-i\beta z+i\omega t],\\ Z_0 H_\phi &= E_0(ik/\chi)\,J_1(\chi\rho)\,\exp[-i\beta z+i\omega t],\end{aligned}\right\} \quad \ldots\ldots(1)$$

where ρ, ϕ and z are the usual cylindrical coordinates, Z_0 is the intrinsic impedance of free space, k is the wave number $=2\pi/$free space wavelength, χ and β are the components of the phase constant in the ρ and z directions respectively and $k^2=\chi^2+\beta^2$.

When $\beta<k$, the phase velocity of this wave is greater than the velocity of light; χ is real, and from the properties of the Bessel function for real argument E_z has a maximum at $\rho=0$ and varies in the usual sinusoidal fashion with increasing ρ. This is the type of solution familiar in ordinary laboratory waveguides in which the boundary surface coincides with a zero of E_z.

In the present application to electron acceleration the phase velocity is required less than the velocity of light; that is, $\beta>k$. χ is now imaginary and in accordance with the properties of the Bessel function for imaginary argument, E_z increases monotonically with increasing radial distance. It is apparent that a wave of this type cannot be contained within an ordinary smooth metallic surface. Examination of the radial field impedance, however, indicates the type of boundary surface which is required. The field impedance is

$$-E_z/H_\phi = Z_0(i\chi/k)\{J_0(\chi\rho)/J_1(\chi\rho)\}. \quad \ldots\ldots(2)$$

When χ is imaginary this impedance is an inductive reactance for all values of ρ. Now, an inductive boundary surface can be simulated by making deep corrugations in a metallic surface to stop the axial energy flow in that region. Reactive energy is then stored inside the deep corrugations and by a suitable choice of depth any desired value of reactive impedance can be presented at the corrugation mouths.

The simplest type of wave which can exist inside each corrugation has an axial component of electric field and circular component of magnetic field. In other words the corrugation has the appearance of a short-circuited radial transmission line and will present any desired reactance at its mouth depending on its depth.

Let us now derive the relationship between guide dimensions, phase velocity and frequency. A crude approach, which is qualitatively accurate for guide wavelengths long compared with the corrugation width, assumes the field in the axial region given by equations (1) and equates the impedance derived in (2) to the impedance looking into the corrugation at its mouth. This approximation was first used by Cutler (1944).

A better approximation can be obtained, however, if we are able to make a sufficiently accurate estimation of the variation of tangential electric field at the mouths of the corrugations. It is found subsequently that the relationship between frequency and phase velocity is not critically dependent on this choice, hence a reasonable estimate of this field leads to a solution of high accuracy. We have therefore assumed the tangential field across the mouth of the nth corrugation at $\rho=a$ to be

$$E'_z=\{C\exp(-i\beta_0 nD)\}/\{1-(2x_n/d)^2\}^{\frac{1}{2}}, \quad \ldots\ldots(3)$$

and zero over the intervening metal walls. The symbols used have the following significance : a = radius of inner boundary of guide, b = radius of outer boundary of guide, D = corrugation pitch, i.e. distance between centre of corrugation walls, d = width of corrugation mouth, $\beta_0 = 2\pi/\lambda_g$, where λ_g is the guide wavelength. x_n is measured from the centre of the nth corrugation.

Now the general circularly symmetrical solution in the axial region of the guide must be represented by summation of solutions of the form derived in (1) by giving β (or χ) all possible values. But we see from (3) that the phase change per corrugation width is $\beta_0 D$, hence β can only take the values given by

$$\beta_m D = \beta_0 D + 2\pi m. \qquad \ldots\ldots(4)$$

The complete solution for the field for $\rho < a$ is therefore

$$\left.\begin{aligned} E_\rho &= \sum_{-\infty}^{\infty} A_m (i\beta_m/\chi_m) J_1(\chi_m \rho) \exp[-i\beta_m z + i\omega t], \\ E_z &= \sum_{-\infty}^{\infty} A_m J_0(\chi_m \rho) \exp[-i\beta_m z + i\omega t], \\ Z_0 H_\phi &= \sum_{-\infty}^{\infty} A_m (ik/\chi_m) J_1(\chi_m \rho) \exp[-i\beta_m z + i\omega t], \end{aligned}\right\} \qquad \ldots\ldots(5)$$

where β_m is given by (4) and $k^2 = \beta_m^2 + \chi_m^2$. The coefficients A_m are found in the usual manner of Fourier analysis such that, at $\rho = a$, E_z is given by (3). That is

$$\begin{aligned} A_m J_0(\chi_m a) D &= C \exp(-i\beta_0 nD) \int_{nD-d/2}^{nD+d/2} \frac{\exp(i\beta_m z)}{\{1-(2x_n/d)^2\}^{\frac{1}{4}}} dz \\ &= (C\pi d/2) J_1(\beta_m d/2). \end{aligned} \qquad \ldots\ldots(6)$$

Substituting this value for the coefficients in (5) gives the complete field in the region $\rho < a$, in accordance with the assumption made in (3).

We now turn our attention to the fields inside the corrugations. A similar analysis might be carried out to obtain a series solution for this field. Since, however, the corrugation width is small compared with the free space wavelength in the present application, only the transmission line mode is of any consequence; hence the fields in the nth corrugation are to a sufficient degree of accuracy given by

$$\left.\begin{aligned} E_z &= BF_0(k\rho) \exp(-i\beta_0 nD), \\ Z_0 H_\phi &= iBF_1(k\rho) \exp(-i\beta_0 nD), \end{aligned}\right\} \qquad \ldots\ldots(7)$$

where $B = C\pi/2F_0(ka)$,

$$\left.\begin{aligned} F_0(ka) &= J_0(ka) Y_0(kb) - Y_0(ka) J_0(kb), \\ F_1(ka) &= J_1(ka) Y_0(kb) - Y_1(ka) J_0(kb), \end{aligned}\right\} \qquad \ldots\ldots(8)$$

and b is the radius of the outer surface of the guide.

The required frequency equation is now obtained from the condition that the magnetic fields given by (5) and (7) must match at their common boundary. Since this can be done accurately at only one point in the corrugation mouth we equate the magnetic fields averaged over the opening. This results in the frequency equation

$$\frac{F_1(ka)}{F_0(ka)} = \frac{d}{D} \sum_{-\infty}^{\infty} (ik/\chi_m) \frac{J_1(\chi_m a)}{J_0(\chi_m a)} J_0(\beta_m d/2) \left\{\frac{\sin(\beta_m d/2)}{\beta_m d/2}\right\}. \qquad \ldots\ldots(9)$$

This is the required relationship between guide dimensions, wave velocity and frequency and we shall discuss its accuracy later. Let us return now to a qualitative description of the physical implications of the foregone analysis.

The fields inside the corrugations require no further elucidation. To our approximation these are simple radial transmission line solutions with a constant phase shift in the field between adjacent sections. Since an inductive impedance is required at the corrugation mouth the depth must be slightly less than an effective quarter-wave transmission line.

In the axial region of the guide, the field is given qualitatively by the first term ($m=0$) of the series given by (5), when the phase change of the field per corrugation is large. For phase velocities less than the velocity of light, the field in the inner region is concentrated close to the corrugation mouths, falling off towards the guide centre in exponential fashion in the nature of a surface wave. For the acceleration of slow particles this is an undesirable feature of the corrugated guide. Of particular interest for electron acceleration is the case when the phase velocity equals the velocity of light. Then $\beta=k$ and making $\chi\to 0$ reduces (1) to

$$\left.\begin{aligned} E_\rho &= \tfrac{1}{2}iE_0k\rho\exp(-ikz+i\omega t)\\ E_z &= E_0\exp(-ikz+i\omega t)\\ Z_0H_\phi &= \tfrac{1}{2}E_0k\rho\exp(-ikz+i\omega t)\end{aligned}\right\}. \qquad \ldots\ldots(10)$$

The axial electric field is then independent of its distance from the guide centre. It is also of interest to note that the impedance of this wave is equal to the intrinsic impedance of free space, that is, the wave impedance of a plane wave in free space.

As in unloaded waveguides, there is a low frequency cut-off which is approximately equal to the cut-off for an ordinary guide having a radius equal to the outer radius of the corrugated guide. In addition there is also a high frequency cut-off which is peculiar to transmission systems having a periodic structure. In general the higher components of the field given by (5) are only important close to the corrugation mouths. However, when the frequency is increased the phase velocity decreases until ultimately the phase change per corrugation width is 180°. From (4) we see that $\beta_{-m-1}=-\beta_m$ or, in other words, a standing wave is produced in the guide. For a travelling wave system it will be necessary to use a sufficient number of corrugations per wavelength to avoid this resonance condition.

2.2. *Experimental check of frequency equation*

The theoretical analysis described above was carried out in conjunction with an extensive investigation of corrugated guides by Mullett and Loach (1948). For a detailed comparison of theory and experiment reference should be made to their paper. Suffice it to say here that approximations of varying degrees of accuracy were examined and discarded in favour of the above theory, which was considered sufficiently accurate (Harvie 1948) for design purposes.

2.3. *Axial field at guide centre*

So far our analysis has given a satisfactory solution for phase velocity. Equal in importance, in the design of an accelerating tube, is an accurate estimate of the axial field at the guide centre. Assuming for the moment that only the

fundamental component ($m=0$) is of importance, the Poynting vector for the power flow can be integrated in the normal way across the inner cross-section of the guide. We get for the axial field at the guide centre

$$E_0=\left\{\frac{2WZ_0\chi^2}{\pi a^2k\beta\{J_1^2(\chi a)-J_0(\chi a)J_2(\chi a)\}}\right\}^{\frac{1}{2}}. \qquad \ldots\ldots(11)$$

This is shown in figure 1 as a function of phase velocity for various values of inner radius. It will be noticed that as the phase velocity is decreased the field at the centre also decreases because the major portion of the power flow then takes place in the region near the mouths of the corrugations. For the same reason the

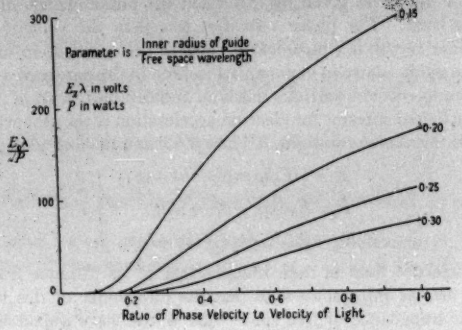

Figure 1. Dependence of axial electric field on phase velocity and inner guide radius.

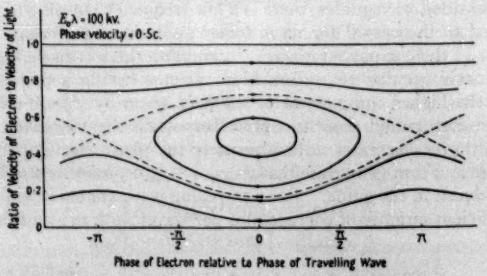

Figure 2. Electron motion in uniform travelling wave.

power flow due to the higher components of the field is only important close to the corrugations. A rough calculation has shown that for a guide of inner radius 0·2λ, with ten corrugations per free space wavelength and a phase velocity 0·4 times the velocity of light, approximately 98% of the power is carried by the lowest component ($m=0$).

The field at the centre of the guide is therefore given to a sufficient degree of accuracy by (9) for guides likely to be used for linear accelerators.

When the phase velocity is equal to the velocity of light, (11) reduces to

$$E_0=(480W)^{\frac{1}{2}}(\lambda/\pi a^2). \qquad \ldots\ldots(12)$$

Equations (9) and (11) are the basic equations, which we shall use in later sections for design purposes.

§3. DESIGN OF LINEAR ACCELERATOR TUBE

3.1. *Motion of electrons in travelling wave*

We now turn our attention to the motion of electrons injected into a travelling wave; in particular, we consider the early stages of an accelerator when the electron velocity is appreciably different from the velocity of light. We recall that it is our intention to introduce electrons into the travelling wave and increase the phase velocity in such a way that stable bunches of electrons are formed slightly in advance of the peak accelerating field. In general the equations of motion for an electron inside a circular corrugated guide are insoluble, but in order to arrive at suitable design data for the variation of phase velocity along the accelerator, we shall assume that electrons are constrained to the axis. In fact electrons bunch at a position of radial defocusing and a paraxial magnetic field is required to confine the electrons to the axial region. The coil design for this field has been carried out by Harvie (1948) and will not be discussed here.

It is instructive to consider first the simple case of an electron in a travelling wave with constant phase velocity. The equation of motion for the constrained electron of charge e is

$$d(m\dot{z})/dt = -Ee\sin(\beta z - \omega t) \qquad \ldots\ldots(13)$$

where m = relativistic mass of particle, $\beta = 2\pi/$guide wavelength, ω/β = phase velocity of wave, E = amplitude of electric field. Multiplying either side of (13) by $(\dot{z} - \omega/\beta)$ and integrating with respect to time t gives the energy equation

$$mc^2[1 - \omega\dot{z}/\beta c^2] = (Ee/\beta)\cos(\beta z - \omega t) + \text{constant}. \qquad \ldots\ldots(14)$$

This can be written in the equivalent form

$$E_1/E_0 - (\omega/c\beta)[(E_1/E_0)^2 - 1]^{\frac{1}{2}} = (E/\beta E_0)[\cos\beta y + \text{constant}] \qquad \ldots\ldots(15)$$

where E_1 = sum of rest and kinetic energies, E_0 = rest energy, $y = z - \omega t/\beta$; βy is the phase of the particle relative to a position of constant phase in the travelling wave where the field is zero.

The cosine term on the right-hand side indicates that the variation of energy with phase is periodic. This is demonstrated by a typical case in figure 2. Those electrons injected with a velocity approximately equal to the wave velocity subsequently oscillate around a stable phase position of zero field. Fast electrons progress continuously forward whilst slow electrons fall continuously backwards. In neither of these cases does an electron gain any energy per cycle. In order to do this it is necessary to start the wave off with a velocity almost equal to that of the injected electrons and slowly increase its phase velocity. The stable phase position now falls back towards the peak of the accelerating field, its position depending on the mean rate at which the electrons are accelerated. Let us suppose then that the phase velocity of the wave is increased in such a way that an electron injected at a phase $-A$, say, is maintained at this phase throughout its subsequent motion. That is, if the amplitude of the field is constant, this electron is accelerated by a constant field $E\sin A$. Its energy equation is therefore

$$mc^2 = Eez\sin A + \text{constant}. \qquad \ldots\ldots(16)$$

This relationship gives the required phase velocity of the wave, which is of course equal to the velocity of this electron.

It is of further interest to examine the subsequent motion of those electrons which enter the guide at phases other than $-A$. For this purpose we write the differential equation of motion of the electron as

$$d(m\dot{z})/dt = -Ee \sin [f(z) - \omega t], \qquad \ldots\ldots(17)$$

where $f(z)$ is the phase change of the wave along the guide, and is already determined (except for a constant) by the constraint put on the stable electron. That is

$$f(z) - \omega t = -A. \qquad \ldots\ldots(18)$$

Integration of (16) gives a relationship between z and t which when substituted in (18) gives

$$f(z) = \frac{\omega m_0 \boldsymbol{c}}{Ee \sin A}\left[\left\{\frac{Ee \sin A}{m_0 c^2} z + 1\right\}^2 - 1\right]^{\frac{1}{2}} + \text{constant}. \qquad \ldots\ldots(19)$$

By numerical integrations of (17) with $f(z)$ given by (19), the phase oscillations of electrons introduced with a velocity of $0{\cdot}4\boldsymbol{c}$ into a guide commencing with this wave velocity, are shown in figure 3 (*a*) for various initial phase angles. The

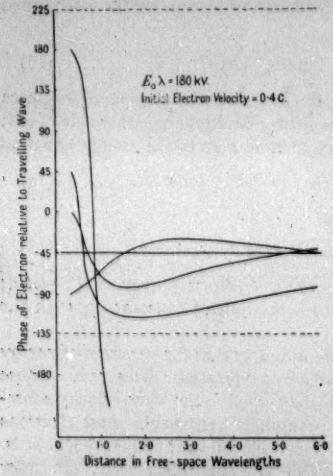

Figure 3 (*a*). Variation of electron phase with distance.

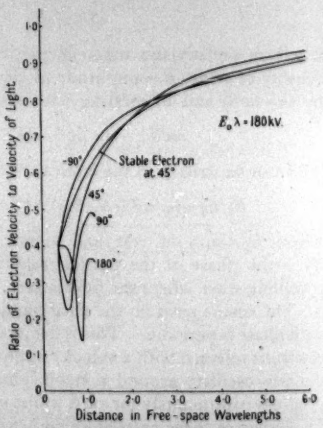

Figure 3 (*b*). Variation of electron velocity with distance.

amplitude of the wave is 0·18 MV. per free space wavelength and the stable phase position is 45° in advance of the peak accelerating field. The corresponding variation in velocity of these electrons is shown in figure 3 (*b*). Those electrons entering near the stable phase position oscillate with decreasing amplitude as their energy increases. If, however, an electron is introduced too far in advance of the stable phase, as for example the electron initially at 180°, it fails to receive sufficient energy for it to be trapped by the wave. Only those electrons initially between $-135°$ and roughly 60° are raised to higher energy levels with a mean velocity equal to that of the wave. It is apparent that, if the stable phase position had been close to the peak accelerating field, the mean rate of acceleration would be greater, but fewer electrons would be trapped.

3.2. *Length of tapered section*

For energies above one or two megavolts, equation (15), for a travelling wave with constant phase velocity, can be written as

$$E_1/E_0(1-\omega/\mathbf{c}\beta)+\tfrac{1}{2}(\omega E_0/\mathbf{c}\beta E_1)=(E/\beta E_0)(\cos\beta y+\mathbf{c}). \quad \ldots\ldots(20)$$

If now the wave velocity, ω/β, is taken equal to the velocity of light, $\mathbf{c}$, and it is required that electrons of initial energy E_1 remain within $\pm 10°$ of the peak accelerating field in attaining extremely high energies, then the following inequality must hold :

$$E_1 > \pi E_0^2/(2E\lambda\cos 80°)=(2{\cdot}3/E\lambda). \quad \ldots\ldots(21)$$

For high energy accelerators $E\lambda$ is likely to be at least 1 MV., hence tapering of the tube can cease for electron energies above 3 MV. without fear of serious phase slip.

3.3. *Numerical design data*

Equations (9), (11) and (16) are the basic equations which we shall now use to obtain numerical data for designing accelerator tubes. It will be noted that the amplitude of the wave at the guide centre has been assumed independent of distance in the previous section. We see from equation (11) or figure 1 that this can only be achieved for different phase velocities by varying the inner radius of the guide. In the following table guide dimensions are given as a function of phase velocity such that the field at the centre is 175 kv. per free space wavelength for a transmitted power of 1 MW. For a phase velocity equal to that of light the inner radius is the 0·2 times the free space wavelength.

Table 1. Phase velocity versus guide dimensions

$D/\lambda=0{\cdot}1$; $d/D=0{\cdot}75$; $E\lambda=175\sqrt{W}$ volts at $\rho=0$; W in watts

Phase velocity	Inner radius		Outer radius	
Velocity of light	Free space wavelength		Free space wavelength	
		δ_2 *		δ_2 *
0·4	0·136025	−3086	0·41814	−180
0·5	0·150615	−2137	0·42166	−110
0·6	0·162992	−1549	0·42403	− 67
0·7	0·173779	−1166	0·42569	− 45
0·8	0·183376	− 905	0·42688	− 34
0·9	0·192053	− 720	0·42772	− 27
1·0	0·200000	− 585	0·42830	− 23

* δ_2 in the above table is the modified second difference.

The above table can be used to design an accelerator tube for any arbitrary power and any chosen variation of phase velocity with distance. In particular the 40-centimetre tapered guide described in a separate paper (Fry, Harvie, Mullett and Walkinshaw 1947) was constructed on the assumption that a power of one megawatt was available, and such that the stable phase was 45° in advance of the peak accelerating field. The dimensions of this guide are easily obtained from (16) in conjunction with table 1, and we shall not give these in detail. The predicted behaviour of the electrons in this guide has already been shown in figures 3 (*a*) and 3 (*b*).

We shall conclude this section with two other tables similar to table 1. The first of these is for a guide differing from that just discussed in corrugation pitch and wall thickness and subsequently in corrugation depth. The inner radius is the same, that is, 0·2 times the free space wavelength for a phase velocity equal

to the velocity of light and such that constant peak field is maintained at the guide centre for other phase velocities. Owing to the high-frequency cut-off it is inadvisable to reduce the number of corrugations per guide wavelength to less than four or five, hence only phase velocities near the velocity of light are of interest.

Table 2. Phase velocity versus guide dimensions

$D/\lambda=0{\cdot}2$; $d/D=0{\cdot}875$; $R\lambda=175\sqrt{W}$ volts at $\rho=0$; W in watts

Phase velocity / Velocity of light	Inner radius / Free space wavelength	δ_2	Outer radius / Free space wavelength
0·8	0·183376	−905	0·4248
0·9	0·192053	−720	0·4244
1·0	0·200000	−585	0·4237
1·1	0·207356		0·4229

The final table is for a high peak field accelerator. Harvie (1948) has shown that the efficiency of the linear accelerator increases with decreasing inner diameter. Engineering tolerances and frequency sensitivity of the guide set a limit to its smallness, but experience has shown that a smaller radius than 0·2 times the free space wavelength for a phase velocity equal to that of light can be used. The following table is for a guide which has a peak accelerating field of 500 kv. per free space wavelength per megawatt transmitted power. The efficient length of a single section of this accelerator tube at a frequency of 3000 Mc/s. is likely to be of the order of two metres.

Table 3. Phase velocity versus guide dimensions

$D/\lambda=0{\cdot}1$; $d/D=0{\cdot}75$; $E\lambda=500\sqrt{W}$ volts at $\rho=0$; W in watts

Phase velocity / Velocity of light	Inner radius / Free space wavelength	δ_2	Outer radius / Free space wavelength
0·4	0·08791	−175	0·3956
0·5	0·09501	−114	0·3964
0·6	0·10090	− 80	0·3969
0·7	0·10597	− 59	0·3974
0·8	0·11044	− 45	0·3978
0·9	0·11445	− 36	0·3982
1·0	0·11810	− 29	0·3985

ACKNOWLEDGMENTS

The work on linear accelerators has been the result of the combined efforts of a large number of people and the author wishes to acknowledge collectively the experimental work and ideas of his colleagues in addition to those specifically referred to already. This work was carried out by the Electronics Group of the Atomic Energy Research Establishment, Malvern, and the author wishes to thank the Director for permission to publish these results and acknowledge his indebtedness to Miss R. Hensman and Miss M. Kingston for their assistance in the computations.

REFERENCES

Cutler, C. C., 1944, *Electromagnetic Waves Guided by Corrugated Conducting Surfaces*, CRB 45/593 Bell Telephone Lab.

Fry, D. W., Harvie, R. B. R-S-, Mullett, L. B., and Walkinshaw, W., 1947, *Nature, Lond.*, **160**, 351.

Harvie, R. B. R-S-, 1948, *Proc. Phys. Soc.*, **61**, 255.

Mullett, L. B., and Loach, B. G., 1948, *Proc. Phys. Soc.*, **61**, 271.

Stratton, J. A., 1941, *Electromagnetic Theory* (New York: McGraw-Hill), p. 360.

Travelling Wave Linear Accelerators

By R. B. R.-Shersby-Harvie
Atomic Energy Research Establishment, Harwell

Communicated by J. D. Cockcroft; MS. received 15 *April* 1948

ABSTRACT. Acceleration of electrons by means of an electromagnetic wave travelling down a circular corrugated tube is considered. The relevant properties of corrugated tubes are derived and the factors influencing electron energies. Some numerical results are also quoted for a wavelength of 10 cm. The problems of high energy accelerators are discussed briefly and illustrated by calculations which have been made for a 500 Mev. accelerator.

§1. Introduction

Preliminary investigations were started on the type of accelerator which is about to be described towards the end of 1945. Successful linear accelerators using radio-frequency accelerating fields had been previously reported (Sloan and co-workers 1931, 1934), and it was apparent that as a result of wartime advances in centimetre-wave magnetrons and waveguide technique, linear accelerators compared favourably with other forms of particle accelerators. Work began on electron accelerators, electrons being chosen both because of the technical simplicity associated with them and because there were important practical applications for comparatively low energies, 20 to 50 Mev., in the field of medical therapy. The type first investigated was that in which electrons are accelerated by electromagnetic waves travelling down a circular corrugated waveguide; the successful operation of an experimental model has been reported by Fry and co-workers (1947).

The object of the present paper is to set out the main factors influencing the design of a travelling wave accelerator. Although it is not proposed to make detailed comparisons with other types of linear accelerator, mention will be made of some other methods which are available. The most important and obvious alternative is to accelerate the electrons by passing them through a series of resonant cavities excited from a radio-frequency source. Successful experiments using this method have been reported from several sources (Bowen, Pulley and Gooden 1946, Halpern *et al.* 1946, Allen and Symonds 1947) and other more ambitious projects are being worked upon (Schiff 1946, Alvarez 1946, Haxby *et al.* 1946, Akeley 1946, Morrison 1947, Schultz *et al.* 1947). It appears that these methods can yield energies comparable with the travelling-wave system, given the same amount of radio-frequency energy and the same overall length of accelerator (Walkinshaw 1947). There are, however, important practical differences not fully resolved, and neither type has as yet been proved superior to the other.

Another type of combined travelling-wave and resonator accelerator using a rectangular corrugated guide has been investigated by Mullett (1946) but was not pursued, mainly on account of difficulties of manufacture of the necessary equipment. Travelling-wave systems using various configurations of bent waveguides have also been considered and rejected for reasons of difficulty with focusing, practical inconvenience or sometimes inefficient accelerating performance, for example the coiled-up waveguide (Hudspeth 1946). Other variations of these methods and a proposal to use a circular waveguide lined with a dielectric tube have also been put forward (Willshaw 1945).

The circular corrugated waveguide travelling-wave type accelerator has at least not been found inferior to other methods for the acceleration of electrons; it has been shown (Cowhig 1946) that different methods must be employed for the acceleration of particles at velocities much less than that of light.

§2. DESCRIPTION

The basic principles of the travelling-wave accelerator will be described briefly to save reference to other papers.

An electromagnetic wave with a longitudinal electric field component is set up in a corrugated tube; this is a circularly symmetrical wave with a field configuration such as is shown in section in figure 1. If a bunch of electrons situated at X is travelling at a velocity equal to the phase velocity of the wave, the electrons will be subjected to an electric field tending to accelerate them. This acceleration can be continued indefinitely, provided the phase velocity of the wave follows the velocity of the electrons as they accelerate; this is ensured by suitable dimensions of the corrugated tube.

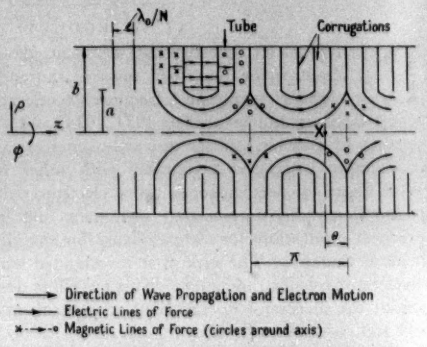

Figure 1. Diagrammatic view of fields in corrugated tube for the case where $v = c$.

If the bunch of electrons be situated at a phase angle θ with respect to the wave, the position of the bunches will be longitudinally stable provided $0 < \theta < \pi/2$, but will tend to diffuse away from the axis of the tube. Thus some form of focusing must be used; this has so far taken the form of a steady longitudinal magnetic field, the effect of which is discussed in Appendix C. Electrons are injected along the axis in a continuous stream and become bunched, due to the natural longitudinal stability of the accelerating process (Walkinshaw 1948).

Details of the practical construction of an accelerator are given by Fry and co-workers (1947), Mullett (1947), and Mullett and Loach (1948).

§3. SOME PROPERTIES OF THE CORRUGATED WAVEGUIDE

3.1. *General*

The performance of an accelerator is mainly determined by the properties of the corrugated waveguide. For a general view of the subject it is only necessary to consider these properties for the case where the phase velocity is constant and equal to c, the velocity of light; the velocity of an electron is

$$u = c\{1 - (m_0c^2/E)^2\}^{\frac{1}{2}}, \qquad \ldots\ldots(1)$$

where m_0 = rest mass of electron, E = total energy of electron; hence, since the rest energy m_0c^2 is approximately 0·51 MeV., the velocity of the electrons will be very close to that of light except for a short length near the start of an accelerator.

This initial part, where the velocity is changing rapidly, is vital to the satisfactory working of the accelerator—the waveguide design for this part is dealt with by Walkinshaw (1948)—but the energies obtainable and the general characteristics are almost entirely determined by the main length over which the electrons and the wave will have a velocity very near to that of light. Consequently it will be assumed henceforth that the phase velocity of the wave is actually equal to the velocity of light.

3.2. *The fields in the waveguide*

The fields in the corrugated waveguide can be very simply calculated by a method due to Cutler (1944). This method gives results of sufficient accuracy for the present argument, although more refined calculations (Walkinshaw 1948) are necessary to design the waveguide to the high degree of precision required in an actual accelerator. Cutler assumes that the protuberances on the guide walls are very thin, and very close together compared with the wavelength. Hence the walls may be considered to have a uniform impedance (Booker 1947), giving simple boundary conditions. The fields in the guide are derived in Appendix A. The following are some special features of the wave when $v = \mathbf{c}$: (i) the accelerating field, E_z, is uniform over the open part of the tube, so that electrons which are not properly aligned on the axis will still receive the same accelerating field; (ii) equation (A 7) shows that, with the same amount of power flowing in each case, the accelerating field is inversely proportional to the square of the inner radius; (iii) as the inner radius decreases, the fields inside the corrugations tend to those in an ordinary TM_{010} resonator, and, for the small inner radii used, the fields are not very different from those in the outer portions of such resonators.

3.3. *Attenuation of the waveguide*

It will be assumed that the electronic current passing down the guide is so small that power absorption due to it is negligible, and that the sole cause of attenuation is absorption of the wave by the walls of the tube. This may not be true in certain practical cases, but the effect is readily allowed for in cases of large electron currents, and the small current case is of sufficient importance to justify its exclusive study.

To calculate absorption by the walls it will be assumed that the fields remain the same as those already given, even when a finite corrugation spacing is used. Walkinshaw (1947) has shown that it is not desirable to use corrugation spacings exceeding about one-fifth of a wavelength, i.e. $N = 5$ in figure 1, for which this assumption is justified. The usual methods (Schelkunoff 1943) are used for finding the attenuation in waveguides.

The attenuation constant is

$$\alpha = w/2W \text{ nepers/metre}, \qquad \ldots\ldots(2)$$

where W = power flow past any point in the guide, and w = power per metre absorbed by walls at the same point. The power absorbed is given by

$$w = (R/2) \iint H.H^* \, ds, \qquad \ldots\ldots(3)$$

where H = magnetic field on the metal surfaces of the guide, H^* = complex conjugate of H, R = intrinsic resistance of the metal $= \sqrt{(\pi\mu\mathbf{c}/\lambda_0 g)}$, μ = permeability of metal, g = conductivity of metal. The integration is carried out over the whole

surface of the metal boundaries over a unit length of pipe, the fields being assumed the same as in the absence of attenuation. It follows from (2) and (3) that the attenuation can be written

$$\alpha = \alpha_0 \lambda_0^{-3/2}, \qquad \ldots\ldots(4)$$

where α_0 is a function of the properties of the metal and the geometry of the guide. When the phase velocity is fixed (e.g. $v = c$), the geometry is specified by a/λ_0, the ratio of the inner radius of the guide to the wavelength, and N, the number of corrugations per wavelength.

Most of the loss is found to occur in the plane dividing walls between the corrugations, so that the attenuation is roughly proportional to N; the variation with a/λ_0 is not so simple and is best found numerically. The attenuation has been computed for a copper tube with $N = 10$ and with $v = c$, and the result is shown in figure 2, which gives α_0 as a function of a/λ_0.

It has been found by experiment (Mullett 1948) that the measured attenuations of the guides which have been made have been roughly twice the calculated values. Thus the theoretical attenuation for $N = 10$ may be taken as approximately equal to the practical attenuation, for $N = 5$, which approaches the optimum design of guide.

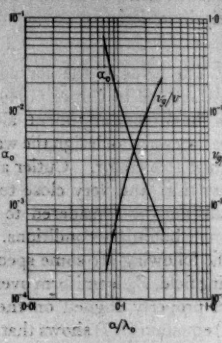

Figure 2. Attenuation and group velocity in corrugated tube.
Attenuation constant is $\alpha = \alpha_0 \lambda_0^{-\frac{3}{2}}$ nepers/metre.
Curve gives α_0 for the case where $N = 10$ corrugations/wavelength, $v = c = 3 \times 10^8$ metres/sec., $g = 5{\cdot}8 \times 10^7$ mhos/metre (typical copper).
Group velocity (v_g) is for the case where $v = c$.

3.4 *Electron energy obtainable*

The energy gained by an electron in travelling down the tube may now be calculated. The maximum energy gained in a length z is

$$V(\text{ev.}) = \int_0^z |E_z| \, dz. \qquad \ldots\ldots(5)$$

This is a maximum because it assumes that the electron travels all the time in the maximum accelerating field. This is not quite attainable in practice because insufficient electrons would be captured at the start of the accelerator (Walkinshaw 1948) and because it is not a position of stable phase equilibrium. However, experiments with the 0·5 MEV. accelerator (Mullett 1947) have shown that about half the possible electron output can be obtained at a phase corresponding to an accelerating field greater than 90% of the maximum; under these conditions the output current may be restored to its full value by injecting more electrons at the beginning. This, together with the possibility of varying the phase along the accelerator, indicates that (5) over-estimates the attainable energies by not more than 10%. No correction will be included in the results, but the effect should not be forgotten.

The power travelling down the tube is

$$W = W_0 \exp(-2\alpha z), \qquad \ldots\ldots(6)$$

where W_0 = power fed into the beginning of the waveguide at $z = 0$. Substituting

from (6) and (A8) into (5) and integrating, $V \simeq 6{\cdot}98(\lambda_0/a^2)\sqrt{W_0}\{1-\exp(-\alpha z)\}/\alpha$, whence from (4)

$$V/\sqrt{(\lambda_0 W_0)} \simeq 6{\cdot}98(\lambda_0/a^2)\{1-\exp(-\alpha_0 z\lambda_0^{-3/2})\}/\alpha_0. \quad \ldots\ldots(7)$$

This relationship has been computed numerically, and figure 3 shows $V/\sqrt{(\lambda_0 W_0)}$ as a function of $z\lambda_0^{-3/2}$ for four different values of (a/λ_0) and for $v=c$ and $N=10$. To give an indication of the magnitudes involved, the same diagram has been plotted for the particular case where $\lambda_0=10$ cm. and $W_0=2\times10^6$ watts, and is shown in figure 4. The envelope of the family of curves, a dotted line in figures 3 and 4, shows the maximum attainable energy for any given length of accelerating tube, each length corresponding to a definite value of (a/λ_0).

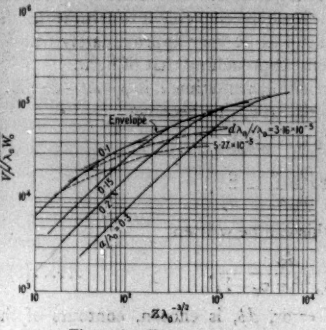

Figure 3. Electron energy.

Computed energy for the case where
$N=10$ corrugations/wavelength,
$v=c=3\times10^8$ metres/sec.,
$g=5{\cdot}8\times10^7$ mhos/metre (copper),
λ_0 = free space wavelength (metres),
z = distance along tube (metres),
V = electron energy (ev.),
a = inside radius of tube (metres),
W_0 = radio wavelength power (watts).

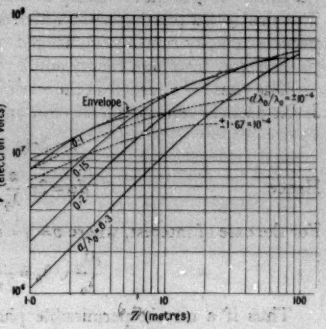

Figure 4.

Energy obtainable for the case where
$\lambda_0=0{\cdot}1$ metre,
$W_0=2\times10^6$ watts,
$N=10$ corrugations/wavelength,
$v=c=3\times10^8$ metres/sec.,
$g=5{\cdot}8\times10^7$ mhos/metre.

It should be noted that the energy limitation represented by the envelope curve is entirely due to attenuation; other, often more serious, limitations will be discussed later. It can be shown * that, using the optimum value of a/λ_0, the attainable electron energy is about 90% of that in the ideal, but hypothetical, case where all the power is dissipated in the tube and the accelerating field is uniform along the length. The conditions on the envelope curve are very close to those which give this 90% of the ideal energy. Thus it will be seen that the system of acceleration is not inherently inefficient in spite of the progressive falling off in accelerating field along the tube and the power remaining at the end, which has to be absorbed in an artificial load. Improvement could be effected by such means as reducing a/λ_0 as the end of the accelerator is approached, but the advantage is too small for such complications to be practicable.

* The problem is formally identical to that of determining the effect of aperture distribution in linear aerial arrays, and has been studied in detail in this connection.

3.5. *Effect of wavelength and temperature variation, and group velocity*

In an ideal accelerator the phase velocity of the wave would remain unchanged as the applied frequency is altered. In a corrugated waveguide this is by no means the case, and the phase velocity changes rapidly with applied frequency because a large amount of energy is stored in the corrugations and the guide acts as a dispersive medium. This is expressed by means of the concept of group velocity (Appendix B), and figure 2 shows v_g/v, plotted as a function of a/λ_0.

If the waveguide is designed to have the correct phase velocity at a certain wavelength, then altering this wavelength will change the phase velocity, and the particles being accelerated will fail to remain in the correct phase relationship with the wave. Due to the low group velocity in the guide, this effect can be very serious. To calculate the phasing errors which occur it will be convenient to assume that the particle velocity remains unchanged, which will be very approximately true for particles having a high energy and a velocity approaching that of light.

The phase of a particle in the wave, at position z and time t, is $\phi = \omega t - 2\pi z/\lambda_g$. If the particle velocity is constant, and equal to u, this becomes

$$\phi = 2\pi(z/\lambda_0)\{c/u - \lambda_0/\lambda_g\}.$$

Hence

$$d\phi = 2\pi \frac{z}{\lambda_0}\frac{d\lambda_0}{\lambda_0}\left\{\frac{\lambda_0}{\lambda_g}\frac{v}{v_g} - \frac{c}{u}\right\}.$$

For the case of interest, where $v = u = c$, this can be written

$$\frac{d\lambda_0}{\lambda_0}\sqrt{\lambda_0} = \frac{d\phi}{2\pi z\lambda_0^{-3/2}(v/v_g - 1)}. \qquad \ldots\ldots(8)$$

Thus if a certain permissible phase error, $d\phi$, is chosen, contours of the corresponding permissible wavelength error, $\sqrt{\lambda_0}d\lambda_0/\lambda_0$, can be drawn on figures 3 and 4. Two such contours are shown for the case of a phase error of $2\pi/10$ radians. The arbitrarily chosen error of $2\pi/10$ is probably rather larger than can be tolerated in practice, and so the results shown are a conservative estimate of the extremely high wavelength stability which is required. The inherent instability of most practical sources would impose very serious limitations on the performance, and it will usually be necessary to incorporate some device for adjusting the wavelength of the source. By this means it should be possible to counteract all but the most rapid variations of wavelength.

Thermal expansion of the waveguide has practically the same effect as the same proportional change of wavelength, but in the opposite sense. Consider a uniform linear expansion of the waveguide accompanied by the same proportionate increase of wavelength. The wavelength in the guide, λ_g, will increase in the same proportion and the phase velocity will remain unchanged; hence the phasing of the electrons with respect to the wave will be unaffected. If the wavelength is now restored to its original value, the effect of the change will be the same as if only the linear expansion had taken place. Hence, for small changes, the phase errors caused by a uniform linear expansion are the same as those caused by the same proportionate change of wavelength in the opposite sense.

The coefficient of expansion of copper is about $1{\cdot}6 \times 10^{-5}$. Thus a change of 1° c. in guide temperature is equivalent to a wavelength change $d\lambda_0/\lambda_0 = -1{\cdot}6 \times 10^{-5}$. In figure 4, therefore, the wavelength tolerance contours of $d\lambda_0/\lambda_0 = \pm 10^{-4}$ and $\pm 1{\cdot}67 \times 10^{-4}$ are equivalent to temperature tolerances of $\mp 6°$ c. and $\mp 10°$ c. respectively.

The actual phase errors in any accelerator will be the sum of the errors caused by wavelength and temperature changes. Where only wavelength tolerances are given these should be considered as representing the sum of both tolerances.

The practical effect of temperature changes is not nearly so serious as that of wavelength changes because they occur slowly, and any uniform change can be compensated by altering the wavelength of the power source. Thus it is only necessary to reduce temperature differences between different parts of the waveguide, and the effect of any remaining temperature differences will certainly be less than that of the same uniform temperature changes, which have already been calculated.

The foregoing estimate of the permissible wavelength variations has been based upon the assumption of a single frequency of oscillation. In practice, linear accelerators must usually be operated from pulsed sources in order to obtain sufficient radio-frequency power; this involves the application of a whole spectrum of frequencies. The steady-state stabilities give a first approximation to those required under pulsed conditions, but various anomalies and difficulties arise in connection with the use of very short pulses, and the problem requires further investigation. The minimum pulse duration which can be used is governed by the time required to build up the wave in the corrugated tube; to a first approximation this is equal to the length of tube divided by the group velocity. The accelerator will only be operative during that portion of the applied pulse which occurs after the wave has had time to build up.

3.6. *Dimensional tolerances*

The effect of one class of dimensional variation—thermal expansion—has already been considered and, from the results which were obtained, it will have been evident that the waveguide dimensions must be so accurately determined that no normal workshop process could be used to manufacture the guide. It also appears most unlikely, from the results of experiment (Mullett and Loach 1948), that the guide could be designed with sufficient accuracy, even were the former limitation removed, except perhaps by long and costly experiment. However, these difficulties can be circumvented to some extent, and it is necessary to discuss the point in more detail, because it has an important bearing upon the design of an accelerator.

It has already been shown that the phase velocity of the wave must correspond to the electron velocity so closely that the relative phase difference between electron and wave does not become excessive. Nevertheless relatively large errors in phase velocity are permissible locally provided they are not cumulative. Thus an accelerator could be constructed from sections of guide with relatively large velocity errors if some subsequent means of phase adjustment can be provided between the sections. It is anticipated that this can be done by interposing between sections short lengths of corrugated guide, which can be made or selected from a stock. This procedure should be easily applicable, provided the number of adjustment points which are required does not become excessive. It is also advisable to distinguish between systematic and accidental errors in the guide; the former are probably mainly due to design and the latter to construction.

Little can be said of the systematic errors, since it is not possible to predict their variation with the shape of the guide (a/λ_0). Among the experimental

results of Mullett and Loach (1948) on a guide with $a/\lambda_0 = 0{\cdot}2$ and $\lambda_0 = 10$ cm. is one showing phase errors of about 18° in a 2-metre length which appear to be mainly systematic errors. It is only possible to assume that in guides with different values of a/λ_0 the proportional dimensional errors will remain the same; it should be possible to reach this standard with a reasonable amount of experiment. On this basis it follows that the number of adjustment points will remain constant in accelerators with constant wavelength tolerance $d\lambda_0/\lambda_0$ and wavelength λ_0, but with varying a/λ_0 and total length. It also follows that the spacing between adjustment points is proportional to λ_0 if a/λ_0 remains constant. The experimental result quoted shows a phase error of the order of that tolerable, and it can thus be said that adjustment points should be spaced about 2 metres apart in a guide with $a/\lambda_0 = 0{\cdot}2$ and $\lambda_0 = 10$ cm. On this assumption a guide with $a/\lambda_0 = 0{\cdot}1$ and $\lambda_0 = 10$ cm. would require adjustment points at about 20 cm. spacings.

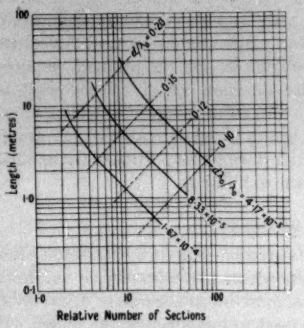

Figure 5.

Relative number of sections required for adjustment of random errors for the case where $\lambda_0 = 0{\cdot}10$ metres, $v \simeq c = 3 \times 10^8$ metres/sec.

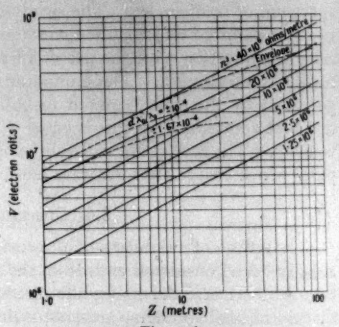

Figure 6.

Efficiency of accelerator of figure 4. Parameter n^2 = efficiency.

The accidental errors are assumed to be caused by random errors in the dimensions of each cavity in the corrugated guide. These will cause a certain phase error, and the phase errors in each cavity are supposed to be capable of addition to give the total error in a length of guide. Since the sum of such a number of independent errors gives a resultant error whose mean is proportional to the square root of the number of additions made, the mean phase error in a section of waveguide will be proportional to the square root of its length, in contrast to the case of systematic errors where the resultant phase error was taken as proportional to the length. Over a moderate range of sizes, workshop practice is such that the proportional dimensional errors may be assumed constant. Thus the length of sections between the adjustment points required to compensate for random errors will be proportional to the wavelength λ_0 and can be computed as a function of a/λ_0 by means of the group velocity as already discussed in connection with thermal expansion. This type of computation has been carried out,

and figure 5 shows the relative number of adjustment sections required as a function of length of accelerator for different values of wavelength tolerance and for the case $\lambda_0 = 10$ cm. and $N = 10$. The absolute number of sections required is not determinate at present through lack of experimental evidence, upon which estimates of errors must of course be based. However, although it is known that the accidental errors are in practice negligible compared with the systematic for $a/\lambda_0 = 0{\cdot}2$, it is clear that the effect of the former increases much more rapidly as a/λ_0 is reduced. Estimates of probable tolerances indicate that the random errors are almost certain to predominate for the case $a/\lambda_0 = 0{\cdot}1$, $\lambda_0 = 10$ cm. and $N = 10$.

It will be shown in § 5 that there are certain advantages to be gained by reducing a/λ_0 as far as possible. One limit to this process is the resulting increase in waveguide errors and the number of adjustments required to compensate for them. The tolerable number of adjustments is a practical limitation, but it could be very serious if, for example, it were necessary to adjust separately each corrugation cavity. It is hoped that in due course further experimental results will become available to enable absolute values to be given to the errors.

Two favourable factors have not been mentioned. Firstly, increasing the corrugation pitch (i.e. reducing N) may reduce the accidental errors by reducing the number of cavities, and it has already been mentioned that pitches corresponding to $N \simeq 5$ are desirable. Secondly, a certain amount of compensation for cumulative errors may sometimes be possible by adjusting the wavelength of the power source.

§ 4. EFFICIENCY OF ACCELERATORS

Accelerator performance is affected by the alteration of various waveguide design parameters; help in choice of such parameters is obtained by consideration of concept of accelerator "efficiency", a figure of merit, defined as n^2, where $n^2 = V^2/W_0 L$ ohms/metre; V and W_0 have the same meanings as before and L = length of accelerator in metres. The efficiency figure has several useful properties. Since both power and length are expensive in cost and space, high efficiency is an indication of economy. Again, high energy accelerators will usually have to be constructed by operating a number of smaller accelerators in cascade. It can be shown that the efficiency of such an accelerator is the same as that of its component accelerators, so that a knowledge of the efficiency of the components enables the overall length and power requirements to be rapidly assessed; for the same reasons the efficiency is an excellent basis of comparison even between accelerators of widely different design, although it does not take into account wavelength differences and many other features of practical importance. Physically, the efficiency figure is almost the same as the "dynamic resistance" of a unit length of the accelerator, and it is often useful to think of it as such.

Constant efficiency contours may be plotted on diagrams such as figures 3 and 4 (see figure 6). The constant efficiency curves are simply straight lines with the efficiency proportional to the square of the intercept on the ordinate. It will be seen at once that the efficiency increases as a/λ_0 is reduced, although a limiting maximum value is eventually reached, and that this increase of efficiency is more marked in accelerators with a wide wavelength tolerance. Hence there is good reason for attempting to use accelerators made up of a number of sections

with small a/λ_0 rather than of a smaller number of sections with large a/λ_0; either the total length or total power will be reduced thereby.

The efficiencies obtainable with the corrugated guide appear very low compared with that of the Sloan and Coates accelerator (Sloan 1934), which was some 15–20 times higher; this is primarily due to the fact that the Sloan and Coates accelerator was designed to accelerate heavy ions, moving very much more slowly than light, so that the field in a cavity resonator (or other resonant circuit) may be used for acceleration several times without introducing much additional loss.

§5. GENERAL DESIGN PROCEDURE

There are so many variables to take into account that it is impossible to lay down any rigid rules of design; it is best to set down the most important considerations and leave details to be determined for any specific case.

One of the first things to decide upon in designing an accelerator is the radio wavelength to be used. As the wavelength is reduced, the efficiency increases slowly (the precise law depends upon the wavelength tolerance and a/λ_0 chosen) and the mass of metal in the waveguide and vacuum system decreases. On the other hand, more power is available from radio valves at longer wavelengths and, while magnetrons can be paralleled (Cowhig and Jones 1947), this may be an important point if a very high energy accelerator is required. Against this, however, is the fact that large tubes store more energy, so that longer pulses are required at longer wavelengths: roughly speaking, the build-up time is proportional to wavelength. Less important points are that wavelength reduction enables the size of focusing coils and their power consumption to be reduced, although too short a wavelength may not allow a sufficient aperture for the passage of electrons. In general it appears that as short a wavelength as possible is desirable, consistent with obtaining the necessary power.

For a given wavelength and output energy, the approximate efficiency obtainable is known in terms of the product of length and power. The balance between length and power is mainly one of economy and individual requirements. Short accelerators using high power also require stronger focusing fields and more focusing power than longer ones using less radio-frequency power.

The last important choice is probably that of the value of a/λ_0. Efficiency demands small a/λ_0, although there is not much to be gained by going below a certain value. Besides the additional difficulty involved in construction of the guide when a/λ_0 is reduced, and the resultant increase in the number of phase adjustment points required, the number of separate component accelerators comprised in the whole accelerator is increased and the power has to be split up and fed in at a greater number of points. It is necessary to arrive at a compromise for a long accelerator composed of several sections, but, if the object is to produce the shortest possible accelerator, it will be necessary to reduce a/λ_0 as far as possible. The difficulties increase very rapidly as a/λ_0 is reduced, so that there is a sharp limit to the smallest guide which can be made, although this limit is not yet known; tubes with a/λ_0 as small as 0·15, at a wavelength of 10 cm., have been made without difficulty at Telecommunications Research Establishment. It is estimated that the limit probably lies in the region of $a/\lambda_0 = 0{\cdot}1$.

None of the factors mentioned above is of course unaffected by the others, although there is a certain degree of independence. As an example of design

procedure some data are reproduced which were computed by Taylor (1946) to investigate the construction of a 500 MeV. accelerator. The length has been fixed arbitrarily and figure 7 shows the power required, as a function of the number of component accelerator sections, for three different wavelengths and wavelength tolerances. Many other facts require consideration, but this chart shows clearly the effect of some of the variables and the magnitudes involved. It should perhaps be added that no decision has been made to construct such an accelerator.

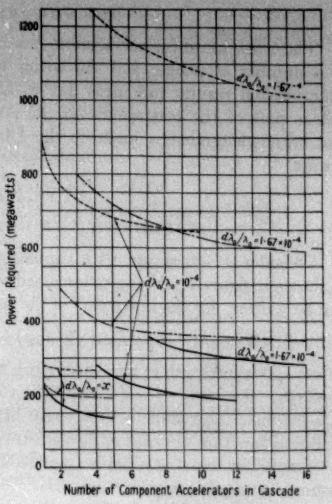

Figure 7. Accelerator for 500 MeV.
Total length = 50 metres.
———— $\lambda_0 = 0{\cdot}10$ metres.
- — - — - $\lambda_0 = 0{\cdot}25$ metres.
– – – – – $\lambda_0 = 0{\cdot}50$ metres.
Frequency tolerance x is such that energy is limited by attenuation.

§6. ADDITIONAL REMARKS

The electron energy obtainable from accelerators has been discussed comprehensively, but little has been said about the beam current obtainable. There are two important limitations to the current–space charge and damping of the wave. Nothing useful is known about the former, but attention is drawn to the fact that the experimental 0·5 MeV. accelerator passed currents of up to about 100 ma. during the pulse. The latter limitation merely means that no more electronic energy can be got out of the device than the radio-frequency put in. Thus it should not be difficult to design linear accelerators giving relatively large mean or peak currents, provided sufficient power is available. Indeed, there seems no reason why high energy efficiencies should not be attainable.

There are three major advantages where exceedingly high energies are involved (greater than, say, 1000 MeV.): the fact that the cost is roughly proportional to the electronic output energy required, which appears to be so far a unique feature of linear accelerators, the small amount of power lost by radiation, and the short electron path, as compared with orbital machines, which reduces the vacuum problems. Also, in all linear accelerators the actual electrons are readily led out of the machine.

The construction of two further accelerators is at present contemplated. The first, which is nearly completed, is effectively an extension of the former 0·5 MeV. machine. It is designed to give 4 MeV. and has the specification: length = 2 metres; power = 2 MW.; wavelength = 10 cm.; $a/\lambda_0 = 0{\cdot}2$; injection energy = 50 kev. Its main object is to investigate focusing problems in longer accelerators than the 0·5 MeV. machine. The second is a 20 MeV. accelerator of the same length, but much higher efficiency (small a/λ_0).

ACKNOWLEDGMENTS

The work on linear accelerators has been the result of the combined efforts of a number of people, and the writer wishes to acknowledge collectively the experimental results and ideas due to his colleagues. This work was carried out as part of the programme of the Atomic Energy Research Establishment, and acknowledgment is made to the Director for permission to publish these results.

APPENDIX A

FIELDS IN THE CORRUGATED TUBE

Consider a waveguide with dimensions and cylindrical coordinate system as shown in figure 1. Using rationalized M.K.S. units, the wave which is of interest can be written, for the inner part of the tube, as

$$E_z = -iE_0 J_0(\chi\rho); \quad E_\rho = E_0(\beta/\chi)J_1(\chi\rho); \quad Z_0 H_\varphi = E_0(k/\chi)J_1(\chi\rho), \qquad \ldots\ldots(A1)$$

where λ_0 = wavelength in free space (m.), λ_g = wavelength in corrugated tube (m.), $k = 2\pi/\lambda_0$, $\beta = 2\pi/\lambda_g$, $\chi = k[1 - \mathbf{c}/v^2)]^{\frac{1}{2}}$, v = phase velocity of wave in m/sec., Z_0 = intrinsic impedance of free space in ohms, $= (\mu_0/\epsilon_0)^{\frac{1}{2}} \simeq 120\pi$, J_n = first kind of Bessel function of order n, E_0 = arbitrary constant.

The factor $\exp i(\omega t - \beta z)$ is implied for each field component; the losses are assumed negligible for the moment.

It will be seen that for phase velocities greater than light this wave is the same as the familiar TM_{01} wave used in smooth-walled tubes (Schelkunoff 1943).

Again the fields within the corrugations can be written (Schelkunoff 1943)

$$E'_z = BJ_0(k\rho) + CY_0(k\rho); \quad Z_0 H'_\varphi = iBJ_1(k\rho) + iCY_1(k\rho). \qquad \ldots\ldots(A2)$$

At the boundary where $\rho = b$ it is necessary to have $E'_z = 0$. Hence from (A2) it follows that

$$BJ_0(kb) + CY_0(kb) = 0. \qquad \ldots\ldots(A3)$$

Thus the radial impedance looking into the corrugations, $Z_\rho = -E'_z/H'_\varphi$, is given by

$$Z_\rho = iZ_0 \frac{Y_0(kb)J_0(ka) - J_0(kb)Y_0(ka)}{Y_0(kb)J_1(ka) - J_0(kb)Y_1(ka)}. \qquad \ldots\ldots(A4)$$

To satisfy the boundary conditions at the surface of the corrugations the radial impedance of the wave in the inner part of the tube must be the same as that in the corrugations. Thus from (A1) this impedance can also be written

$$Z_0 = iZ_0(\chi/k)J_0(\chi a)/J_1(\chi a). \qquad \ldots\ldots(A5)$$

Simultaneous solutions of (A4) and (A5) give waveguide dimensions in terms of phase velocity or vice versa. Examination shows that any phase velocity can be obtained by a suitable choice of dimensions.

The strength of the fields in the corrugations can be related to those in the centre part by noting that $E'_z = E_z$ and $H'_\varphi = H_\varphi$ when $\rho = a$.

It is also necessary to know the value of the constants in terms of the power flowing down the tube. Integrating the Poynting vector over the inner portion of the tube,

$$2W = E_0^2(k/\chi)^2(\mathbf{c}/v)(\pi a^2/Z_0)\{J_1^2(\chi a) - J_0(\chi a)J_2(\chi a)\}, \qquad \ldots\ldots(A6)$$

where W = power flowing down tube in watts.

The special case where $v = \mathbf{c}$ is of particular importance for present purposes. Substituting this value of v in (A1) and (A6), it is found that the longitudinal field is given by

$$E_z = -i(4/ka^2)\sqrt{(WZ_0/\pi)} \text{ volts/metre}, \qquad \ldots\ldots (A7)$$

or, substituting the values of constants, $E_z \simeq -i(6{\cdot}98/a^2)\lambda_0\sqrt{W}$.

APPENDIX B

GROUP VELOCITY IN THE TUBE

The group velocity in a waveguide can be defined as (Lamont 1942)

$$v_g = \mathbf{c}\left(\frac{\lambda_g}{\lambda_0}\right)^2 \frac{d\lambda_0}{d\lambda_g} = \frac{v^2}{\mathbf{c}}\frac{d\lambda_0}{d\lambda_g}. \qquad \ldots\ldots (B1)$$

A method of finding the group velocity is described which it is believed gives a clearer physical picture of the relevant factors than a direct derivation from $d\lambda_0/d\lambda_g$. The results also emerge in a form well adapted for computation from the integrals required in computing the attenuation, and show how the attenuation and group velocity are related.

Results will be used which have been obtained in connection with the deformation of electromagnetic cavity resonators, as given, for example, by MacLean (1945).

Consider a portion of a loss-free corrugated waveguide formed into a resonator with a loosely fitting piston at one end as shown in figure 8. The corrugations must also be loosely fitting, so that they can be pushed along by the piston, and they are again assumed indefinitely thin and closely spaced. Let the cavity be set oscillating in the desired mode and let the length be equal to one wavelength, λ_g, of this mode. Let the piston now be slowly pushed in a small distance, dz, while the cavity continues to perform free oscillations. Then if F be the time-averaged force on the piston due to the electromagnetic fields, the work done on the piston is $F\,dz$ = increase of oscillating energy $= d\mathscr{E}$, say. But it has been shown (MacLean 1945) that $\mathscr{E}\lambda_0 =$ constant, or $d\lambda_0/\lambda_0 = -d\mathscr{E}/\mathscr{E}$. Hence, since $dz = -d\lambda_g$, substitution in (B1) gives

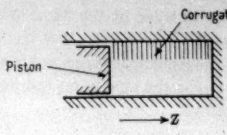

Figure 8.

$$v_g = vF/(\mathscr{E}/\lambda_g). \qquad \ldots\ldots (B2)$$

The expression $\mathscr{E}/\lambda_g$ is of course just the electromagnetic energy per unit length.

To evaluate (B2) two well known relationships in electromagnetic theory are used: the time-averaged force on a perfectly conducting surface, reflecting an electromagnetic wave, $F = \frac{\mu}{4}\iint H.H^*ds - \frac{\epsilon}{4}\iint E.E^*ds$ newtons, and the time-averaged energy stored in a volume, $\mathscr{E} = \frac{\mu}{4}\iiint H.H^*dv + \frac{\epsilon}{4}\iiint E.E^*dv$ joules. Substituting these in (B2) and using the field equations (A1), there results

$$v/v_g = (v/\mathbf{c})^2\left\{1 + \frac{\iint H'_\varphi.H'^*_\varphi ds_2}{\iint H_\varphi.H^*_\varphi ds_1}\right\}, \qquad \ldots\ldots (B3)$$

where the integral in the numerator is across the corrugated section of the guide and that in the denominator is across the open part. It will be seen that the

integral in the numerator is proportional to the losses in the dividing walls of the corrugations—which is the major part of the total losses—while that in the denominator is proportional to the power flow down the guide. Thus v/v_g is very nearly proportional to the attenuation. v_g/v has been computed for the case $v=c$, and the result is shown in figure 2.

It is interesting to notice that an observer moving down the guide at the group velocity v_g will observe no net energy flow past him, the forward flow of energy in the centre part being balanced by the backward flow in the corrugations which are moving past the hypothetical observer. Details of the appearance of waveguide fields to moving observers have been published (Hershberger 1945). This confirms that the group velocity is in this case also the velocity of energy flow, and indicates another method of deriving the group velocity.

APPENDIX C

FOCUSING

The need for focusing

(i) Consider a positively charged particle travelling down the waveguide parallel to the axis with velocity v. Let v be also the phase velocity of the electromagnetic wave at the same point as the particle. Gaussian (mixed) units will be used.

The particle is subjected to an outward radial force given by $F_\rho = eE_\rho - H_\varphi e v/c$, where e is the charge on the particle. But from waveguide theory $H_\varphi = (v/c)E_\rho$; therefore

$$F_\rho = eE_\rho\{1-(v/c)^2\}. \qquad \ldots\ldots(C1)$$

From waveguide theory it again follows that E_ρ is positive in the bunching and accelerating region of the wave (i.e. the region where E_z is positive and $\partial E_z/\partial z$ is negative). Hence, from (C1), F_ρ is positive in this region and the guide is diffusing. In fact E_ρ is always of the opposite sign to $\partial E_z/\partial z$.

(ii) Consider a similar case where the particle velocity is u but the wave velocity is still v. Then, arguing as before, we find that

$$F_\rho = eE_\rho\{1-uv/c^2\}. \qquad \ldots\ldots(C2)$$

Hence in this case the guide would only be focusing in the bunching region if $uv>c^2$; the wave would then have a greater velocity than the particle, which would involve phase changing at intervals, but the method provides a form of focusing not obtainable with a realizable form of magnetic field, and might be valuable in a long high-energy accelerator. It is not practicable to make use of this form of focusing unless the particle velocity is fairly close to c.

Magnetic focusing

It is possible to prevent the particles being diffused by immersing the accelerator in a steady longitudinal magnetic field. Ideally this field must be so designed that the particles are guided down the waveguide with the minimum expenditure of energy in the focusing magnet. This problem has not been solved to date, and we content ourselves with examining the field required to produce a particular form of guiding.

We assume that particles are to be guided down the accelerator in a helical path of small radius, r, centred on the axis of the accelerator, and consider the

case of an "equilibrium" particle, i.e. one in the stable phase position, and with constant phase angle.

Let H_z and H_ρ be the components of a circularly symmetrical steady magnetic focusing field and let the particle position be (ρ, ϕ, z).

Then the equations of motion are $d(m\rho^2\dot{\phi})/dt = -(e/\mathbf{c})\rho\dot{\rho}H_z + (e/\mathbf{c})\rho\dot{z}H_\rho$, which on integration gives

$$mr^2\dot{\phi} \simeq -\frac{e}{\mathbf{c}}\frac{r^2}{2}H_z + C, \qquad \text{.....(C3)}$$

where C is a constant, which we shall discuss later, and

$$d(m\dot{\rho})/dt - m\rho\dot{\phi}^2 = eE_\rho - (e/\mathbf{c})\dot{z}H_\varphi + (e/\mathbf{c})\rho\dot{\phi}H_z.$$

Now since $H_\varphi = (\dot{z}/\mathbf{c})E_\rho$ and $\dot{\rho} = 0$, we find from these equations

$$H_z^2 = 4\left[\left(\frac{\mathbf{c}}{e}\right)^2\left(\frac{C}{r^2}\right)^2 + \frac{m\mathbf{c}^2}{e}\frac{E_\rho}{r}\left\{1 - \left(\frac{\dot{z}}{\mathbf{c}}\right)^2\right\}\right].$$

Now, except at the beginning of an accelerator, it is nearly true to say that the particle energy is the same as if its velocity were $\dot{z}$. Hence we get

$$H_z^2 = 4\left[\left(\frac{\mathbf{c}}{e}\right)\left(\frac{C}{r^2}\right)^2 + \left(\frac{m_0\mathbf{c}^2}{e}\right)^2\frac{eE_\rho}{r}\frac{1}{m\mathbf{c}^2}\right]. \qquad \text{.....(C4)}$$

Thus (C4) gives the longitudinal component of the required field. It will be seen that it is desirable that C should be finite in order to secure stability, but not too large, as this would lead to unnecessary expenditure of focusing energy in the later stages of an accelerator; space charge should also contribute towards stability, but its effect is not easily estimated. For purposes of practical computation C is assumed negligible.

Note that if C is finite the focusing field H_z never vanishes. There are two explanations for this, depending upon the sign of C. In one case the particles eventually follow a path parallel to the accelerator axis without any angular momentum but in a field of finite H_z; although there is no focusing action, removal of H_z would itself create angular momentum. In the other case there is a residual angular momentum, which requires the focusing field to be continued.

In a practical accelerator the above formula for the focusing field does not hold near the beginning of the accelerator, since the electrons are not easily injected in bunches or in the proper direction to satisfy the conditions postulated. Calculations of the focusing field have been made for other special cases, corresponding to different electron trajectories, and the results have been surprisingly similar to the above. It is therefore concluded that the electron injection arrangements are not critical and that it is unlikely that any other trajectory can be found which would require substantially less focusing field.

Extension to practical cases

It has so far been the custom to design accelerating waveguides so that the peak longitudinal field on the axis, E_0, remains constant. It is therefore better to write (C4) in terms of E_0 and other convenient quantities.

From waveguide theory we have $E_\rho = E_0(\beta/\chi)J_1(\chi\rho)$, where $\beta = 2\pi/\lambda_g$, $\chi = (2\pi/\lambda_0)\{1 - (\mathbf{c}/v)^2\}^{\frac{1}{2}}$, and $v = \dot{z} =$ phase velocity of wave.

Assuming as before that the particle velocity is approximately $\dot{z}$, and putting $E_\rho = \hat{E}_\rho \cos\theta$, where θ is the particle-to-wave phase angle, we have from (C4)

$$H_z^2 = 4\left[\left(\frac{\mathbf{c}}{e}\right)^2\left(\frac{C}{r^2}\right)^2 + \frac{m_0\mathbf{c}^2}{e}\frac{E_0\cos\theta}{r}I_1\left(\frac{2\pi r}{\lambda_0}\frac{\mathbf{c}}{\dot{z}}\frac{m_0}{m}\right)\right].$$

We can put $$C \simeq 0; \quad I_1\left(\frac{2\pi r}{\lambda_0}\frac{\mathbf{c}}{\dot{z}}\frac{m_0}{m}\right) \simeq \frac{1}{2}\left(\frac{2\pi r}{\lambda_0}\frac{\mathbf{c}}{\dot{z}}\frac{m_0}{m}\right),$$

whence, writing the energy in terms of electron volts, we obtain as a practical formula

$$H_z^2 = 4(m_0\mathbf{c}^2/e)(E_0\cos\theta)(\pi\mathbf{c}/\lambda_0\dot{z})V_0/(V+V_0). \qquad \ldots\ldots(C5)$$

Example

Formula (C5) has been used to compute the longitudinal axial component of the magnetic focusing induction required for the 0.5 MEV. accelerator already referred to. Figure 9 shows B_z as a function of z for a number of different values of the radio-frequency input power W_0. It should be noted that changing W_0 changes both the strength of the radio-frequency fields and the stable phase angle θ, so that the focusing field changes more rapidly than it would if due to only one of these effects. For $W_0 = 0{\cdot}5$ MW. the focusing field is zero.

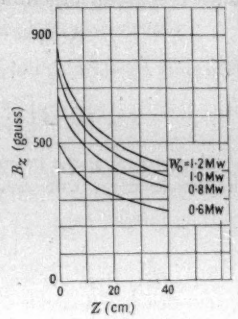

Figure 9.

REFERENCES

AKELEY, E. S., 1946, *Phys. Rev.*, **69**, 50, 255, 1946, *J. Appl. Phys.*, **17**, 1056.

ALLEN, W. D., and SYMONDS, J. L., 1947, *Proc. Phys. Soc.*, **59**, 622.

ALVAREZ, L. W., 1946, *Phys. Rev.*, **70**, 799.

BOOKER, H. G., 1947, *J. Instn. Elect. Engrs.*, **94**, pt. iii, 171.

BOWEN, E. G., PULLEY, O. O., and GOODEN, J. S., 1946, *Nature, Lond.*, **157**, 840.

COWHIG, W. T., 1946, *T.R.E. Memo.*, S1/M178/WTC.

COWHIG, W. T., and JONES, E. J., 1947, *T.R.E. Report*, A.E. 1008.

CUTLER, C. C., 1944, *Bell Tel. Labs. Report*, MM-44-160-218.

FRY, D. W., R.-SHERSBY-HARVIE, R. B., MULLETT, L. B., and WALKINSHAW, W., 1947, *Nature, Lond.*, **160**, 351.

HALPERN, J., EVERHART, E., RAPUANO, R. A., and SLATER, J. C., 1946, *Phys. Rev.*, **69**, 688.

HAXBY, R. O., *et al.*, 1946, *Phys. Rev.* **70**, 797.

HERSHBERGER, W. D., 1945, *J. Appl. Phys.*, **16**, 465.

HUDSPETH, E. L., 1946, *Phys. Rev.*, **69**, 671.

LAMONT H. R. L., 1942, *Wave Guides* (London : Methuen & Co.).

MACLEAN, W. R., 1945, *Proc. Inst. Radio Engrs.*, **33**, 539.

MORRISON, P., 1947, *J. Appl. Phys.*, **18**, 133.

MULLETT, L. B., 1946, *T.R.E. Report*, T2021 ; 1947, *Ibid.*, AE1006, AE1007.

MULLETT, L. B., and LOACH, B. G., 1948, *Proc. Phys. Soc.* **61**, 271.

SCHELKUNOFF, S. A., 1943, *Electromagnetic Waves* (New York : D. Van Nostrand).

SCHIFF, L. I., 1946, *Rev. Sci. Instrum.* **17**, 6.

SCHULTZ, H. L., *et al.*, 1947, *Phys. Rev.*, **72**, 346.

SLOAN, D. H., and COATES, W. M., 1934, *Phys. Rev.*, **47**, 539.

SLOAN, D. H., and LAWRENCE, E. O., 1931, *Phys. Rev.*, **38**, 2021.

TAYLOR, H. E., 1946, *T.R.E. Report*, A.E.1000.

WALKINSHAW, W., 1947, *T.R.E. Report*, A.E. 1005 ; 1948, *Proc. Phys. Soc.*, **61**, 246.

WILLSHAW, W. E., and LAMONT, H. R. L., 1945, *Confidential Report from Research Labs. of General Electric Co. Ltd.*, No. 8766(B).

Experimental Work on Corrugated Waveguides and Associated Components for Linear Electron Accelerators

By L. B. MULLETT and B. G. LOACH
Atomic Energy Research Establishment, Harwell

Communicated by J. D. Cockcroft; MS. received 17 *March* 1948

ABSTRACT. This paper describes experimental work carried out on corrugated waveguides in connection with the development of an electron linear accelerator.

The general problem of feeding R.F. power from a conventional rectangular waveguide is considered and several successful "feeds" are described.

Finally, the work carried out on corrugated circular waveguides with continuously varying phase velocities and their associated "feeds" for the 0·5 MeV. and 4 MeV. sections of long accelerators is described in some detail. It is shown that the experimental results are in close agreement with the theoretical treatment of Harvie, Cutler and Walkinshaw.

§1. INTRODUCTION

The development of the linear accelerator in the form described by Harvie (1948), involved a considerable programme of experimental work on corrugated (or loaded) waveguides. From the wide variety of possible modes and geometrical systems, the corrugated circular waveguide carrying an E_{01} type of mode was very soon chosen as the most likely basis for a travelling-wave type of accelerator. One other possible geometry was considered—a rectangular waveguide loaded on one of the broad faces with rectangular corrugations somewhat longer than a half-guide wavelength—and a certain amount of theoretical and experimental work was carried out on this system, although this work was later abandoned in favour of the circular corrugated waveguide system.

The programme of experimental work was initially directed towards testing the accuracy of various theoretical treatments (of ever increasing complexity) in order to establish a means of designing systems with predetermined laws relating phase velocity and accelerating field to distance.

The design wavelength is 10·00 cm. throughout.

§2. CONSTRUCTION

A mechanical form taken by a corrugated circular waveguide is shown in figures 1 and 2. Separate sections are machined from pure copper with a general tolerance of $\pm 0{\cdot}0005$ in. on all internal dimensions. These sections are self located by spigots and are soft-soldered together on the outside as shown in figure 2. Other forms of construction are being considered. Each section has four 3/16 in. diameter holes spaced 90° apart both for measurement purposes and for evacuation in the actual accelerators.

§3. WAVEGUIDES HAVING CONSTANT PHASE VELOCITIES

(i) *The first experimental waveguide*

The theoretical approach was an improved form of that originally given by Cutler (1944). The phase velocity was designed to be equal to the velocity of

light for an air wavelength of 10·00 cm. The inner hole was chosen to give a maximum axial field of 100 kv/cm. for a radio frequency power of 2 MW. (this being the highest power readily available at present). The dimensions were as follows: number of corrugations per wavelength $N=10$, pitch of corrugations $D=1$ cm., ratio of width of corrugation to pitch $K=0{\cdot}75$, inner radius of corrugations $a=1$ cm., outer radius of corrugations $b=3{\cdot}944$ cm. Unlike all subsequent guides, the manufacturing tolerances were of the order of $\pm 0{\cdot}001$ in., although care was taken to prevent any build-up of tolerances over the total length (25 cm.), and the material used was brass, the sections being clamped together without soldering.

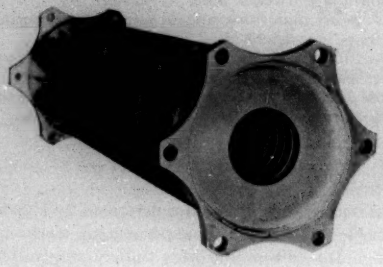

Figure 1. 40 cm. length of corrugated circular guide.

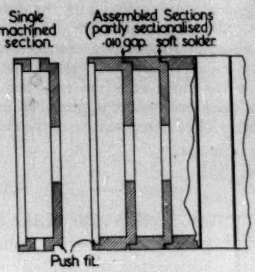

Figure 2. Construction of corrugated circular waveguide. The sections are clamped together and the 0·010 in. gap is filled with soft solder as shown.

Measurements of phase velocity were carried out using a low power klystron oscillator and a coaxial line test bench. The feed into the guide was a coaxial probe, approximately a quarter wavelength long, introduced along the axis. The amount of power fed into the corrugated guide was only a small fraction of that available and could not be improved upon by any simple change of dimensions, but was adequate for this purpose. A tuned crystal detector of standard form (Huxley 1947) fitted with a small pick-up loop was inserted through the measuring holes in the outer wall so as to be lightly coupled to the magnetic field. The phase of the magnetic field in the corrugations varied with distance in the same manner as the phase of the fields on the axis at the centre of each corrugation.

With the end of the guide short-circuited by a flat metal plate the standing wave pattern was plotted in a similar manner to those shown for later cases, e.g. figure 3. The distance between adjacent minimum values gives half the guide wavelength, from which the phase velocity is given by $v_p = \mathbf{c}\lambda_g/\lambda$ where λ is free space wavelength, λ_g is the wavelength in the guide, $\mathbf{c}$ is the velocity of light. For $\lambda = 10{\cdot}00$ cm. the guide wavelength was of the order of 10 cm. At shorter air wavelengths the phase velocity decreased as expected and standing wave patterns were readily plotted for guide wavelengths as short as 3 cm. ($v_p = 0{\cdot}3\,\mathbf{c}$). At longer air wavelengths the guide wavelength became indeterminate because of a rapid onset of attenuation. This was later found to be mainly due to the poor frequency spectrum of the oscillator combined with the fact that the low-frequency cut off was less than 10 Mc/s. from the design

frequency (2998 Mc/s). Trouble was also experienced with bad contacts between the unsoldered sections.

(ii) *Accurate experimental results*

The first guide had indicated that a less frequency sensitive system should be employed in the early stages. A guide was therefore designed on the basis of 25 kv/cm. (for 2 MW. of R.F. power) with dimensions $N=10$, $D=1$ cm., $K=0{\cdot}75$, $a=2$ cm., $b=4{\cdot}288$ cm., total length of guide 40 cm.

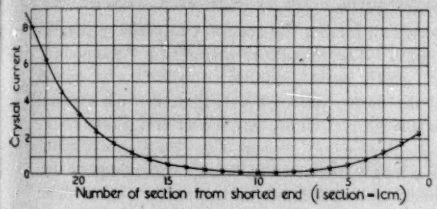

(*a*) $\lambda=10{\cdot}604$ cm.; λ_g indeterminate.

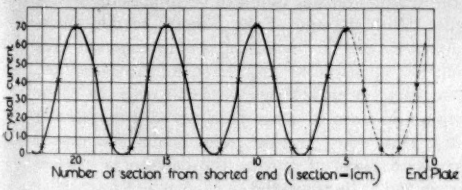

(*b*) $\lambda=10{\cdot}002$ cm.; $\lambda_g=10{\cdot}00$ cm.

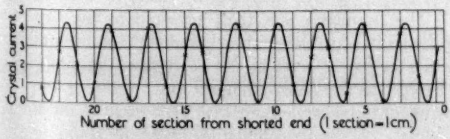

(*c*) $\lambda=9{\cdot}200$ cm.; $\lambda_g=4{\cdot}7$ cm.

Figure 3. Corrugated circular guide. Variation of standing wave pattern with frequency. $a/\lambda=0{\cdot}2$; $K=0{\cdot}75$; 1 cm. pitch.

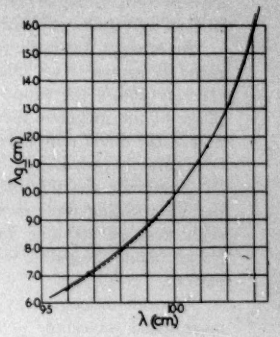

Figure 4. $\lambda-\lambda_g$ corrugated circular guide. (1 metre length.) $a/\lambda=0{\cdot}2$; $K=0{\cdot}75$; 1 cm. pitch.

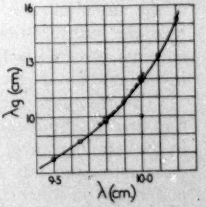

× simple theory.

Figure 5. $\lambda-\lambda_g$ for corrugated circular guide with 2 cm. pitch. $K=0{\cdot}875$. $a/\lambda=0{\cdot}2$. b calculated on simple theory to give $\lambda_g=10$ cm. for $\lambda=10$ cm.

——⊙—— experimental
— — — — new theory (Walkinshaw).

Typical standing wave curves for the short-circuited guide for values of air wavelength around 10·0 cm. are shown in figures 3 (*a*), (*b*), (*c*). Graphs of the relation between the air and guide wavelengths showed fairly close agreement between the experimental results and the theory used to design the guide.

The length of the guide was eventually increased to 100 cm. in order to obtain a reliable measurement of attenuation. The accuracy of the standing wave measurements was again improved and slight irregularities in manufacture and

assembly were smoothed out. The final curve of λ and λ_g (figure 4) shows remarkable agreement with the more rigorous theoretical treatment (Walkinshaw 1948).

The group velocity can also be obtained from this curve. The general expression is

$$\text{Group velocity } v_g = \mathbf{c}(d\lambda/d\lambda_g)(\lambda_g/\lambda)^2;$$

at $\lambda_g = \lambda$ (i.e. the design wavelength), $v_g = \mathbf{c}(d\lambda/d\lambda_g)$. The slope of the curve at $= 10{\cdot}0$ cm. is $d\lambda_g/d\lambda = 10{\cdot}75$, giving a value for v_g of $0{\cdot}093\,\mathbf{c}$, which is again in close agreement with the theoretical value.

An attempt was made to increase still further the accuracy of phase measurement by means of a "phase meter". The apparatus included a "magic T" (Huxley 1947), the properties of which were used for comparing the actual phase of the magnetic field near the outer wall of a corrugation with a small part of the direct power from the R.F. source, whose amplitude and phase could be accurately varied.

The guide was terminated in a long wooden cone, which was adequate for normal standing wave measurements and could not be improved upon. The slight residual standing wave produced a large cyclic variation on the phase pattern along the guide, which was little better than plotting the standing wave pattern.

Accurate measurement of the attenuation was found to be impossible by the more usual waveguide methods. With the end of the 1-metre section short-circuited, the standing wave pattern showed no obvious signs of attenuation—the standing wave ratio at the input end appeared as large as at the short-circuited end. The normal method resorted to in such a case is to measure the shape of the minimum, but, assuming a minimum to occur precisely at a monitoring hole, the next measurable point is 1 cm. away, and the range of detector crystal currents involved is far too great. Instead of moving the detector a method involving slight frequency changes had to be employed.

The procedure was as follows: With an air wavelength of 10·00 cm. a corrugation near the input end was chosen which was as close as possible to a minimum in the standing wave. The input frequency was then slightly changed until an exact minimum was obtained. The frequency was then adjusted to the two points (one on either side) where the crystal current was twice that at the minimum (allowance being made for changes in power level in the corrugated guide by monitoring in the corrugation nearest to the short-circuited end). The guide was sufficiently long for the experiment to be carried out with very small changes in frequency (of the order of 1 Mc/s). A simple calculation gives the standing wave ratio, n, in terms of the total frequency excursion, the length l from the measuring point to the short-circuited end of the guide, and the group velocity v_g already obtained:

$$n = (\pi l/v_g)(\Delta f/f) \quad (n<1),$$

$$\text{attenuation} = (10/l)\log[(1+n)/(1-n)] \quad \text{db/metre}.$$

The procedure was repeated with a measuring point near the centre of the guide. The difference between the total losses measured in the two cases gave the attenuation for twice the length of guide between the two measuring points, independent of any imperfections in the short-circuiting plate. The average value so obtained was 0·85 db/metre—this being approximately twice theoretical.

This is an encouraging figure since even plain waveguides will give values twice theoretical merely due to imperfections of the metal and its surface. Careful cleaning of the guide gave no appreciable improvement, and the excess loss was therefore assumed to be in the joints between the sections.

(iii) *Reduction of the number of corrugations per guide wavelength*

It is desirable from the point of view of attenuation to reduce the number of corrugations per guide wavelength, and it has been shown theoretically (Walkinshaw 1948) that optimum efficiency of an accelerator is obtained when N is approximately 4.

A guide was therefore constructed with a corrugation pitch of 2 cm. ($N=5$ at $\lambda=\lambda_g=10$ cm.). The dimensions were: $K=0{\cdot}875$, $a=2$ cm., $b=4{\cdot}171$ cm., obtained from early theory, total length 40 cm. The measurement of guide wavelength became even more difficult because of the reduced number of discrete measuring points per guide wavelength. A curve showing the relationship between the guide and air wavelengths is given in figure 5. Although the experimental results (full line) differed considerably from the values given by the early theory used to design the guide (represented by the cross at $\lambda_g=\lambda=10$ cm.) there was extremely close agreement with the final treatment (Walkinshaw 1948) whose validity had not been so obviously demonstrated for guides with 1 cm. pitch ($N=10$).

(iv) *General phase velocity measurements*

In order to demonstrate the general behaviour of this type of guide, phase velocity measurements were carried out with a set of guides having the characteristics shown in table 1.

Table 1

Guide no.	Pitch (cm.)	K	a (cm.)	b (cm.)*	Guide no.	Pitch (cm.)	K	a (cm.)	b (cm.)*
1	1	0·75	1·0	3·944	4	2	0·875	1·0	3·894
2	1	0·75	1·5	4·085	5	2	0·875	1·5	4·002
3	1	0·75	2·0	4·288	6	2	0·875	2·0	4·171

* b for $\lambda_g=\lambda=10$ cm. from original theory.

An oscillator of much narrower frequency spectrum than had been available previously was used throughout. The resulting standing wave patterns for the guides with an inner radius as small as 1 cm. were quite good in spite of their high frequency sensitivity.

Figures 6 (*a*) and 6 (*b*) show graphs of λ_g against λ for the guides having 1 cm. and 2 cm. pitches respectively.

(v) *Corrugated guides with phase velocities less than that of light*

Two guides were constructed having phase velocities of 0·4 **c** and 0·87 **c** for $\lambda=10$ cm., these corresponding to the input and output ends of a proposed 0·5 Mev. accelerator. Both guides had a pitch of 1 cm. and $K=0{\cdot}75$. At the input end, $a=1{\cdot}3602$ cm. and $b=4{\cdot}1814$ cm.; at the output end, $a=1{\cdot}8948$ cm. and $b=4{\cdot}2751$ cm. Guide wavelengths of 4 cm. and 8·7 cm. were obtained for $\lambda=10$ cm. in close agreement with the theory.

It was therefore concluded that, for all experimental purposes, an adequate theoretical approach had been established.

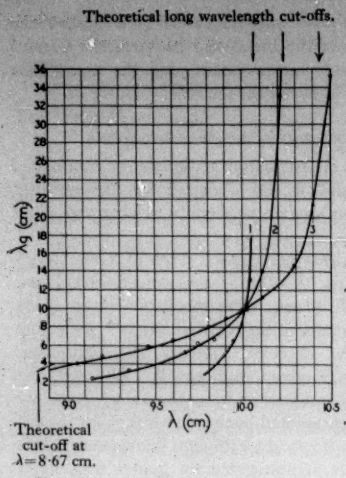

Figure 6 (*a*). Circular corrugated guides.
Corrugation pitch 1 cm.
Varying a/λ.

Type	a/λ	$2a$
1	0·1	2 cm.
2	0·15	3 cm.
3	0·2	4 cm.

(All guides calculated to give $\lambda_g = 10{\cdot}0$ cm. at $\lambda = 10{\cdot}0$ cm.)

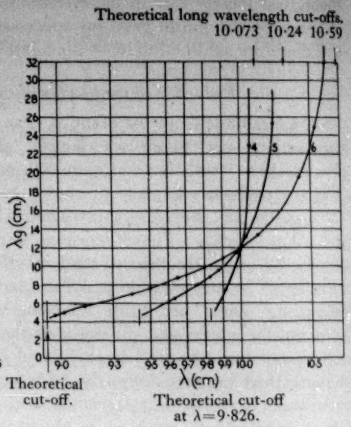

Figure 6 (*b*). Circular corrugated guides.
Corrugation pitch = 2 cm.
Varying a/λ.

Type	a/λ	$2a$
4	0·1	2 cm.
5	0·15	3 cm.
6	0·2	4 cm.

(All guides calculated to give $\lambda_g = 10{\cdot}0$ cm. at $\lambda = 10{\cdot}0$ cm.)

§4. FEEDS FOR CORRUGATED GUIDES

The design of suitable feeds from the standard rectangular waveguide to the circular corrugated guide presented many difficulties. The primary consideration is that the feed should allow the electrons to be injected along the axis of the corrugated guide, and in doing so should not expose the beam to appreciable fields until it enters the accelerating field proper.

The simple quarter wavelength probe along the axis was very soon discarded for anything except low power measurements.

The obvious method of slowly tapering from a smooth E_{01} guide to the corrugated guide is very clumsy; the beam is subjected to undesirable fields, and its only virtue, that of wide bandwidth, is quite unnecessary for the application considered.

(i) *Annular hole feed*

Several mechanically suitable feeds were tried, one of which yielded quick results since some theoretical design was possible. It consisted of a coaxial line tapered to a low impedance and fed directly into the first corrugation as shown in figure 7. The electron beam could enter through a hole down the centre of the inner conductor and R.F. power was fed to the coaxial line from a standard rectangular waveguide ($3 \times 1\frac{1}{2}$ in. o.d.) by means of a "door knob" transformer (Huxley 1947).

The conditions which it was essential, or desirable, to satisfy were: (*a*) the coaxial line should be of a convenient impedance (40 ohms); (*b*) the coaxial line to be below cut-off for the first waveguide mode (H_{11}) so as to eliminate any possibility of propagation of an asymmetrical mode from the rectangular guide into the corrugated guide; (*c*) the inner conductor to be as large as possible when satisfying the above conditions; (*d*) the coaxial line to be tapered to match into the first corrugation at a point between its inner and outer radius; (*e*) the electric fields should be limited to 100 kv/cm. or less for an R.F. power of 2 MW. to reduce the possibility of breakdown.

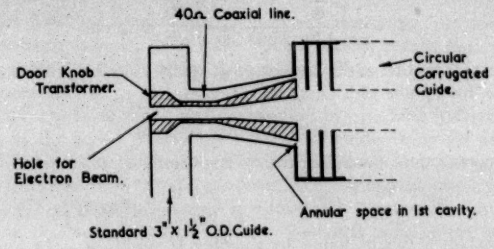
40Ω. Coaxial line.
Door Knob Transformer.
Circular Corrugated Guide.
Hole for Electron Beam.
Annular space in 1st cavity.
Standard 3" x 1½" O.D. Guide.

Figure 7. Arrangement of annular hole feed.

Since the corrugated guide is effectively a high Q device we expect the value of the field strength at any point to be independent of the point at which the power from the source is introduced.

In order to obtain a match the wave impedance looking into the annular hole must be identical with that of a matched coaxial line with the same inner and outer radii, i.e.

$$E'_\varrho/H'_\varphi = E''_\varrho/H''_\varphi, \qquad \ldots\ldots(1)$$

where E'_ϱ is a radial component of electric field assumed to have been introduced into the corrugation by the annular gap, H'_φ is the magnetic field in the corrugation at the mean radius of the annular gap, E''_ϱ and H''_φ are the fields in a coaxial line.

If the coaxial line is terminated everywhere by its own impedance all the power will be transmitted through the annulus, and integrating the Poynting vector over the annular space it follows that

$$\int_s E'_\varrho H''_\varphi \, ds = \int_s E''_\varrho H''_\varphi \, ds. \qquad \ldots\ldots(2)$$

If it is assumed that the field variations between the inner and outer radii of the annulus are small for both the coaxial line and the corrugation, then the integration signs can be removed. Hence if H'_ϱ and H''_φ are equated at the mean radius of the annulus, the equality of E'_ϱ and E''_ϱ follows automatically.

The 40-ohm coaxial line chosen to satisfy the required conditions had inner radius $r = 1{\cdot}03$ cm. (0·406 in.) and outer radius $R = 2$ cm. (0·787 in.). This allowed a fairly large diameter hole (5/8 in. maximum) for the electron beam. The fields in a coaxial line (in M.K.S. units) are:

$$E''_\varrho = A'(1/\rho), \qquad \ldots\ldots(3)$$

$$H''_\varphi = A'(\epsilon/\mu)^{\frac{1}{2}}(1/\rho). \qquad \ldots\ldots(4)$$

The constant A' is found by integrating the Poynting vector over the cross-sectional area normal to the axis of propagation:

Mean power

$$\overline{W} = \tfrac{1}{2}\int_s E''_\varphi H''_\varphi \, ds, \qquad \ldots\ldots(5)$$

Hence

$$A' = \left[\frac{\overline{W}}{\pi}\left(\frac{\epsilon}{\mu}\right)^{\frac{1}{2}} \frac{1}{\ln R/r}\right]^{\frac{1}{2}} \qquad \ldots\ldots(6)$$

and

$$H''_\varphi = \frac{1}{\pi\rho}\left[\frac{\overline{W}}{120} \cdot \frac{1}{2{\cdot}303 \log R/r}\right]^{\frac{1}{2}} \text{ amp/cm.} \qquad \ldots\ldots(7)$$

In the centre portion of the corrugated guide by a similar process, in the limit as $v_p \to \mathbf{c}$ (i.e. for a guide with phase velocity $= \mathbf{c}$):

$$H_\varphi = (\rho/\pi r^2)(\overline{W}/30)^{\frac{1}{2}} \text{ amp/cm.} \qquad \ldots\ldots(8)$$

Inside the corrugations the magnetic field is given by

$$H'_\varphi = \frac{iB}{120\pi}\left[J_1(2\pi\rho/\lambda) - \frac{J_0(2\pi b/\lambda)}{Y_0(2\pi b/\lambda)} Y_1(2\pi\rho/\lambda)\right]. \qquad \ldots\ldots(9)$$

The constant B can be found by equating H_φ to H'_φ at $\rho = a$, and hence H'_φ and H''_φ can be equated for a range of values of ρ. As ρ increases the gap width becomes very small, an undesirable feature since the inner of the coaxial line is liable to sag.

For the guide having $a/\lambda = 0{\cdot}2$ and a pitch of 1 cm. the value of ρ was chosen to be 2·5 cm. so that the feed would be clear of higher order modes near the mouth of the corrugation. The gap width was then 0·218 cm. and the electric field E''_φ across it 21·9 kv/cm. (for 2 MW. R.F. power). An experimental feed made up precisely as calculated was tested, and found to have a standing wave ratio of 0·56/1 which varied very little with changes in frequency.

The effect on the standing wave ratio of eccentricity of the inner portion of the feed with respect to the outer, and of axial displacement of the inner, was extremely small, but the introduction of the hole for the electron beam had a marked effect. An optimum of the standing wave ratio (0·7/1) was obtained for a hole diameter of 1·10 in., probably due to the conditions in the end cavity of the corrugated guide approximating more exactly to the theoretical case.

No high power measurements were made at this stage but it seemed clear that no breakdown troubles would occur. The annular hole appeared to be the limiting factor, but even here the calculated fields showed a wide margin of safety. That these assumptions were true was borne out by later experience with an actual accelerator.

A similar feed was designed and constructed for the very critical guide with $a/\lambda = 0{\cdot}1$. The mean radius chosen was 1·50 cm. giving a gap width of only 0·058 cm. Even so the feed showed signs of working, its standing wave ratios being 0·53/1, 0·52/1 and 0·29/1 at air wavelengths of 9·90, 9·93 and 9·97 cm. respectively.

The measure of success obtained led to this type of feed being adopted for the first linear accelerator. The fields in the corrugated guide are more complicated when the guide has a phase velocity less than $\mathbf{c}$. Then $1 - (\mathbf{c}/v_p)^2$ becomes negative.

Hence the magnetic field within the inner diameter of the corrugations is given by

$$H_\psi = E_0\left[\frac{\mu}{\epsilon}\left\{\left(\frac{c}{v_p}\right)^2 - 1\right\}\right]^{-\frac{1}{2}} I_1\left[\frac{2\pi\rho}{\lambda}\left\{\left(\frac{c}{v_p}\right)^2 - 1\right\}^{\frac{1}{2}}\right], \quad \ldots\ldots(10)$$

where E_0 is the accelerating field along the axis. The calculation then proceeds as before.

(ii) *Short door-knob feed*

One other feed has been found to work experimentally. It offers several advantages over the annular hole feed. The length of coaxial line, which was difficult to assemble correctly and greatly obstructed the electron beam, has been effectively removed.

The object was to feed the first corrugation by attaching it directly and at right angles to the broad face of the rectangular guide, using for convenience a hole of the same size as the inner diameter of the corrugated guide. The coaxial line and door-knob transformer were then compressed into a short door-knob forming a circular projection of appropriate dimensions (as shown in figure 8) from the outer broad face of the rectangular guide to the first hole of the corrugated guide. For almost any diameter of post, P, with its corresponding radius of curvature S, it is possible to obtain a good match by adjustment of its

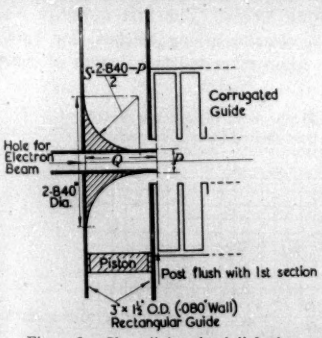

Figure 8. Short " door knob " feed.

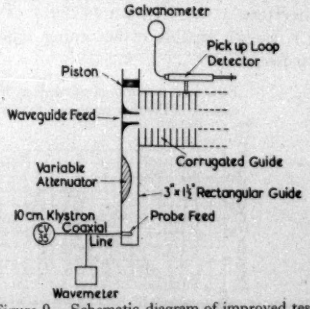

Figure 9. Schematic diagram of improved test gear using short " door knob " feed.

length Q, using the terminating piston in the rectangular guide as another variable. It is then found that with small diameters the post does not reach the entrance to the first cavity, with large diameters the post projects into the cavity, and as P is further increased the optimum position no longer gives a perfect match. It is possible to choose a diameter which will give a perfect match with the post flush with the first section.

This feed has been used for uniform guides with values of a/λ as small as 0·1 although the setting of the variables to obtain a perfect match is rather critical. It is also being incorporated in a 4 MeV. accelerator, and although no high power tests have yet been carried out, no breakdown troubles are expected.

The test equipment and procedure is very much simplified when a purely waveguide feed of this type is used, as shown in figure 9. The mechanical arrangement allows the door-knobs to be interchanged with great ease.

§ 5. CORRUGATED CIRCULAR WAVEGUIDE WITH CONTINUOUS VARIATION OF PHASE VELOCITY

A theoretical treatment for guides of uniform phase velocity being established, the design of a waveguide system for an actual accelerator followed similar lines. The velocity of the injected electrons was chosen to be 0·4 **c**, equivalent to a gun voltage of 45 kv. In order to simplify the manufacture a constant corrugation pitch of 1 cm. was chosen. The number of corrugations per guide wavelength at the beginning of the accelerator was therefore considerably less than ten, but the theory had been shown to be accurate down to five corrugations. In order to simplify the computation of electron energy against distance down the accelerator, the inner diameter of the corrugations was reduced at low phase velocities in order to maintain a constant accelerating field on the axis.

Two such systems have been designed (Walkinshaw 1948) and manufactured.

(i) 0·5 MeV. *bunching section of a long accelerator*

It was originally considered that the initial section of a linear accelerator working from 45 kev. injected electrons up to the order of 0·5 MeV. would present the major difficulties, since we have large variations of phase velocity, strong bunching forces, and also strong defocusing forces. The first objective was therefore a short length (40 cm.) of an accelerator giving 540 kev. for 1 MW. R.F. power capable of becoming efficient when extended to a length of some 10 metres.

Figures at maxima on graph (e.g. 40·0, 4·0) represent: the detector crystal current at the maximum and the distance from cavity 1 (in cm.), respectively

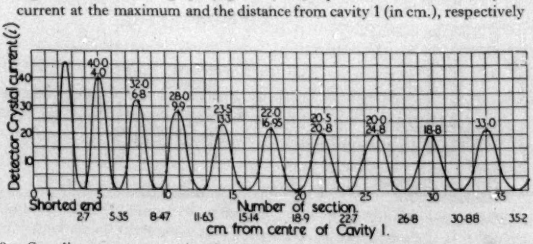

Figure 10. Standing wave pattern in 40 cm. tapered guide for 0·5 MeV. linear electron accelerator. Voltage maxima are obtained from $\sqrt{}$(crystal current) $\times$ (factor taking into account changes in wall thickness).

(*a*) *Corrugated guide.* The phase along the guide was again obtained from a plot of the standing wave pattern with one end short-circuited. The maxima and minima determine phase intervals of $\pi/2$. The theoretical and experimental phase curves are shown in figure 10. The agreement is a remarkable tribute to the theory, manufacture and measurements. It can be seen from the standing wave pattern that the magnetic field which is measured near the outer wall of the corrugations decreases from the 0·4 **c** end. This is not due to attenuation. At $v_p < \mathbf{c}$, both the magnetic field H_φ and electric field E_z varying, as I_1 and I_0

functions of ρ (Bessel functions of an imaginary argument), have minimum values on the axis. The inner hole having therefore been reduced to give uniform accelerating field on the axis, the fields at the outside of the guide will be greatest at the low velocity end. The maxima in the standing wave pattern represent in the ideal case the squares of the magnetic fields (H_φ) at the outer wall. By working at very low crystal currents and applying corrections for crystal law, and certain mechanical factors, H_φ was obtained with some measure of accuracy, and compared graphically with calculated values. The agreement was close, considering the complexity of the measurements, and was a convincing demonstration of the uniformity of the axial accelerating field.

(*b*) *Input and output* R.F. *feeds.* Feeds of the tapered coaxial line type were chosen for this accelerator. The dimensions were finally obtained from a consideration of sets of graphs such as that shown in figure 12 for the output end, and are given in table 2.

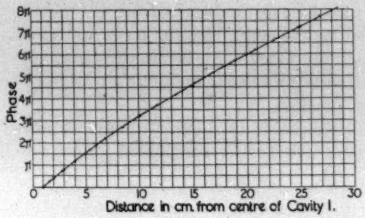

Figure 11. Phase in 40 cm. tapered guide.
Next points: 28·8, 8·2π; 30·88, 8·7π; 33·0, 9·2π; 35·2, 9·7π.
From voltage max. and min. curve (figure 10).
Adjusted to same phase at 2nd maximum (4·0).

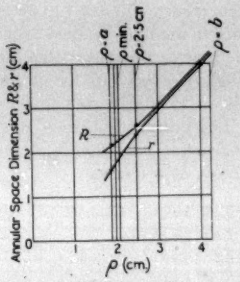

Figure 12.
Design data for output feed.
(0·5 MeV. accelerator.)

Table 2

	ρ (cm.)	a (cm.)	b (cm.)	Z_0 (ohms)
Input feed	1·8	1·725	1·875	5·0
Output feed	2·5	2·409	2·591	4·4

Experimental feeds were made to these dimensions and the size of the electron hole was adjusted to give the best match. The sharp edges of the annular gap and the electron hole were slightly rounded. The standing wave voltage ratios were then 0·55/1 for the input feed and 0·53/1 for the output feed. It was found impracticable, by alteration of those dimensions easy to vary, to obtain a better match for the feeds alone. However, it was again found possible, when the feeds combined with their waveguide to coaxial transformers were assembled in the end sections of the accelerator envelope, to obtain an improved match by axially adjusting the inner portions of the feeds, thereby obtaining standing wave ratios of 0·58/1 and 0·76/1 for the input and output feeds respectively. The final matching was carried out by the use of inductive irises in the main rectangular guide as near to the waveguide to coaxial transformers as possible, and gave standing wave ratios of 0·976/1 for the input end and 0·94/1 for the output end. The standing wave ratio of the corrugated waveguide system

complete with feeds was found to be 0·895/1 looking into the input (0·4 **c**) end and 0·94/1 looking into the output (0·87 **c**) end, the discrepancy being attributed to the attenuation of the corrugated guide.

When finally assembled as an accelerator (Fry, Harvie, Mullett and Walkinshaw 1947) with a vacuum-tight steel dummy load and a directive feed for monitoring, the overall standing wave ratio presented to the magnetron was found to be better than 0·95/1 at a wavelength of 10·00 cm.

(ii) 4 MeV. *section of a long accelerator*

The second experimental waveguide system was again designed as the initial section (2 metres) of an accelerator capable of being extended to some 10 metres in length. The peak accelerating field per megawatt of R.F. power was chosen to be the same as for the 0·5 MeV. accelerator, but the power required to give an initial stable electron position of 45° was increased to 2 MW. The first 40 cm. length was designed so that the R.F. phase velocity was slightly greater than the velocity of the stable electron, in order to decrease the phase angle linearly from 45° to 35°, and hence to increase the field experienced by the stable electron as the amplitude of the phase oscillations within the bunch decreased. At 40 cm. the phase velocity is slightly reduced to that of the stable electron so as to maintain a constant phase angle of 35° for the remainder of the 2 metres.

The corrugation pitch was again chosen to be 1 cm. throughout, and the construction was almost identical with that of the corrugated guides for the 0·5 MeV. accelerator.

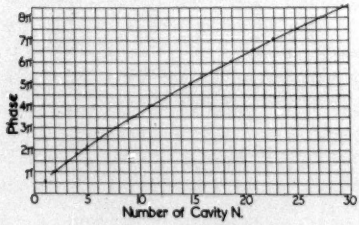

× Practical. ○ Theoretical.

Figure 13 (*a*). Phase at beginning of 2 metre tapered guide (for 4 MeV. linear electron accelerator).

Relatively adjusted to coincide at 7π ($N=23$) since this is an extremely accurate point.

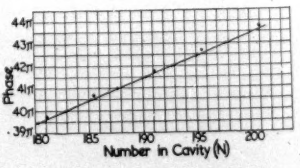

× practical. ○ theoretical.

Figure 13 (*b*). Phase at end of 2 metre tapered guide.

In order to correct the phase the wavelength should be decreased, i.e. effectively deeper corrugations. This could not be achieved with metallic screws.

(*a*) *Phase measurements.* A standing wave curve was plotted for the complete 2 metre length and a curve of phase against length obtained. Figures 13 (*a*) and (*b*) show the interesting regions near the beginning and end of the accelerator. The theoretical phase curve has been adjusted to fit the experimental curve at cavity 23, this being an accurately defined experimental point. Slight fluctuations in phase in the cavities before this are relatively unimportant since the electron velocity will be well below **c** and can adjust itself to the wave. The error between theoretical and experimental phase at the end of the 2 metres is 18° (in 22 wavelengths), corresponding to a mean wavelength error of 1 part in 400. This error is cumulative throughout rather than random, hence it would appear that errors due to

manufacturing tolerances are negligible and that the purely theoretical error is far smaller than had been expected. In the actual accelerator such an error could be corrected by a small change in frequency. There was also some indication on the graph of the phase jump in the region of the 40th section.

The 18° phase error in 22 wavelengths is tolerable for this accelerator. Longer accelerators would require some correction to be applied at intervals of this order—or possibly less (Harvie 1948). The introduction of 3/16 in. diameter dielectric or metal rods into the corrugations has been tried, and although a phase correction of the required order could be produced with only a few rods, it was necessarily in one direction only and was accompanied by a sharp rise in attenuation (possibly due to the setting up of an asymmetrical mode) especially in the case of the dielectrics. Short correcting sections of corrugated guide provide the best solution.

(*b*) R.F. *feeds.* The short door-knob feed was used for this accelerator. For the 0·4 **c** end of the accelerator the inner diameter of the corrugated guide was 2·72 cm.; the largest diameter of post which would give a perfect match when flush with the first section was 1·7 cm. This gave a 1·5 cm. diameter hole for the injection of electrons from the gun.

At the output end of the accelerator it is permissible for the post to project into the last section; the post diameter was therefore increased to the maximum of 3·2 cm. with a projection into the last cavity of approximately 3 mm. in order to obtain a perfect match. This gives an electron hole of 3 cm. diameter and a prospect of higher beam current leaving the accelerator. If the hole into the corrugated guide is increased in order to fit a still larger diameter of post, it is difficult to obtain a good match since the projection into the corrugated guide becomes excessive. The rectangular piston had to be soldered into the guide to obtain good contact and also to form a vacuum joint, hence it was found desirable to have a preset screw projecting through the centre of the piston and acting as a very fine variable. In this way final standing wave ratios of 0·96/1 to 0·97/1 were obtained for the input and output feeds.

The behaviour of these feeds to changes in frequency is of considerable interest. It is necessary that a good match should be maintained over the working band of frequencies. If an arbitrary figure of $\pm\frac{1}{8}$ Mc/s. for the magnetron frequency stability is chosen as a basis for design, then this particular accelerator could be extended to a length of some 10 metres, and the associated components (in particular the feeds here described) need only be efficiently matched over a bandwidth of this order.

The bandwidth of the present feeds for a standing wave ratio of 0·9/1 or better are for the input ± 3 Mc/s., for the output ± 4 Mc/s. The BM 735 magnetron, which will again be used, can be pulled in frequency by the order of ± 3 Mc/s. It will therefore be possible even with this two metre length to change the phase at the end of the accelerator by at least $\pm 0{\cdot}4\pi$ without deterioration of the R. F. system. This will adequately cover the interesting regions of operating conditions.

(*c*) *Overall performance.* The standing wave ratio of the complete corrugated guide and feeds was 0·96/1.

The attenuation of the complete system was determined by replacing the dummy load with a short-circuited guide and measuring the standing wave ratio in the input rectangular guide. The mean value obtained was 2·5 db. By removing 40 cm. sections the guide itself was found to have a loss of approximately 0·9 db. per metre, leaving a residue of about 0·7 db. for the two feeds and various

joints in the rectangular guides. This attenuation is again twice the theoretical value but is not excessive for this accelerator. It will, however, be desirable in future accelerators of efficient lengths to increase the pitch to 2 cm., except in the initial region, so as to halve the losses. It will also be acceptable (although not imperative) if new methods of construction now in hand give losses near to the theoretical values.

ACKNOWLEDGMENTS

The authors wish to express their appreciation of the assistance given to them by their colleagues during the carrying out of this work in the Electronics Group of the Atomic Energy Research Establishment at the Telecommunications Research Establishment, Malvern. Acknowledgment is made to the Director, Atomic Energy Research Establishment, Ministry of Supply, for permission to publish these results.

REFERENCES

CUTLER, C. C., 1944, *Bell Tel. Labs. Report*, MM/44/160/218.

FRY, D. W., HARVIE, R. B. R-S-, MULLETT, L. B., and WALKINSHAW, W., 1947, *Nature, Lond.*, **160**, 351.

HARVIE, R. B. R-S-, 1948, *Proc. Phys. Soc.*, **61**, 255.

HUXLEY, L. G. H., 1947, *A Survey of the Principles and Practice of Waveguides* (Cambridge : The University Press), pp. 80, 188, 95 (in order of reference in text).

WALKINSHAW, W., 1948, *Proc. Phys. Soc.* **61**, 246.

Effect of Azimuthal Inhomogeneities in the Magnetic Field of a Betatron or Synchrotron

BY F. K. GOWARD

Telecommunications Research Establishment, Malvern

MS. received 14 *February* 1948

ABSTRACT. Azimuthal inhomogeneities in the magnetic field of a betatron or synchrotron cause a forced oscillation of the electron; this forced oscillation may be analysed into oscillations whose frequencies are simple multiples of the rotational frequency of the electron. The complete motion of the electron may be described by adding to the forced oscillation the normal free oscillation of the electron, the period of which is not, in general, commensurate with the rotational frequency.

In this paper are considered quantitatively some particular examples of the types of electron oscillation which may be encountered, with special emphasis on the problems of injecting an electron into an inhomogeneous field, and of extracting an electron by an applied inhomogeneity.

§ 1. INTRODUCTION

THE effects on the electron orbits of azimuthal inhomogeneities in the magnetic field of a betatron or synchrotron have been considered by several workers (Bohm and Foldy 1946, Clark *et al.* 1946, Goward and Dain 1947); no simple general explanation of the effects and their occurrence and application has, however, been given. It is hoped that the description given here, and the illustrative examples considered, will emphasize the practical importance of these inhomogeneities. There is, admittedly, some doubt as to the correctness of a simple theory of electron orbits in a betatron type field

(Kerst 1941, Kerst and Koch 1947), but discrepancies between theory and practice can only be attributed to physical conditions extra to those considered here.

§ 2. MOTION OF ELECTRON IN INHOMOGENEOUS FIELD

The undisturbed axial field of a betatron or synchrotron normally follows the radial law

$$H_z = H_0(r/r_0)^{-n}, \qquad \ldots\ldots(1)$$

where H_0 is the field at some particular radius, r_0, and $0<n<1$. An electron with velocity v_0, where

$$v_0 = (e/mc)H_0 r_0 \qquad \ldots\ldots(2)$$

would describe an orbit at r_0, if injected tangentially at r_0.

Consider that a small axial disturbing field is added, its magnitude varying sinusoidally with θ, i.e. the total field is

$$H_z = H_0(r/r_0)^{-n}(1+\delta_m \sin m\theta), \qquad \ldots\ldots(3)$$

where $\delta_m \ll 1$, and m is any integer. The equation of radial motion in this field, for an electron of velocity v_0, is

$$d^2r/dt^2 = v_0^2/r - (e/mc)v_0 H. \qquad \ldots\ldots(4)$$

Restricting to small displacements, x, from r_0, where $r = r_0 + x$, equation (4) becomes, using equations (2) and (3) and neglecting terms in x^2 etc.,

$$d^2x/dt^2 = (v_0^2/r_0)[(1 - x/r_0 \ldots\ldots) - (1 - nx/r_0 \ldots\ldots)(1+\delta_m \sin m\theta)]. \qquad \ldots\ldots(5)$$

This is conveniently put in terms of θ by the substitutions $d\theta/dt = \omega_0$ and $\omega_0 = v_0/r_0$ giving

$$d^2x/d\theta^2 = r_0[-x/r_0 + nx/r_0 - \delta_m \sin m\theta + (nx/r_0)\delta_m \sin m\theta].$$

The last term may be neglected, since it is a product of two small quantities, giving

$$d^2x/d\theta^2 + (1-n)x = -r_0\delta_m \sin m\theta. \qquad \ldots\ldots(6)$$

The general solution of this equation is

$$x = [r_0\delta_m \sin m\theta/(m^2+n-1)] + [A \sin (1-n)^{\frac{1}{2}}\theta + B \cos (1-n)^{\frac{1}{2}}\theta], \qquad \ldots\ldots(7)$$

the first term representing the forced oscillation, and the second term the free oscillation, A and B being arbitrary constants determined by the initial conditions of the electron. In injection problems the two terms may be comparable, but in extraction problems there is no free oscillation initially and the disturbing field is normally introduced slowly, compared with the oscillation period, so that no free oscillations are excited.

Any arbitrary disturbing field may be synthesized by a Fourier series of terms corresponding to equation (3), i.e.

$$H_z = H_0(r/r_0)^{-n}\left[1 + \sum_{m=0}^{\infty} \delta_m \sin (m\theta + \alpha_m)\right], \qquad \ldots\ldots(8)$$

where α_m allows for azimuthal shift of the disturbing field. This gives, for the electron motion,

$$x = \left[r_0 \sum_{m=0}^{\infty} \epsilon_m \sin (m\theta + \alpha_m)\right] + [A \sin (1-n)^{\frac{1}{2}}\theta + B \cos (1-n)^{\frac{1}{2}}\theta], \qquad \ldots\ldots(9)$$

where

$$\epsilon_m = \delta_m/(m^2+n-1). \qquad \ldots\ldots(10)$$

The terms of equation (10) usually become negligible as the order of the harmonic, m, becomes large.

To illustrate the above analysis, some examples of practical importance will now be studied.

§ 3. INJECTION INTO A BETATRON

The effect of eddy-current disturbing fields on injection into a betatron may conveniently be studied by taking an example, the original Kerst-type 2·3 or 4 MEV. betatron. The magnet construction in this machine leads naturally to out-of-phase fields which are of significant magnitude at injection, and these fields vary in a conveniently regular manner with azimuth.

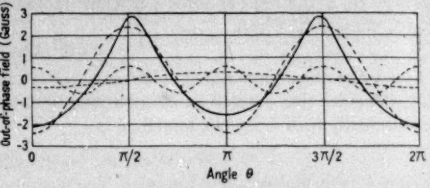

Figure 1. Measured field at injection (full curve), and its harmonic components (dotted curves).

NOTE: Zero out-of-phase field is taken as the mean height of the full curve. For 2 kv. injection voltage and $r_0 \times 7{\cdot}5$ cm. this zero corresponds to 19·9 gauss main field.

Some measurements on these fields for a 4 MEV. betatron, whose radial field varies according to the law $H = H_0(r/r_0)^{-0{\cdot}7}$, where $r_0 = 7{\cdot}5$ cm., the equilibrium orbit radius, are shown in figure 1. The curve is arbitrarily arranged so that its mean ordinate is zero; this is permissible, since a mean value different from zero merely entails injecting the electrons at a time slightly different from that with no eddy-currents present. Taking an injection voltage of 2 kv., which corresponds to a mean field of 19·9 gauss at 7·5 cm. radius, harmonic analysis of the full curve of figure 1 gives

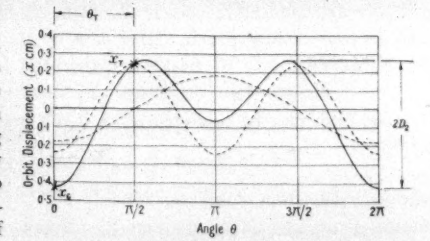

Figure 2. Forced oscillation of orbit (full curve), and its harmonic components (dotted curves). The oscillation corresponds to the field disturbance of figure 1.

$$H_z = H_0(r/r_0)^{-n}\left[1 + \sum_{m=1}^{\infty} \delta_m \cos m\theta\right], \qquad \ldots\ldots(11)$$

where $\delta_1 = -0{\cdot}017$, $\delta_2 = -0{\cdot}120$, $\delta_3 = 0{\cdot}005$, $\delta_4 = 0{\cdot}028$ etc. The forced oscillation therefore has the coefficients $\epsilon_1 = -0{\cdot}024$, $\epsilon_2 = -0{\cdot}032$ and all other coefficients are of the order of 0·001 or less, and may be neglected. Thus the equation of the forced oscillation is

$$x = -0{\cdot}18[\cos\theta + (4/3)\cos 2\theta] \text{ cm.} \qquad \ldots\ldots(12)$$

This oscillation is shown in figure 2, where it may be noted how the lower harmonics are accentuated: this is an important point to notice in practical betatron design, as has been observed experimentally by Adams, Kerst and Scag (1947).

In the injection process the forced oscillation of equation (12) combines with a free oscillation, the free oscillation amplitude being determined by the condition that it must combine with the forced oscillation to give an electron coincident with the gun initially. A typical oscillation is shown by the full line of figure 3 (*a*), the oscillation being a combination of the forced oscillation of overall amplitude 0·7 cm. and a free oscillation of overall amplitude 2·9 cm. The injection gun is shown at $r = 8{\cdot}5$ cm. by the points G_1, G_2, ... etc., and the target at $r = 4{\cdot}7$ cm. by the points T_1, T_2, ... etc.; the target is at right angles to the injection gun. A pure free oscillation of the same amplitude as the free oscillation component of figure 3 (*a*) is shown in figure 3 (*b*), i.e. the oscillation is of 2·9 cm. overall amplitude about a mean radius of 7·05 cm. The figures drawn do not assume damping, since damping will be considered separately later. For this undamped case it may be seen that the target in figure 3 (*a*)

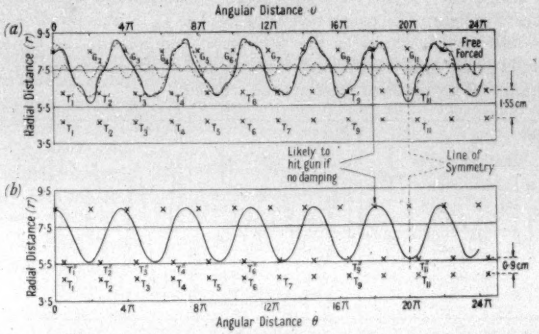

Figure 3. Oscillations in betatron. (*a*) Forced+free oscillations. (*b*) Free oscillation.

can be moved 1·55 cm. from its nominal radial position to T_1', T_2', ... etc., without intercepting the electron at T_7' or T_9'. In figure 3 (*b*), however, a movement of 0·9 cm. only is permissible, to T_1'', T_2'', ... etc. Thus, with the forced oscillation present, the target may be 0·65 cm. closer to the gun, radially, for the same amplitude of free oscillation. This 0·65 cm. is clearly the radial distance $x_T - x_G$ in figure 2.

Considering now the maximum permissible oscillations with the gun and target fixed at G_1 and T_1, the amplitudes of the free and forced oscillations are again fixed by the conditions that the gun and target must not be hit and that the electron must be coincident with the gun initially. A free oscillation is permissible, therefore, of overall amplitude approximately 0·65 cm. greater than that permissible with no forced oscillation present, i.e. of 4·45 cm. overall amplitude. This figure is approximate because there is a slight change in the amplitude of the forced oscillation dependent on the mean radius about which the oscillation occurs (see equation (9)); this slight change may be neglected.

A general statement can be made for this particular type of betatron, with an external gun and an internal target at fixed radial distances; if the target is at an angle θ_T relative to the gun (see figure 2), then a free oscillation is permissible, on injection, of amplitude A_2, where

$$A_2 = A_1 + \tfrac{1}{2}(x_T - x_G); \qquad \ldots\ldots(13)$$

A_1 is the maximum permissible free oscillation amplitude with no forced oscillation present and is therefore half the radial separation between the gun and the target; $x_T - x_G$ is defined in figure 2. The largest effect occurs if the target is placed at an angle θ_T such that $|x_T - x_G|$ has its maximum value, $2D_2$. Then the limiting values of A_2 are given by

$$A_2 = A_1 \pm D_2, \qquad \ldots\ldots(14)$$

where A_2 takes its maximum or minimum value as the phase of the free oscillation changes by π relative to the gun. This effect of the phase of the forced oscillation may be seen in the initial states shown in figure 5, which is discussed more fully later. The presence or absence of the forced oscillation does not in any way affect the number of revolutions before the electron hits the gun in this undamped case. The only factor which will affect this number is the possibility of the electron hitting the "donut" at some point. This follows from the fact that the full curve in figure 3 (*a*) passes below the level of T_1'. It is possible, however, that the relative magnitudes of the oscillation components, as expressed by equation (13), may have a significant effect on the injection process by changing the damping. This problem must now be studied.

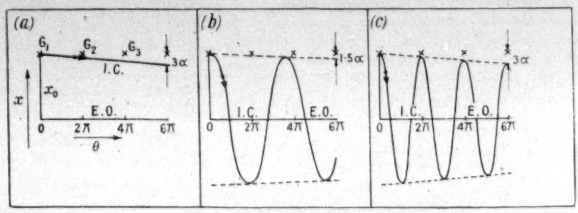

Figure 4. Types of damping.
(*a*) Shrinkage of instantaneous circle : $x = x_0(1 - \alpha\theta/2\pi)$.
(*b*) Damping of free oscillation : $x = x_0(1 - \alpha\theta/4\pi)\cos(1-n)\frac{1}{2}\theta$.
(*c*) Damping of forced oscillation : $x = x_0(1 - \alpha\theta/2\pi)\cos m\theta$.
NOTE : I.C. denotes instantaneous circle; E.O. denotes equilibrium orbit.

Theories of the mechanism of injection which have been advanced (Kerst and Serber 1941) rely on damping to miss the gun, which is considered to be substantially a point. These theories are not in accord with experiment, failing in particular to explain the approximately linear variation of beam current with injection voltage, and the possibility of injecting with a gun which requires an inordinate damping to miss it. Nevertheless, it seems reasonable to assume that damping is important as a contributory factor in injection and to examine the effect on the damping of the presence of the forced oscillations. Kerst and Serber state that two forms of damping are possible:

(*a*) An electron may be injected tangentially at a field value and energy such that its radius of curvature is equal to the radius at which the gun is placed. The orbit then shrinks, as shown in figure 4 (*a*), the shrinkage being such that

$$\Delta x/x = -\Delta H/H. \qquad \ldots\ldots(15)$$

From this it follows, since the field H rises linearly with time during injection, that

$$x = x_0(1 - \alpha\theta/2\pi), \qquad \ldots\ldots(16)$$

α is the damping factor, and the relation holds when x/x_0 is near unity.

(*b*) An electron may be injected at a field value and energy such that its radius of curvature would be r_0, were it injected tangentially at radius r_0. A free oscillation is then obtained, as shown in figure 4(*b*), the damping of the oscillation being half that of equation (16).

To these forms of damping, which may be called, respectively, shrinkage of the "instantaneous circle" towards the equilibrium orbit and damping of the free oscillations about the instantaneous circle, must now be added a further type of damping, the damping of the forced oscillation. The disturbing eddy current field producing the forced oscillation remains constant with time, whereas the main field rises linearly with time. Thus δ_m, the relative amplitude of the disturbing field, varies inversely with time, and ϵ_m does likewise by equation (10). The oscillation amplitude therefore varies inversely with field, i.e.

$$|x| = k/H, \qquad \ldots\ldots(17)$$

which gives a relation of the form of equation (15). Thus the damping of the forced oscillation is the same as the shrinkage of the instantaneous circle and is double the damping of the free oscillation. The expression for damping assumes that δ_m changes inappreciably during one revolution, so that no free oscillations are excited during the change.

Returning now to the example which has been considered for the undamped case, the dampings may be compared with and without forced oscillations present; the argument will be restricted to oscillations which are as large as the space between the gun and target will permit.

The maximum permissible free oscillation, with no forced oscillation present, has an amplitude of 1·9 cm. about an instantaneous circle of 6·6 cm.; this is shown in the left-hand portion of figure 5(*a*). After r revolutions the amplitude of the oscillation is damped by $0{\cdot}95\alpha r$ cm. It will be convenient to consider always that $r = 9$, since this corresponds to the point G_{10} when the electron is likely

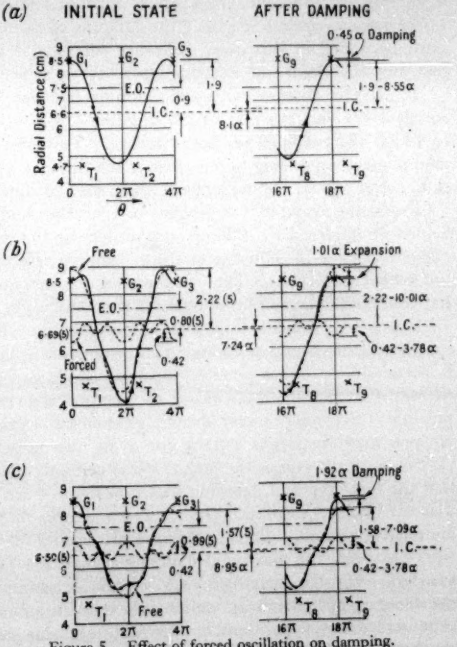

Figure 5. Effect of forced oscillation on damping.
(*a*) No forced oscillation; (*b*) harmful forced oscillation; (*c*) helpful forced oscillation.

to hit the gun. The free oscillation damping is therefore $8{\cdot}55\alpha$ cm. From this must be subtracted the expansion of the instantaneous circle, $0{\cdot}9\alpha r$ cm. or $8{\cdot}1\alpha$ cm. (The orbit expands because the equilibrium orbit is at a greater radius than the instantaneous circle.) The net damping is therefore $+0{\cdot}45\alpha$ cm. These damping effects are shown in the right-hand portion of figure 5 (*a*). The relative dampings are drawn to an approximately correct scale, but the absolute magnitude is not to scale.

The combination of a free and forced oscillation is shown in figure 5 (*b*). The free oscillation is large and of amplitude $1{\cdot}9+\frac{1}{2}(0{\cdot}65)=2{\cdot}22_5$ cm., about an instantaneous circle of radius $6{\cdot}69_5$ cm.; its damping after nine revolutions is therefore $10{\cdot}01\alpha$ cm. From this must be subtracted an expansion in the instantaneous circle of $9\times 0{\cdot}80_5\alpha=7{\cdot}24\alpha$ cm. Further, the damping of the forced oscillation, $9\alpha x_G$ or $3{\cdot}78\alpha$ cm., must also be subtracted. This gives a net damping of $-1{\cdot}01\alpha$ cm. Thus the presence of the forced oscillation spoils the chance of injection.

The above effect is, however, dependent on the phase of the forced oscillation, and the forced oscillation shown in figure 5 (*c*) may be shown to have the opposite effect. The free oscillation is now reduced to an amplitude of $1{\cdot}9-\frac{1}{2}(0{\cdot}65)=1{\cdot}57_5$ cm. about an instantaneous circle of radius $6{\cdot}50_5$ cm. The free oscillation is damped by $7{\cdot}09\alpha$ cm., from which must be subtracted the expansion of the instantaneous circle $8{\cdot}95\alpha$ cm.; the damping of the forced oscillation, $3{\cdot}78\alpha$ cm., must be added in this case. The net damping is therefore $1{\cdot}92\alpha$ cm., which increases the chance of injection over that with no forced oscillation present.

It may be observed that the damping increase $(1{\cdot}92\alpha-0{\cdot}45\alpha)$ cm., which equals $1{\cdot}47\alpha$ cm., is equal to the decrease $(1{\cdot}01\alpha+0{\cdot}45\alpha)$ cm., to the accuracy to which the example has been worked. This change is in fact equal to the damping corresponding to one quarter the distance x_T-x_G in the forced oscillation, i.e. to $9(0{\cdot}65\alpha/4)$ cm., a result which may be shown to be correct in general.

From this example it is possible to generalize and say that injection may be helped or hindered by different magnitudes and angular distributions of eddy-current fields. In addition to these damping effects the betatron will clearly not work if the forced oscillation is such that it cannot be contained within the space between the gun and target, or between the donut walls, irrespective of damping.

It is a little difficult to generalize beyond this. Firstly, in the example the special case has been considered of an instantaneous circle as far from the gun as is permissible. Other possible injection conditions have been neglected, and therefore no consideration taken of the time interval over which injection is possible. Secondly, a very specific geometrical arrangement has been studied, whereas many betatrons use the gun as its own target, or have the donut walls very close to the gun or the target. It is certainly possible to observe, however, that the three types of damping shown in figure 4 are all of the same order, and that the changes introduced by various mixtures of free and forced oscillation are relatively small. Thus in the example, even if the condition of equation (14) were observed, the maximum damping change is $4{\cdot}5\,D_2\alpha$, whereas for injection as in figure 4 (*a*) the damping is $9A_1\alpha$. Thus for a damping change equal to 10% of the damping of figure 4 (*a*), we have the condition $D_2=\frac{1}{5}A_1$, and this is therefore suggested as an upper limit to the eddy currents permissible, i.e. the overall amplitude of the forced oscillation should not exceed one-fifth of the radial separation of the gun and target.

In concluding this section it should be re-emphasized that the above considerations are not intended to indicate how normal injection into a betatron is accomplished. The assumptions of a gun which is almost a point and of the significance of damping are the recognized doubtful assumptions made by Kerst and Serber (1947). The treatment given here, while not attempting to elucidate the problem of why most betatrons work, may perhaps indicate why some do not.

§ 4. EJECTION OF ELECTRON BEAM BY A STEP FIELD

As a further example, consider the forced oscillation caused by the "step field" shown in figure 6; such a step field may be used for ejecting the electrons from their normal orbit. The disturbing field, H_D, may be analysed into Fourier components thus (note that $m=0$ does not give the $\frac{1}{4}\theta_1$ term):

$$H_D=(2\Delta H_0/\pi)[\tfrac{1}{4}\theta_1-\sin\tfrac{1}{2}\theta_1\cos\theta+\tfrac{1}{2}\sin\theta_1\cos 2\theta\ldots.+(-1)^m m^{-1}\sin\tfrac{1}{2}m\theta_1\cos m\theta]. \quad \ldots\ldots(18)$$

If it is assumed that the addition of the disturbing field does not change the value of n, then the forced oscillation is

$$x=[r_0\Delta H_0\theta_1]/[2\pi H_0(n-1)]+r_0\sum_{m=1}^{\infty}\epsilon_m\cos m\theta, \quad \ldots\ldots(19)$$

where

$$\epsilon_m=\frac{2}{\pi}\frac{\Delta H_0}{H_0}\left[\frac{(-1)^m\sin\tfrac{1}{2}m\theta_1}{m(m^2+n-1)}\right]. \quad \ldots\ldots(20)$$

This series converges rapidly if $\theta_1\simeq\pi$, but less rapidly if $\theta_1\simeq 0$ or 2π.

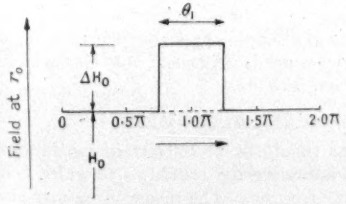

Figure 6. Step field.

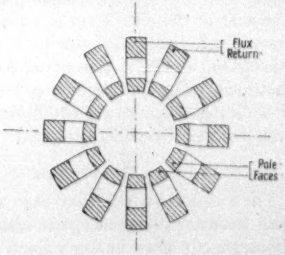

Figure 7. Circularly symmetrical magnet.

For the important case when $\theta_1=\pi$, ϵ_2, ϵ_4, and even coefficients, vanish, leaving as the only significant terms

$$\epsilon_0=\frac{2}{\pi}\frac{\Delta H_0}{H_0}\left[\frac{1}{n-1}\frac{\pi}{4}\right], \quad \epsilon_1=\frac{2}{\pi}\frac{\Delta H_0}{H_0}\left[-\frac{1}{n}\right]. \quad \ldots\ldots(21)$$

Clark *et al.* (1946) considered the special case of $\epsilon_0=0$, and equations (19) and (21) then give their result, namely

$$\frac{x}{r_0}=-\frac{2}{\pi n}\frac{\Delta H_0}{H_0}\cos\theta. \quad \ldots\ldots(22)$$

For general considerations, however, such as finding the optimum length of a step field for ejecting the electrons, the slow or non-convergence of equation (19) makes it better to ignore the approach via the Fourier analysis and to treat the problem directly, as was done by Goward and Dain (1947).

§ 5. EFFECT OF PERIODIC DISCONTINUITIES IN A CIRCULARLY SYMMETRICAL MAGNET

As a final example, the effect of a large number of similar discontinuities round the circumference of a magnet may be considered. This is of some interest in the design of large synchrotrons, where it is mechanically desirable to leave gaps in the magnet poles between individual segments of the magnet. Figure 7 shows a section through such a magnet, with 12 segments. The disturbing field may then take the form shown diagrammatically in figure 8.

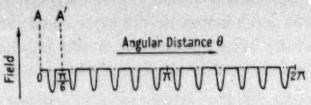

Figure 8. Possible disturbing field with circularly symmetrical magnet.

If w is the number of segments, i.e. the number of disturbances per revolution, equations (8) and (9) become

$$H_z = H_0(r/r_0)^{-n}\left[1+\sum_{m=0}^{\infty}\delta_m \sin(mw\theta+\alpha_m)\right], \qquad \ldots\ldots(23)$$

$$x = \left[r_0\sum_{m=0}^{\infty}\epsilon_m \sin(mw\theta+\alpha_m)\right]+[A\sin(1-n)^{\frac{1}{2}}\theta + B\cos(1-n)^{\frac{1}{2}}\theta)], \qquad \ldots\ldots(24)$$

where

$$\epsilon_m = \delta_m/(m^2w^2+n-1). \qquad \ldots\ldots(25)$$

Because of the m^2w^2 term in equation (25), the forced oscillation is, in general, very much smaller for this kind of disturbance than for the same disturbance spread out so that AA′ in figure 8 occupies 2π. The $m=0$ term is an exception, however, being independent of w; this has a simple physical explanation, since it indicates a shift of the equilibrium orbit which is dependent only on the mean value of the disturbing field, taken over one revolution.

§ 6. CONCLUSION AND ACKNOWLEDGMENT

The examples which have been studied should be of interest to synchrotron and betatron designers, particularly in indicating the tolerances to which field homogeneity must be maintained during injection. The theory given may also suggest new methods of ejecting the electron beam; an instance of this will be described in the appendix.

This work was carried out in the Atomic Energy Research Establishment Group at the Telecommunications Research Establishment, Malvern, and acknowledgment is made to the Director for permission to publish this paper.

APPENDIX

EFFECT OF RADIAL DISTURBING FIELDS

In the main text we have studied the effects of azimuthal asymmetries, formed by the addition of axial fields to the main field. The problem of adding radial fields to give azimuthal asymmetry may be considered in a very similar way.

The undisturbed radial field of a betatron or synchrotron may be obtained by applying the condition that curl H is zero, i.e. that

$$\partial H_z/\partial r = \partial H_r/\partial z. \qquad \ldots\ldots(26)$$

This gives, for the radial magnetic field,

$$H_r = -nzH_0/r_0, \qquad \ldots\ldots(27)$$

to a good approximation. Consider, now, the addition of a radial field, varying sinusoidally with azimuth, so that the field becomes

$$H_r = -nzH_0/r_0 + H_0\beta_m \sin(m\theta + \alpha_m). \qquad \ldots\ldots(28)$$

The equation of axial motion, for an electron of velocity v_0, is

$$d^2z/dt^2 = (\boldsymbol{e}/\boldsymbol{mc})v_0H_r, \qquad \ldots\ldots(29)$$

which reduces, using equations (2) and (28), to

$$d^2z/d\theta^2 = -nz + r_0\beta_m \sin(m\theta + \alpha_m). \qquad \ldots\ldots(30)$$

The general solution of this equation is

$$z = [-r_0\gamma_m \sin(m\theta + \alpha_m)] + [C \sin(n^{\frac{1}{2}}\theta) + D \cos(n^{\frac{1}{2}}\theta)], \qquad \ldots\ldots(31)$$

where

$$\gamma_m = \beta_1/(m^2 - n). \qquad \ldots\ldots(32)$$

Arbitrary disturbing fields may be synthesized by expressing them as Fourier series, as in the main text.

It may be seen, from equations (9) and (31), that an azimuthally constant disturbing field, for which $m=0$ and $\alpha_m = \pi/2$, gives a displacement $(1/n)-1$ times as great as would the same field applied axially: this is in agreement with the well known axial instability observed as n approaches zero.

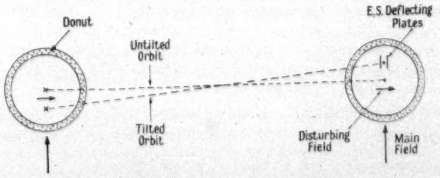

Figure 9. Beam ejection by radial disturbing field.

The effect of a disturbing field varying as $\sin\theta$, i.e. $m=1$, is of particular interest and importance. The orbit is caused to tilt, its maximum displacement from $z=0$ being $r_0\beta_1/(1-n)$. As n approaches 1, the displacement becomes resonant and very large. This large displacement suggests a method of extracting the beam in a betatron or synchrotron, since the beam could be made to pass into electrostatic deflecting plates. This is shown diagrammatically in figure 9.

REFERENCES

Adams, G. D., Kerst, D. W., and Scag, D. T., 1947, *Rev. Sci. Instrum.*, **18**, 799.
Bohm, D., and Foldy, L., 1946, *Phys. Rev.*, **70**, 249.
Clark, J. S., Getting, I. A., and Thomas, J. E., Jr., 1946, *Phys. Rev.*, **70**, 562.
Coward, F. K., and Dain, J., 1947, *Nature, Lond.*, **159**, 636.
Kerst, D. W., 1941, *Phys. Rev.*, **60**, 47.
Kerst, D. W., and Koch, H. W., 1947, *Rev. Sci. Instrum.*, **18**, 681.
Kerst, D. W., and Serber, R., 1941, *Phys. Rev.*, **60**, 53.

LETTERS TO THE EDITOR

The Measurement of Dielectric Constant in a Waveguide

The dielectric constant of ethyl alcohol has been measured at a wavelength of 12·60 cm. in a waveguide. The standing-wave method was used, the essentials of which have already been described by Williams and Bolton (1945). The wavelength is close to the middle of the dipole dispersion region and the absorption is consequently large. The energy is completely absorbed in the liquid when a few centimetres deep, and the impedance presented at the liquid surface is the characteristic impedance of the guide filled with dielectric.

The liquid was supported on a thin slab of ebonite in a vertical guide, $7 \times 3{\cdot}5$ cm. in cross-section, and an H_{10} wave was used. The minimum depth of ethyl alcohol needed was about 4 cm.: for depths greater than this the impedance measured was constant. The impedance is complex and, using the symbols defined by Williams and Bolton, is given by $Z_0' = i\omega\mu/P_t'$ where $P_t' = \alpha_t' + i\beta_t'$ is the propagation constant. If χ^2 is the constant characterizing the mode of oscillation in the hollow tube, $\chi^2 = P_t'^2 + \omega^2\mu(\epsilon' - i\epsilon'')$, and these three equations are sufficient to determine the real and imaginary parts (ϵ', ϵ'') of the dielectric constant.

The standing wave was observed by a crystal detector moving in a slot above the liquid. The crystal was calibrated by assuming its characteristic to be given by $i = A|E|^k$, where i is the output current and E the strength of the transverse electric field. The value of k was found by a subsidiary experiment using an empty tube closed by a metal plate. The standing wave was then represented by $|E|^2 = B \sin^2 2\pi x/\lambda_t$, where x is the distance from a minimum, and the slope of the graph of $\log i$ against $\log(\sin 2\pi x/\lambda_t)$, which was accurately a straight line, gave k equal to $0{\cdot}960 \pm 0{\cdot}5\%$.

The results of three independent samples of freshly dried and distilled ethyl alcohol gave $\epsilon' = 5{\cdot}5$, $\epsilon'' = 7{\cdot}8$. The accuracy was to within about 1%. The results are plotted in the figure together with other experimental points referred to by Mizushima (1927), Akerlof (1932), Malsch (1932), Bäz (1939) and Slevogt (1939). The semicircle is the locus of Debye's equation and the points suggest that the equation applies to ethyl alcohol. Using the parametric form of the equation the present experimental results give a value of 31 cm. for the relaxation wavelength (Sprungwellenlänge).

The University, Nottingham. H. C. Bolton.

12 June 1948.

Akerlof, G., 1932, *J. Amer. Chem. Soc.*, **54**, 4125.
Bäz, G., 1939, *Phys. Z.*, **40**, 394.
Malsch, J., 1932, *Ann. Phys., Lpz.*, **12**, 865.
Mizushima, S., 1927, *Phys. Z.*, **28**, 418.
Slevogt, K. E., 1939, *Ann. Phys., Lpz.*, **36**, 141.
Williams, G., and Bolton, H.C., 1945, *Phil. Mag.*, **36**, 862.

REVIEWS OF BOOKS

Electrons in Gases, by Sir John Townsend, F.R.S. Pp. 166. (London: Hutchinson's Scientific and Technical Publications, 1948.) 25*s*.

Sir John Townsend, the author of this book, by the number and fundamental character of his contributions, both in theory and experiment, occupies an unrivalled position as an authority in the field of electrical discharges and of electronic motion in gases.

Moreover, his early investigations at the turn of the century on the atomic nature of electricity rank with the greatest of that remarkable time. It will be recalled, for instance, that in 1897 he made the first direct attempt to determine the atomic charge by the method of

falling drops, which, to quote Millikan, " was of much novelty and no little ingenuity. It is also of great interest because it contains all the essential elements of some subsequent determinations." In 1899 and 1900 he showed from the ratio of the mobilities of ions to their diffusion coefficients (which he measured) that the product is the same for gaseous ions as for a monovalent ion in an electrolyte. Thus the charge e is the same on each. These fundamental investigations were followed in 1900 by his discovery that molecules of a gas were ionized in collisions with electrons possessing energies of only 20 electron volts, and by means of his well-known parallel plate apparatus he measured the number of molecules α ionized on the average by an electron in drifting one centimetre in the direction of the uniform electric force. These early experiments on ionization possess a double interest; first, they showed that electrons liberated by ultra-violet light from a metal plate and those liberated from molecules by ionization possessed the same ionizing coefficient α and were presumably identical—a fact of considerable significance at that time; secondly, they form the starting point of the series of investigations on the mechanism of discharges in gases to which we owe most of our understanding of the subject. When n_0 photo-electrons are liberated from a plane cathode, the number reaching the anode after moving in a uniform field between the electrodes is given by Townsend's formula

$$n = n_0 \frac{(\alpha-\beta)\exp(\alpha-\beta)x}{\alpha-\beta\exp(\alpha-\beta)x},$$

in which α has the meaning assigned to it above, and β is the number of molecules ionized by a positive ion in drifting one centimetre in the direction of the electric force which is supposed to be maintained constant as the separation x of the electrodes is varied. Thus in 1903 Townsend was led to propose a theory of sparking in uniform fields according to which a spark first occurs at a separation x such that the denominator in the expression vanishes. The current then remains finite although n_0 is zero. Since he had shown, both by theory and measurement, that the ionizing coefficients α and β in each gas satisfy functional equations $\alpha/p = f(Z/p)$ and $\beta/p = F(Z/p)$, p being the gas pressure and Z the electric force, it was possible successfully to predict the sparking potential for a given separation x of the electrodes from the experimental determinations of these functional relationships. In the following years up to the outbreak of the first World War, the theory was extended to discharges in non-uniform fields and to the conditions that supervene when the applied field is modified by the presence of space charge. This work is lucidly described in his celebrated treatise *Electricity in Gases*, which, in many respects, is still the best account of the principles of the subject.

The appearance of a recent book, *Electrons in Gases*, by Sir John Townsend, describing his further investigations in this field carried out between the wars, is, therefore, a matter of considerable interest to workers in this and related subjects. Although the book forms a useful appendix to *Electricity in Gases*, it is in fact a self-contained work because the author has included all the theory required for an understanding of the whole book. The book is principally concerned with three topics: the study of the behaviour of slow electrons in gases when ionization is unimportant, ionization by collision, and the theory of the spark discharge. After a preliminary chapter which gives the theory of electron diffusion and drift in an electric field, the author proceeds to describe the principle of his diffusion apparatus, which permits the energy factor k—the ratio (agitational energy of electrons)/(agitational energy of the gas molecules)—and the drift velocity W of the electrons to be determined as a function of the ratio (Z/p) of the electric force Z to the pressure p. From k and W, using theoretical formulae, the following parameters of the electronic motion are obtained: the mean free path L at unit pressure (1 mm. Hg), the R.M.S. velocity of agitation V and the mean proportion λ of its energy lost by an electron in a collision with a gas molecule. The dependence of k, W, V and λ upon Z/p in a variety of gases is exhibited in tables and curves.

It was found that L (which is inversely proportional to the collisional cross-section of the molecules) depends upon the energy of the electron, the variation being especially remarkable in the heavier monatomic gases. There are interesting critical paragraphs in which the results of diffusion experiments on L are compared with those of other workers using the methods of Lenard and Ramsauer.

The major part of the remainder of the book is concerned with studies of ionization in gases by collision and other actions, and of theories of discharges. It has long been known

(*Electricity in Gases*) that the increase of the current with distance in a uniform field is represented with equal accuracy both by the formula given above in terms of the coefficients α and β and by an alternative formula in terms of α and γ, where the positive ions are supposed to act by liberating γ electrons per ion at the cathode, and also by a formula in which α, β and γ all occur. It is a remarkable fact that all three formulae are analytically equivalent, so that it is not possible to decide the precise action of the positive ions in contributing to the growth of the current and in electrical discharges, from experiments with uniform fields. When, however, the whole range of phenomena is considered, in particular the properties of brush discharges from wires and points, the author shows that the fashionable view that the action represented by the coefficient β is absent is untenable, but that it is necessary to suppose that positive ions do in fact ionize gas molecules in discharges—that is, the β-effect is always operative. Near the minimum sparking potential the γ-action is also important, but becomes relatively unimportant at the higher pressures. He also describes an experiment which demonstrates the β-action directly.

Other theories of sparking are discussed in full and the hypotheses on which they are based are shown to be untenable. Although a theory of sparking at present in vogue is not discussed, it is rejected by implication, since it is shown that photo-ionization of the gas is not an important factor in contributiong to electrical breakdown. The book contains interesting and acute discussions of many other matters, including the electrical properties of monatomic gases, experiments on critical potentials, and the distribution of the agitational velocities of the electrons.

This is a book which should be read by all who are interested in the fundamental principles of electrical discharges and of electronic motion in gases.

L. G. H. HUXLEY.

Royal Society Mathematical Tables Committee

Mathematical Tables for Science and Industry

It is considered that important investigations in the physical, chemical and engineering sciences, in mathematics and in industry, may be held up by the absence of relevant mathematical tables. Several important tables of a fundamental nature have in the past been produced by the British Association through its Mathematical Tables Committee. The work in this field has now been transferred to the Royal Society on the invitation of the British Association, and a special Royal Society Mathematical Tables Committee has been established to continue and extend the earlier work. This Committee would be glad to receive suggestions from industrial research groups, from individual investigators and from Service departments relating to existing needs in their special fields. Requests for assistance may be met either by advice as to the most economical way of producing the desired tables, or by an undertaking to produce the tables under the auspices of the Royal Society, or, in exceptional cases, by a grant towards the cost of tabulation or to make possible the publication of important tables which may exist only in manuscript. In the first instance inquiries should be addressed to the Assistant Secretary, The Royal Society, Burlington House, London W.1.

CORRIGENDA

"Angular Distribution in Internal Pair Creation", by G. K. HORTON (*Proc. Phys. Soc.*, 1948, **60**, 457).

In figures 1, 2, 3, ordinates *should read* $P\times10^{5}$, *not* $P\times10^{-5}$.

In figure 1, right-hand ordinate scale should be shifted down one unit.

In figure 4, caption *should read*: "2, 4, Magnetic dipole or electric quadrupole. 1, 3, Electric dipole."

Page 460, line 11, *for* larger *read* smaller.